Using CombiCells to investigate the role of co-signalling receptor ligands on T cell activation



Jordan Kramer

Brasenose College

University of Oxford

Supervisors: P. Omer Dushek and P. Anton van der Merwe

This thesis is submitted for the degree of *Doctor of Philosophy*

Trinity Term, 2026

Statement of Contribution

The work presented in this thesis was conducted in the Sir William Dunn School of Pathology at the University of Oxford, and, except where otherwise indicated, all of the research described is my own work. Specific contributions from collaborators are explicitly acknowledged below and at the relevant points in the text and figure captions.

Many of the cell lines utilised in these studies were developed by previous lab members. The CHO-K1 CombiCell line was generated by Johannes Pettmann [1]. The Jurkat T cell lines with extended CD2 and PD-1 variants were generated by Jake Burton and Violaine Andre [2]. The U87 NLuciferase and A375 mCherry cells were created by Jose Cabezas Caballero [2].

Purification of SpyTagged proteins was performed by Yue Jin Oh and Mikhail Kutuzov [1,2]. Experimentally, all microscopy studies and PD-L1 surface density quantifications were performed by Tommy Dam [2]. Primary T cell isolation for SLAM and CAR studies was performed in a rotating manner, with contributions from Dushek lab members Sofía Bustamante Eguiguren, Kirtana Sivasubramanian, Alina Shomuradova, and Pablo Lopez Ribelles.

All studies on the Compact CAR are the result of a highly collaborative research effort including significant experimental contributions from Jake Burton, Jesús A Siller-Farfán, Violaine Andre, Edward Jenkins, Michael Barton, Tommy Dam, Sofía Bustamante Eguiguren, and Jose Cabezas Caballero [2]. The Compact CAR itself was conceptualised by my supervisor, Omer Dushek [2]. While the data presented in this thesis regarding the Compact CAR were collected entirely by the author except when otherwise explicitly noted, the project design and the generation of many of the materials and DNA constructs used are again the result of a highly collaborative effort.

The Dushek group as a whole has offered me incredible support over the last few years including practical day-to-day advice on cloning protocols, cell culture, experimental design, and primary T cell maintenance. This work would not have been possible without their guidance and mentorship.

Acknowledgements

I am deeply grateful for the support I have been shown throughout my DPhil journey. From my incredible college friends, who provide endless entertainment, to the amazing labmates who made coming to work each day an absolute pleasure, my Oxford experience has been characterised as much by the people as by the work.

I would first like to thank my supervisors, Prof. Omer Dushek and Prof. Anton van der Merwe, who took me on as a student and guided me through the trials and tribulations of biological research. Omer in particular was unfailingly generous with his time and his encouragement; I could not have completed my experiments nor my thesis without his support. In addition, my supervisors curated an incredibly friendly and collaborative laboratory environment in which it has been a pleasure to work. I have no end of good things to say about my colleagues and the research team that I have been a part of.

The Dushek lab is an amazing group of individuals who have provided unwavering support, kindness, and friendship. From laser tag to holiday dinners to coffee breaks and tennis sessions, I have no end of joyful memories. I would, in particular, like to thank Sofía for always, always making the time to answer my questions and for providing me with incredible kindness and support over the last four years. It has been an absolute pleasure to work alongside her. I would also like to thank Tommy for our Uni parks walks, Kirtana for the tennis games and excellent commentary, and Colin for the spikeball and daily encouragements. I am so grateful for each and every member of the Dushek lab.

I would like to thank my friends for walks in the park, camping trips, spikeball games, squash evenings, and, more generally, for making the last four years so incredible. Finally, I would like to thank my family, whose support is the only reason I could even dream of studying here.

Abstract

T cells are a central component of adaptive immunity, capable of identifying and eliminating foreign pathogens while remaining tolerant to a far more abundant population of healthy self-cells. This high degree of specificity is mediated in part by the T cell receptor (TCR), which interacts with peptides presented on the major histocompatibility complex (pMHCs). Although the TCR is specialised for antigen recognition, the remarkable sensitivity of the T cell response is aided by a diverse array of accessory receptors, which act to fine-tune T cell activation. However, dissecting the contributions of individual receptors to the complex process of TCR signalling remains challenging, due to the diversity and combinatorial nature of receptor-ligand interactions at the T cell/antigen-presenting cell (APC) interface. In this thesis, we utilise the novel CombiCell platform to generate biologically relevant APCs capable of presenting any desired concentration or combination of ligands. We employ these CombiCells to interrogate the role of individual accessory receptors in T cell activation, examining the impact of these receptors on both TCR-T cell and chimeric antigen receptor (CAR)-T cell sensitivities. The results of this thesis highlight the essential role of accessory receptors in fine-tuning T cell activation and support the use of the CombiCell system for future T cell activation studies.

Keywords— CAR-T cells, CombiCells, SLAM Family, T cell sensitivity

Table of Contents

List of Figures **7**

List of Tables **10**

1 Introduction **1**

1.1 The Human Immune System 1

1.1.1 Innate Immunity 1

1.1.2 Adaptive Immunity 1

1.2 T cell maturation 2

1.2.1 V(D)J recombination 3

1.2.2 Positive and negative selection 4

1.2.2.1 MHC class I and II 4

1.2.2.2 Thymic selection 5

1.3 The TCR complex 6

1.4 TCR signalling 7

1.5 TCR triggering 8

1.5.1 The aggregation model 8

1.5.2 The conformational change model 10

1.5.3 The segregation model 11

1.6 T cell subsets 12

1.6.1 CD4 and CD8 co-receptors 12

1.6.2 $CD4^+$ T cells 13

1.6.3 $CD8^+$ T cells 14

1.6.4 Memory T cells 15

1.6.5 $\gamma\delta$ T cells 15

1.7 Functional outcomes of T cell activation 16

1.7.1 Cytokine production 16

1.7.1.1 IL-2 . . . 17
1.7.1.2 IFN-γ . . . 17
1.7.2 Cell-mediated killing . . . 18
1.7.3 Surface expression of activation markers . . . 18
1.8 Accessory Receptors . . . 19
1.8.1 CD28 . . . 19
1.8.2 CD2 . . . 20
1.8.3 PD-1 . . . 21
1.8.4 SLAM . . . 22
1.8.5 Additional accessory molecules . . . 23
1.9 Immune-based therapies . . . 23
1.10 This thesis . . . 23

2 The role of SLAM-family co-signalling receptors in T cell antigen recognition 25

2.0.1 Introduction . . . 25
2.0.2 SLAM receptors and the CombiCell system . . . 30
2.0.3 This chapter . . . 31
2.1 Results . . . 32
2.1.1 Developing a platform to assess T cell sensitivity to SLAM ligands using CombiCells . . . 32
2.1.2 SLAM ligands have no impact on Jurkat T cell sensitivity . . . 33
2.1.3 Overexpression of SLAM receptor 2B4 leads to increased sensitivity in the presence of SLAM ligand CD48 . . . 35
2.1.4 Further increases in CD48 concentrations do not lead to further increases in T cell antigen sensitivity . . . 40
2.1.5 Primary T cells upregulate SLAM expression following stimulation . . . 42

2.1.6 T cell antigen sensitivity as assessed by surface 4-1BB and CD69 up-regulation is not impacted by SLAM-family co-signalling 43
2.1.7 CD150, but not CD48, Ly9, CD84, or CRACC, reduces T cell cytokine production 43
2.2 Discussion 46

3 The role of extracellular size in TCR and CAR-T cell antigen recognition 53
3.1 Introduction 53
3.1.1 CAR structure 54
3.1.2 CAR-T cell successes 56
3.1.3 CAR-T cell limitations 56
3.1.4 Sensitivity differences between the CAR and the TCR 57
3.1.5 The impact of accessory ligands on CAR and TCR sensitivities 57
3.1.6 The size-matching hypothesis 58
3.1.7 This chapter 60
3.2 Results 61
3.2.1 Developing a platform to study PD-1/PD-L1 mediated CAR-T cell inhibition 61
3.2.2 CAR sensitivity to PD-L1 inhibition can be improved through elongation of PD-1 64
3.2.3 "Compact" CAR demonstrates enhanced sensitivity 67
3.2.4 Compact CAR exhibits improved cell killing to the Standard CAR 70
3.2.5 CAR size-matching fails to achieve TCR-level sensitivities . . 70
3.3 Discussion 75

4 Refining CombiCells by size-matching native and SpyCatcher-coupled surface ligands 78

4.1 Introduction . . . 78
4.1.1 Traditional Antigen Presentation Systems . . . 78
4.1.1.1 Genetically Manipulated Antigen Presenting Cells . . 78
4.1.1.2 Artificial platforms: plates and supported lipid bilayers 80
4.1.2 The CombiCell System . . . 81
4.1.3 This Chapter . . . 84
4.2 Results . . . 85
4.2.1 SpyTagged ligands may increase TCR sensitivity . . . 85
4.2.2 Developing a platform to assess size-matching in CombiCells . 88
4.2.3 Testing the effect of CD2 variants on Jurkat T cell sensitivity to endogenous CD58 and SpyTagged CD58 . . . 90
4.2.4 Truncated SpyCatchers improve T cell sensitivity to endogenous CD58 . . . 93
4.2.5 Transmembrane SpyCatchers lead to further improvements to endogenous CD58 sensitivities . . . 96
4.3 Discussion . . . 102

5 Discussion **106**
5.1 Contextual relevance . . . 106
5.2 Thesis aims . . . 107
5.3 Essential findings, future work, and limitations . . . 108
5.3.1 Investigating the contributions of SLAM-family receptors in antigen recognition . . . 108
5.3.1.1 Essential findings . . . 108
5.3.1.2 Significance, future work, and limitations . . . 109
5.3.2 Determining the role of extracellular size in TCR and CAR-T cell antigen recognition . . . 110
5.3.2.1 Essential findings . . . 110
5.3.2.2 Significance, future work, and limitations . . . 110

5.3.3 Refining the CombiCell system by investigating size-matching between native and SpyCatcher-presented ligands 112
5.3.3.1 Essential findings 112
5.3.3.2 Significance, future work, and limitations 113
5.4 Conclusions 115

6 Materials and Methods 116
6.1 Materials 116
6.1.1 General reagents 116
6.1.2 In-house reagents 118
6.2 Methods 119
6.2.1 Maintenance of immortal cell lines 119
6.2.2 Lentivirus production - pHR 119
6.2.3 Lentivirus production - pLEX 120
6.2.4 Isolation, viral transduction, and maintenance of CD8+ T cells 121
6.2.5 Production of U87 CombiCells 122
6.2.5.1 CRISPR/Cas9 knock-out of U87 proteins 122
6.2.5.2 Lentiviral transduction 123
6.2.6 Production of Jurkat TCR/CAR-T cells 123
6.2.7 Production of additional cell lines 125
6.2.8 CombiCell co-culture assays - adherrent cells 125
6.2.9 CombiCell co-culture assays - suspension cells 126
6.2.10 Peptide pulsing assays 126
6.2.11 Flow Cytometry - detection of T cell activation 127
6.2.12 Flow Cytometry - detection of loaded SpyTagged ligands . . . 127
6.2.13 Flow Cytometry - detection of T cell receptors 128
6.2.14 Flow Cytometry - detection of surface SpyCatcher 128
6.2.15 Surface density quantification of PD-L1 on CHO-K1 CombiCells 130
6.2.16 Longitudinal killing assays 131

6.2.17 Cytokine detection assays . . . 132
6.2.18 AlphaFold SpyCatcher size measurements . . . 132
6.2.19 Elongated CD2 size estimates . . . 133
6.2.20 Data analysis . . . 133
6.2.21 Peptide and protein production . . . 134
6.2.21.1 Peptides . . . 134
6.2.21.2 pMHC tetramer . . . 134
6.2.21.3 SpyTagged proteins . . . 134
6.3 Sequences . . . 136
6.3.1 SpyCatcher Variants . . . 136
6.3.2 SLAM Family Expression Sequences . . . 138
6.3.2.1 SLAM Receptor Sequences . . . 138
6.3.2.2 SpyTagged Ligand Sequences - extracellular domain only . . . 140
6.3.3 TCR and CAR Sequences . . . 141

Bibliography **145**

List of Figures

1.1 Thymocyte development 4
1.2 MHC molecule structures 5
1.3 Structure of the $\alpha\beta$ TCR 7
1.4 TCR signalling 9
1.5 Structures of CD8 and CD4 13

2.1 SLAM family signalling 28
2.2 Using CombiCells as an artificial antigen presentation platform . . . 31
2.3 SLAM family proteins 33
2.4 Validation of ligand loading on CHO CombiCells 34
2.5 SLAM CombiCell assay design and experimental read-out 36
2.6 SLAM ligands have no impact on Jurkat T cell antigen sensitivity . . 37
2.7 Jurkats endogenously express high levels of CD84 and low levels of Ly9, but not 2B4, CRACC, or CD150 38
2.8 Overexpression of 2B4, but not CD150, Ly9, CD84, or CRACC, increases T cell sensitivity 39
2.9 CD48 exerts concentration-independent effect on T cell sensitivity . . 41
2.10 Generation of 1G4 TCR primary T cells 42
2.11 Stimulation increases expression of SLAM receptors CD150, CD84, and CRACC 44
2.12 SLAM ligands have no impact on primary T cell antigen sensitivity as assessed by expression of surface activation markers 45
2.13 CD150 ligand addition leads to decrease in IL-2 production 47

3.1 Production and administration of CAR-T cells 53
3.2 Second-generation CAR structure 54

3.3 Size mismatch between CAR and accessory molecules prevents protein engagement 60
3.4 Generating TCR and CAR Jurkat T cells with size-optimised CD2 . . 62
3.5 Engagement of PD-1 by PD-L1 inhibits TCR-T cell and CAR-T cell activation 63
3.6 Generation of CAR-T cells with size-optimised PD-1 65
3.7 Elongation of PD-1 improves CAR sensitivity to inhibition 66
3.8 Compact CAR exhibits surface expression on primary T cells 68
3.9 Size-matched Compact CAR demonstrates enhanced sensitivity to endogenous ligands 69
3.10 Compact CAR exhibits enhanced killing relative to the standard CAR 71
3.11 Truncated CD28 CAR variants exhibit comparable transduction efficiencies and surface expression levels to the standard CAR 73
3.12 Reducing the length of the extracellular hinge of a CAR has no impact on antigen sensitivity 74

4.1 Genetically modified antigen-presenting cells 79
4.2 Solid-phase antigen presentation platform 80
4.3 Supported lipid bilayer presentation platform 81
4.4 Surface SpyCatcher structure representations 83
4.5 Surface SpyCatcher may alter size matching at the close contact . . . 84
4.6 Generation of U87 CombiCells 86
4.7 Verification of U87 knockout efficacy, SpyCatcher transduction, and ligand loading 87
4.8 SpyTagged CD58 exhibits a higher potency than endogenous CD58 . 89
4.9 Generation of 1G4 Jurkat T cells with elongated CD2 receptors . . . 90
4.10 WT and elongated CD2 receptors exhibit equivalent sensitivity to native CD58 in CombiCell assays 91
4.11 Schematic of hypothesized receptor size matching 93

4.12 Truncated hCD52 surface SpyCatcher variants exhibit no change in transduction efficiency, surface expression, or peptide presentation ability 94
4.13 Elongation of CD2 does not decrease T cell antigen sensitivity to endogenous CD58, despite truncation of surface SpyCatcher 95
4.14 CD2 WT Jurkat T cells show enhanced sensitivity to antigen presented on Δ15 SpyCatcher under endogenous CD58 conditions 97
4.15 Transmembrane surface SpyCatchers have similar loading capacities to GPI-anchored surface SpyCatchers 99
4.16 Truncated CD80 transmembrane surface SpyCatcher exhibits improved sensitivity compared to truncated GPI-anchored surface SpyCatcher . 100
4.17 SpyTagged CD58 at a concentration of 0.1 μM exhibits higher surface expression than endogenous CD58 101
4.18 Summary schematic of surface SpyCatcher truncations and their effects on the extracellular sizes of presented ligands 105

List of Tables

1.1 Major T cell subsets and their defining characteristics 16

2.1 SLAM family naming conventions, structures, and expression patterns. 26

3.1 TCR and CAR Dimensions 59

4.1 Comparison of experimental platforms for ligand presentation and control 81

6.1 Cell lines 116
6.2 Antibodies for flow cytometry 117
6.3 Reagent kits 117
6.4 Instruments and equipment 118
6.5 Software 118
6.6 In-house reagents 118
6.7 Jurkat T cell activation panel 129
6.8 Primary T cell activation panel 129
6.9 SpyTagged ligand loading check panels 129
6.10 T cell receptor expression check panel 130

Abbreviations

ACT Adoptive cell therapy

ADCC Antibody-dependent cellular cytotoxicity

AP Activator protein

APC Antigen-presenting cell

BCR B cell receptor

BSA Bovine serum albumin

BTLA B- and T-lymphocyte attenuator

CAR Chimeric antigen receptor

Cas9 CRISPR-associated protein 9

CD Cluster of differentiation

CHO Chinese hamster ovary

CO_2 Carbon dioxide

CRACC CD2-like receptor activating cytotoxic cells

CRISPR Clustered regularly interspaced short palindromic repeats

DAG Diacylglycerol

DMEM Dulbecco's Modified Eagle Medium

DN Double negative

DNA Deoxyribonucleic acid

DP Double positive

EAT EWS-FLI1-activated transcript

EDTA Ethylenediaminetetraacetic acid

ELISA Enzyme-linked immunosorbent assay

FBS Fetal bovine serum

GPI Glycosylphosphatidylinositol

Grb Growth factor receptor-bound protein

HLA Human leukocyte antigen

ICAM Intercellular adhesion molecule

IFN Interferon

Ig Immunoglobulin

IL Interleukin

IP_3 Inositol trisphosphate

ITAM Immunoreceptor tyrosine-based activation motif

ITSM Immunoreceptor tyrosine-based switch motif

KO Knockout

LAT Linker for activation of T cells

LFA Lymphocyte function-associated antigen

Lck Lymphocyte-specific protein tyrosine kinase

MAPK Mitogen-activated protein kinase

MHC Major histocompatibility complex

NFκB Nuclear factor kappa-light-chain-enhancer of activated B cells

NFAT Nuclear factor of activated T cells

NHEJ Non-homologous end joining

NY-ESO New York esophageal squamous cell carcinoma

PBS Phosphate-buffered saline

PD-1 Programmed cell death protein 1

PD-L1 Programmed cell death ligand 1

PIP_2 Phosphatidylinositol 4,5-bisphosphate

PKC Protein kinase C

PLC Phospholipase C

pMHC Peptide-MHC

Ras Rat sarcoma

RPMI Roswell Park Memorial Institute

SAP SLAM-associated protein

SH Src homology

SHIP Src homology 2 domain-containing inositol 5'-phosphatase

SHP Src homology region 2 domain-containing phosphatase

SLAM Signalling lymphocyte activation molecule

SLB Supported lipid bilayer

SLP SH2 domain-containing leucocyte protein

SOS Son of sevenless

SP Single positive

SPR Surface plasmon resonance

Src Sarcoma

$\mathbf{T}_{CM}$ Central memory T cells

$\mathbf{T}_{EM}$ Effector memory T cells

$\mathbf{T}_{RM}$ Resident memory T cells

Tc Cytotoxic T cell

TCR T cell receptor

Tfh T follicular helper cell

TGF Transforming growth factor

Th T helper cell

TNF Tumour necrosis factor

Treg Regulatory T cell

WT Wild-type

XLP X-linked lymphoproliferative disease

ZAP Zeta-chain-associated protein kinase

1 | Introduction

1.1 The Human Immune System

The human immune system is composed of a complex network of cells, tissues, and signalling molecules that work together to protect the body from disease [3]. It is broadly divided into two branches: the innate immune system and the adaptive immune system [3].

1.1.1 Innate Immunity

The innate immune system acts as the body's first line of protection. It is composed of a range of general defences including physical barriers, enzymes, soluble proteins, and specialised cells [4–6]. The innate immune system can become active within minutes and is designed to identify and eliminate anything it recognises as foreign, providing rapid and generalised protection [5].

1.1.2 Adaptive Immunity

When the innate immune response fails to identify or fully clear an infection, the adaptive immune system is triggered to carry out a targeted host response. This more robust system offers lasting protection in the form of immune memory. However, the adaptive system takes longer to activate, operating on a time scale of days to weeks [5].

Adaptive immunity relies on the activity of two distinct immune cell types: B lymphocytes (B cells) and T lymphocytes (T cells) [7]. B cells mediate the humoral immune response, secreting soluble effector molecules called antibodies to interfere with pathogen activity [7]. In contrast, T cells perform cell-mediated immunity, directly killing infected or abnormal cells and helping to regulate the activity of other

immune cells [7].

A key characteristic of the adaptive immune system is its specificity, with both B and T cells carrying out targeted and precise immune responses [8]. The high specificity of these cells is mediated through specialized receptors on the cell surface called B cell and T cell receptors (the BCR and the TCR, respectively) [8]. When B cells recognize an antigen through the BCR, they can differentiate into antibody-producing cells and secrete antibodies capable of binding to target antigens [9]. Antibody binding can prevent pathogen entry into cells and flag infected cells as targets for cell-mediated killing [7]. Antibody binding also recruits innate immune cells such as macrophages and neutrophils to the site of infection [7]. When T cells identify foreign peptides through the TCR, they undergo multiple transcriptional, epigenetic, and translational changes as a result of activation-induced intracellular signalling cascades [10]. Activated T cells will experience changes in surface protein expression as well as secretion of effector and signalling molecules to directly kill infected cells and facilitate cell-cell communications to coordinate the immune response [11].

1.2 T cell maturation

T cells originate in the bone marrow and migrate to the thymus for maturation, at which time they begin to express a TCR and commit to a specific T cell subset lineage [12].

When immature thymocytes enter the thymic cortex, they are characterised as double negative cells (DNs): they do not express the TCR or the CD4 and CD8 co-receptors [12]. DN thymocytes can be further subdivided into four stages of development based on their surface receptor expression patterns: DN1 cells ($CD44^{+}CD25^{-}$), DN2 cells ($CD44^{+}CD25^{+}$), DN3 cells ($CD44^{-}CD25^{+}$), and DN4 cells ($CD44^{-}CD25^{-}$) [12]. To progress through all four DN stages, T cell progenitors must begin to express a functional variant of the T cell receptor (TCR) (Fig 1.1) [12].

1.2.1 V(D)J recombination

The T cell receptor is composed of two polypeptide chains which together form the antigen-binding domain [13]. The exons for this region are encoded by variable (V), diversity (D), and joining (J) gene segments that can be altered and rearranged prior to TCR expression to increase the diversity of the TCR repertoire [13]. During this process, which is known as V(D)J recombination, lymphoid-specific recombinase enzymes introduce double-stranded breaks at recombination signal sequences flanking the V, D, and J gene segments and then resolve these breaks using nonhomologous end joining (NHEJ) [13]. The number of different V, D, and J gene segments present in the genome allows for a significant yet finite set of rearrangement possibilities, a phenomenon termed combinatorial diversity [14]. However, the process of V(D)J recombination introduces additional variability to the set of potential TCRs: during the repair process, small insertions and deletions will occur at the junctions between segments, greatly increasing the number of potential TCR chain variants [14]. VDJ recombination is therefore essential for generating a diverse TCR repertoire, allowing an estimated 10^{14} - 10^{19} unique receptors to be created from a finite set of initial gene segments [15].

The process of VDJ recombination and TCR expression occurs in parallel with T cell development in the thymus [12]. A nascent variant of the TCR, termed the pre-TCR, is first seen at the DN3 stage, when the fully rearranged TCR β chain associates with a "pre-TCR" (non-rearranged) α chain for expression on the cell surface [12, 16]. Cells capable of initiating T cell signalling through the pre-TCR will then undergo rearrangement at the TCR-α locus [17]. The rearranged α and β chains will pair together to form the mature $\alpha\beta$ TCR, which will eventually replace the pre-TCR on the cell surface [16]. At this stage, expression of the CD4 and CD8 co-receptors also begins, forming a large population of double-positive (DP) thymocytes with fully rearranged TCRs [12]. However, only a small subset of these

DP cells will eventually migrate to the peripheral lymphoid tissues. To select for those cells best suited to the periphery, DPs undergo the processes of positive and negative selection [16].

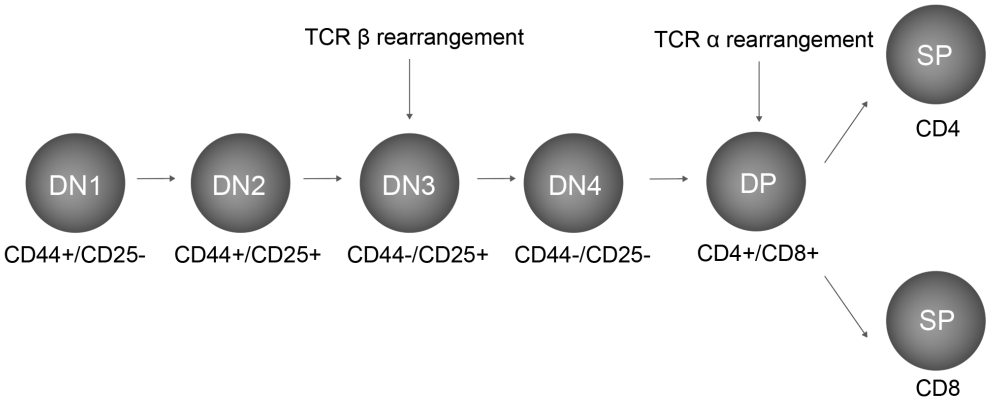

Figure 1.1: Thymocyte development

1.2.2 Positive and negative selection

The TCR is designed to identify short peptide fragments through interactions with specialised peptide-presenting molecules called major histocompatibility complexes (MHCs) [18]. There are two main classes of MHC molecules (I and II), each of which interacts with a different set of T cells (Fig 1.2) [19].

1.2.2.1 MHC class I and II

MHC class I molecules are found on all nucleated cells in the body and are responsible for presenting intracellular protein fragments to $CD8^+$ T cells [20]. MHC class I molecules are heterodimers composed of a polymorphic α chain and a non-polymorphic $\beta 2$ microglobulin [21]. During the process of MHC class I-mediated peptide presentation, molecules inside the cytosol (e.g. viral proteins or tumour antigens) are degraded into short peptides (8-14 amino acids in length) by the intracellular proteasome, loaded onto MHC class I, and transported to the cell surface

to be recognised by $CD8^+$ T cells [20, 22]. These degraded peptides can originate from self-proteins (in the case of healthy cells), or can be fragments of viral proteins or tumour antigens (in the case of infected cells) [20]. $CD8^+$ T cells will interact with these MHC class I-presented peptides, identifying them as either self or non-self [20,23]. When a $CD8^+$ T cell identifies a foreign peptide, it will become activated and can directly kill the infected cell [20, 23].

MHC class II molecules are heterodimers composed of polymorphic α and β chains, both of which contain transmembrane domains [21]. MHC class II molecules are only found on professional antigen-presenting cells (APCs) such as macrophages, dendritic cells, and B cells [20]. These professional APCs use phagocytosis or endocytosis to engulf exogenous antigens from their surroundings (e.g., bacterial toxins and extracellular pathogens) and degrade these molecules in their acidic endosomes [20, 24]. Peptide fragments from these endosomes are then loaded onto MHC class II and transported to the cell surface, where they are presented to $CD4^+$ T cells to initiate an immune response [20, 24].

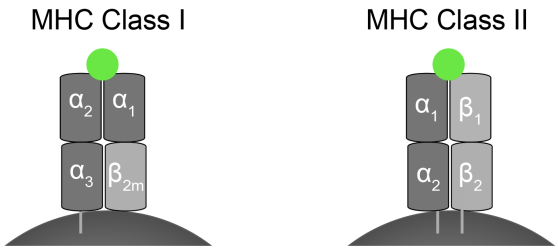

Figure 1.2: MHC molecule structures

1.2.2.2 Thymic selection

MHC presentation is an essential component of T cell maturation in the thymus. For positive and negative selection to occur, double-positive thymocytes must interact with self peptides presented by MHC class I and II molecules (pMHCs) on the surface of epithelial cells in the thymic cortex [25]. Thymocytes with TCRs that

exhibit a high affinity for self-peptide MHC complexes receive signals that trigger apoptosis in a process called negative selection [26]. Thymocytes with TCRs that exhibit a low-to-moderate affinity for self-peptide MHC complexes receive survival signals. These signals indicate to the cell that it has generated a functional TCR capable of recognizing the body's own MHC molecules [26]. The surviving cells will differentiate into mature T cells in a process called positive selection. Around 90% of DP thymocytes will exhibit no affinity for self-peptide MHC complexes [26]. These cells will not receive any essential survival signals and will therefore undergo apoptosis in a process called death by neglect.

The positive selection process also determines T cell lineage, as cells with TCRs that preferentially interact with MHC class I will become $CD8^+$ T cells while cells with TCRs that preferentially interact with MHC class II will become $CD4^+$ T cells [25]. $CD8^+$ T cells will lose their CD4 expression, and $CD4^+$ T cells will lose their CD8 expression, thereby becoming single positive (SP) cells [25].

With the thymic maturation process now complete, these SP T cells are ready for export from the thymus to the peripheral tissues.

1.3 The TCR complex

T cell signalling required for progression through positive and negative selection is mediated by the TCR complex, a group of proteins consisting of the TCR itself, four CD3 chains, and two CD247 (ζ) chains (Fig 1.3) [27].

The TCR itself is a heterodimer composed of two polypeptide chains linked by a disulfide bridge [28]. There are four TCR genes in the human genome encoding the four different polypeptide chains: the TCR α chain, the TCR β chain, the TCR γ chain, and the TCR δ chain [29]. These chains can be paired to create two distinct heterodimers: the $\alpha\beta$ TCR and the $\gamma\delta$ TCR [29]. The vast majority of T cells will

express the $\alpha\beta$ TCR, but a small portion (0.5-5%) express the $\gamma\delta$ variant [30]. $\gamma\delta$ T cells have different functions than the more common $\alpha\beta$ T cells, exhibiting the capacity to recognise non-MHC surface antigens [29].

All TCR chains are composed of an extracellular region for antigen recognition, a transmembrane region, and a short cytoplasmic tail (Fig 1.3) [27]. The extracellular region contains the variable (V) immunoglobulin-like domain responsible for interacting with the pMHC ligand and the constant (C) immunoglobulin-like domain responsible for associating with CD3 proteins on the cell surface through non-covalent hydrophobic interactions. The complete TCR complex consists of the TCR heterodimer, two heterodimers of CD3 proteins (the $\epsilon\delta$ and $\epsilon\gamma$ heterodimers) and the CD3ζ (CD247) homodimer.

[27, 31].

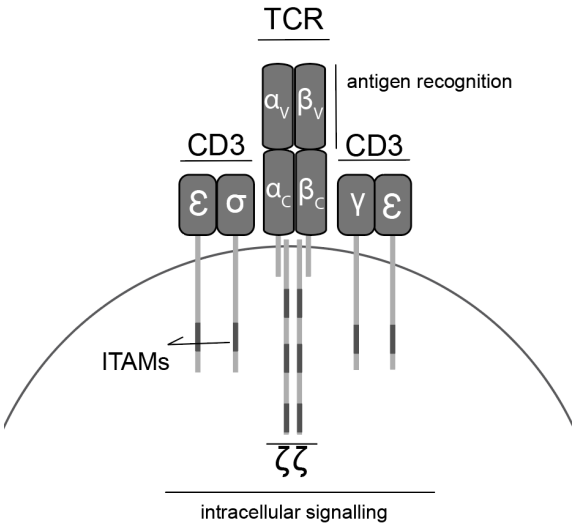

Figure 1.3: Structure of the $\alpha\beta$ TCR.

1.4 TCR signalling

T cell signalling begins when the TCR recognises a specific pMHC ligand and comes into proximity with membrane-anchored lymphocyte-specific protein tyrosine kinase

(Lck), which phosphorylates the immunoreceptor tyrosine-based activation motifs (ITAMs) on the cytoplasmic tails of the CD3 subunits and ζ-chains (Fig 1.4) [32]. These phosphorylated ITAMs serve as high-affinity docking sites for the cytosolic ZAP-70 kinase [33]. ZAP-70 can be phosphorylated both by Lck and by neighbouring ZAP-70 molecules in a process termed trans-autophosphorylation [34]. Activated ZAP-70 coordinates the organisation of a multiprotein signalosome by phosphorylating the transmembrane adapter LAT (linker for activation of T cells), which serves as a scaffold to recruit downstream adaptors and effector molecules such as SLP-76, Grb2, and PLC-γ1 [35]. PLC-γ1 can cleave PIP_2 membrane phospholipids to generate second messengers such as IP_3 and DAG, which then initiate three divergent cascades: the calcium-calcineurin pathway (activating the NFAT transcription factor), the Ras-MAPK pathway (activating the AP-1 transcription factor), and the PKC-θ pathway (activating the NF-κB transcription factor). These transcription factors will help drive gene expression and coordinate T-cell proliferation, differentiation, and effector function.

1.5 TCR triggering

While the intracellular signalling events required to translate TCR/pMHC binding into T cell activation have been well characterised, there remains a considerable amount of controversy regarding the mechanism through which extracellular ligand binding leads to intracellular signalling, also known as the process of TCR triggering [36]. There are three main mechanisms that have been proposed to explain TCR triggering, including aggregation, conformational change, and TCR segregation [36].

1.5.1 The aggregation model

The aggregation model relies on the idea that TCR engagement leads to the clustering of multiple TCR-CD3 complexes together on the plasma membrane [36]. This

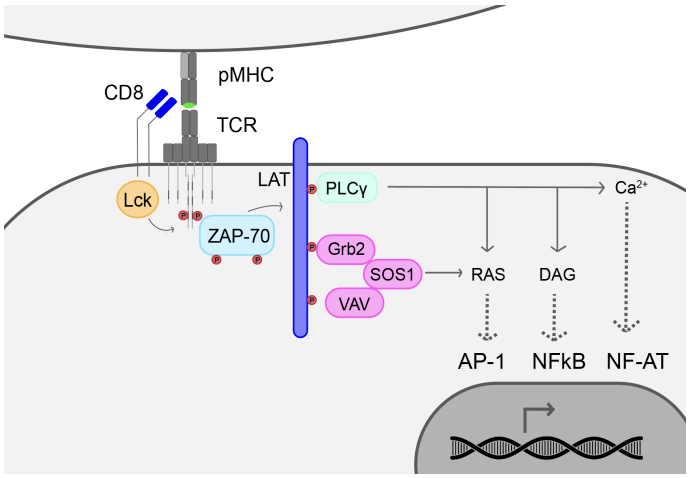

Figure 1.4: TCR signalling. TCR signalling begins when the TCR recognises an antigen presented on an MHC molecule. This triggers an intracellular signalling cascade involving the phosphorylation of ITAMs on CD3 by Lck, which leads to the recruitment and phosphorylation of ZAP-70. Phosphorylated ZAP-70 becomes active and, in turn, phosphorylates transmembrane adapter LAT, which further interacts with downstream effectors, leading to an increase in the activity of the AP-1, NF-κB, and NF-AT transcription factors.

TCR aggregation has the potential to increase the local density of CD3-associated Lck molecules, facilitating the activation of other receptors in the area through trans-phosphorylation [37]. This theory has been tested *in vitro* by studies using soluble antibodies to induce forced aggregation of TCRs, which have shown that artificial TCR aggregation through interactions with trimeric or tetrameric agonist ligands is sufficient to initiate TCR triggering [38].

However, it has been shown that T cell activation can occur in response to even a single pMHC ligand, an antigen surface density that would be far too low to induce effective TCR aggregation [39]. Other aggregation-supporting models, such as the co-receptor heterodimerization model and the pseudodimer model, have attempted to reconcile the extreme sensitivity of the TCR with the idea of TCR-CD3 complex aggregation [36]. The co-receptor heterodimerization model postulates that the CD4 and CD8 co-receptors amplify signalling by recruiting Lck to the TCR/pMHC interface, thereby lowering activation thresholds [40]. However, TCR triggering can

occur even in the absence of co-receptors [41, 42]. The pseudodimer model posits the idea that a single agonist-bound TCR can recruit neighbouring TCRs engaged with self-pMHC complexes to form "pseudodimers", enhancing the local proximity of CD3-associated Lck [43]. Given the high density of self-pMHCs, this model could help explain how T cells can respond to low-density antigens. This model has been supported by studies demonstrating that TCR engagement with self peptide-MHC molecules does, in fact, enhance T cell activation towards agonist peptide-MHC ligands [36, 43, 44].

1.5.2 The conformational change model

In contrast, the conformational change model proposes the idea that TCR engagement induces a conformational change in the TCR itself that can be transduced to the cytoplasm to initiate downstream signalling events [45]. This theory is supported by crystallographic studies of the TCR in both bound and unbound states that indicate the potential for a subtle conformational change in the membrane-proximal AB loop of the constant domain of the TCRα chain which, when mutated, leads to inhibition of TCR triggering [46, 47]. It has been proposed that this AB loop conformational change facilitates TCR clustering [48]. However, the AB loop is often poorly resolved in TCR/pMHC crystal structures, and additional studies with enhanced AB loop resolutions are essential to provide further evidence to support this hypothesis [36].

Other conformational change models have examined the potential for mechanical forces exerted on the TCR-CD3 complex during ligand binding to play a role in TCR triggering [36]. Previous studies have shown that T cells exhibit improved signalling when artificial ligands are anchored to solid surfaces, and the application of mechanical forces to the TCR has the ability to further enhance TCR triggering [49]. Additionally, structural evidence suggests that the CD3$\epsilon\gamma$ heterodimer adopts a rigid conformation that exhibits direct contact with the TCR β chain constant domain,

thereby allowing any force applied to the TCR to be transmitted directly to the CD3$\epsilon\gamma$ heterodimer [50]. The precise mechanism through which these mechanical forces could then be transduced into the cell interior remains unclear, but it has been posited that this process is mediated through the movement of CD3 cytoplasmic tails or through conformational changes in the structure of the TCR-CD3 transmembrane domains; however, further experimentation is required to support these hypotheses [36].

1.5.3 The segregation model

The last model proposed to explain TCR triggering is the TCR segregation model [36]. The TCR-CD3 complex is embedded in the cell surface in dynamic equilibrium with molecules favouring signalling (e.g. Lck) and molecules favouring inhibition (e.g. the CD45 phosphatase) [51, 52]. Studies have shown that treating resting T cells with phosphatase inhibitors leads to an increase in ITAM phosphorylation and ligand-independent T cell activation [53]. Lck itself has been shown to be constitutively active in both resting and active T cells, suggesting that phosphorylation of CD3 ITAMs may involve a balance between kinase and phosphatase activity, and anything which perturbs this balance could influence T cell signalling [54].

There are two prominent models to explain TCR segregation: the kinetic-segregation model and the lipid raft model. The kinetic segregation model relies on the idea that APC/T cell interactions form zones of close contact, interfacing at a distance of around 14-15 nm [55]. Molecules with large extracellular domains (e.g. phosphatases CD45 and CD148) are therefore size-excluded from this zone, shifting the balance in favour of Lck activity and ITAM phosphorylation [55]. This model has been supported through *in vitro* studies showing that CD45 and CD148 are excluded from areas of TCR triggering and that truncation of these molecules or elongation of the pMHC complex is sufficient to prevent TCR triggering [56–59].

The lipid raft model has also been proposed to explain TCR segregation [36]. Lipid rafts support a local environment enriched in Lck and deficient in CD45 [60]. It has been proposed that engagement of the TCR leads to TCR-CD3 lipid raft association, thereby favouring phosphorylation through a local environment rich in Lck [60]. However, some experiments have failed to confirm co-localisation of lipid raft markers with TCR microclusters [61]. There is a need for additional studies to support the lipid raft model of TCR triggering.

Together, the aggregation, conformational change, and segregation models provide evidence for a mechanism of T cell triggering dependent on a delicate balance between tyrosine phosphorylation by constitutively active Lck molecules and dephosphorylation by constitutively active CD45 and CD148 phosphatases. Any mechanism that tilts this balance in favour of phosphorylation can lead to T cell activation, potentially facilitated by TCR-CD3 complex aggregation at sites of close contact and spatial separation of these TCR-CD3 complexes from large phosphatases.

1.6 T cell subsets

There are several types of T cells that can be found in the periphery. These cell types can be characterised by their surface receptor expression and functionality. They can be broadly categorised into two groups: $CD4^+$ "Helper" T cells and $CD8^+$ "Cytotoxic" T cells, although other subsets also exist (e.g. $\gamma\delta$ T cells) [62].

1.6.1 CD4 and CD8 co-receptors

The CD4 and CD8 co-receptors are known to play important roles during thymic development, helping to drive T cell differentiation into $CD4^+$ or $CD8^+$ T cells by determining whether TCRs will bind to MHC class I or class II molecules [63]. However, the role of these co-receptors in T cell activation in the periphery remains under debate. Triggering of the TCR can be induced in the absence of these co-

receptors, but the presence of CD4 and CD8 and their associated Lck molecules can also enhance TCR sensitivity, especially to lower-affinity pMHCs [64, 65].

Structurally, both CD4 and CD8 exhibit extracellular immunoglobulin domains, transmembrane regions, and short cytoplasmic tails that interact with intracellular Lck (Fig 1.5) [66]. CD4 is a monomeric type I transmembrane glycoprotein composed of four extracellular Ig-like domains [66]. In contrast, CD8 is expressed as a dimer, capable of adopting both a homodimeric form (CD8$\alpha\alpha$) and a heterodimeric form (CD8$\alpha\beta$) [66]. Both the α and β CD8 chains contain an extracellular Ig-like domain [66]. CD8$\alpha\alpha$ is commonly found on $\gamma\delta$ TCR T cells and NK cells, whereas CD8$\alpha\beta$ is found on cytotoxic T cells [66]. Despite differences in their extracellular structures, both CD8 and CD4 co-receptors can engage the same MHC molecule as their TCR (e.g. MHC class I and class II molecules for CD8 and CD4 receptors, respectively) [66].

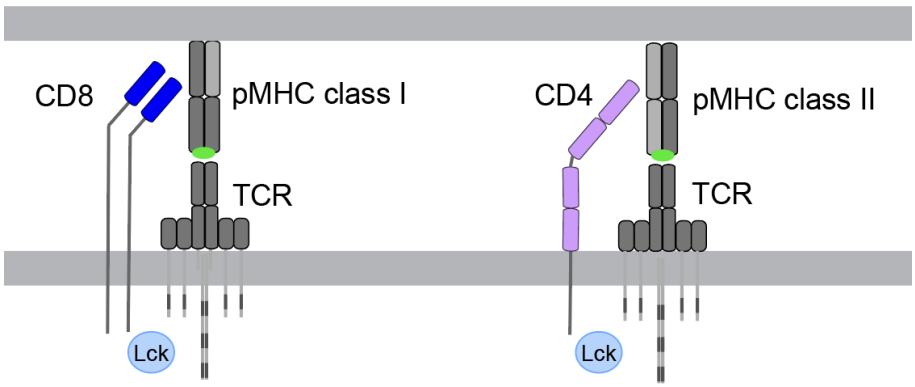

Figure 1.5: Structures of CD8 and CD4

1.6.2 CD4$^+$ T cells

CD4$^+$ T cells are characterised by the cytokines they secrete and can be grouped into several different subsets including Th (T helper) 1 cells, Th2 cells, Th17 cells, Treg (regulatory T) cells, and Tfh (follicular helper) cells [67].

Th1 cells primarily secrete IFN-γ and TNFα [67]. These cells are responsible for coordinating immune responses to intracellular pathogens, including bacterial species and viruses [67]. Th2 cells secrete interleukin (IL)-4, IL-5, and IL-13 and coordinate the immune response against large extracellular pathogens (e.g. parasitic worms) [67]. Th17 cells secrete IL-17 and IL-22 and help protect against extracellular bacteria and fungi by recruiting neutrophils to the site of infection [68]. Th17 cells are also known to play a role in driving chronic inflammation and autoimmune disease [69]. Tfh cells primarily secrete IL-21 and are found in the lymph nodes and spleen, where they promote B cell maturation and antibody production [70, 71]. Treg cells mediate immune suppression through the secretion of anti-inflammatory cytokines IL-10 and transforming growth factor (TGF) β [68].

1.6.3 CD8$^+$ T cells

CD8$^+$ T cells have fewer subset distinctions and are often classified by their differentiation states alone: naive, effector, and memory [72]. CD4$^+$ T cells also have naive, effector, and memory subsets, but are more often classified using the system outlined previously [67].

Following exit from the thymus, naive CD8$^+$ T cells migrate to the periphery where they become activated upon recognition of an antigen [73]. They differentiate into effector CD8$^+$ T cells, which can be further classified as Tc1, Tc2, Tc9, Tc17, and Tc22 cells based on their cytokine secretions [74].

Tc1 cells compose the majority of effector CD8 T cells and mediate T cell cytotoxicity through the production of perforin, granzyme B, IFN-γ, and TNF-α, which they release to destroy infected cells and tumour cells [74, 75]. Tc2 cells are primarily found in intraepithelial tissues and are known to produce Th2-type cytokines including IL-4, IL-5, and IL-13 [74, 75]. These cells are thought to play a role in autoimmune responses (e.g. allergic asthma and contact dermatitis) [76, 77]. Tc9

cells produce IL-9 and, like Tc2 cells, are involved in allergic responses, although Tc9 cells are also commonly found in tumour tissues and may help mediate anti-tumour activity [78, 79]. Tc17 cells produce IL-17 and can help attract neutrophils to sites of infection or inflammation [80]. Tc22 cells secrete IL-22, and while their exact function is under debate, they are thought to exhibit anti-tumour activity [81].

$CD8^+$ T cells are also capable of exerting regulatory function through a specialised subset of cells termed suppressive $CD8^+$ Tregs [82]. These cells help to maintain immune homeostasis and prevent autoimmunity through the secretion of immunosuppressive cytokines such as IL-10 [83].

1.6.4 Memory T cells

Following antigen clearance, a fraction of CD8 and CD4 T cells will differentiate into memory T cells [84]. These cells have the ability to immediately proliferate if re-exposed to a previously encountered antigen, facilitating the unique property of immune memory that is characteristic of the adaptive immune system [84]. Memory T cells can be subdivided into central memory (T_{CM}), effector memory (T_{EM}), and tissue-resident memory (T_{RM}) cells [84]. T_{CM} cells patrol the lymph nodes while T_{EM} cells circulate through the blood and T_{RM} cells remain inside tissues [85, 86].

1.6.5 $\gamma\delta$ T cells

$\gamma\delta$ T cells expressing the $\gamma\delta$ variant of the TCR compose between 0.5 and 5% of all T cells and can primarily be found in the epithelial tissues of the gut, lungs, and skin [87, 88]. These unique cells can interact with antigens even without MHC presentation, allowing them to detect both exogenous and endogenous pathogens, and they do not require co-stimulation [88,89]. $\gamma\delta$ T cells produce IFN-γ and IL-17 in response to antigen and can release perforin and granzyme to directly kill target cells that have been marked with antibodies through a process called antigen-dependent

Table 1.1: Major T cell subsets and their defining characteristics

Category	Subset	Primary Function
$CD4^+$ T cells	Th1	Intracellular pathogen defence (IFN-γ)
	Th2	Helminth immunity, allergy (IL-4, IL-5, IL-13)
	Th17	Bacteria and fungi defence (IL-17)
	Tfh	B cell help in germinal centres (IL-21)
	Treg	Immune suppression and tolerance (IL-10)
$CD8^+$ T cells	Tc1	Direct killing of infected or tumour cells
	Tc2	Produce Th2-type cytokines (IL-4, IL-5, IL-13)
	Tc9	Produce IL-9, involved in autoimmunity
	Tc17	Produce IL-17, recruit neutrophils
	Tc22	Produce IL-22, involved in tumour infiltration
	Treg	Maintain immune homeostasis
Memory T cells	T_{CM}	Commonly found in lymph nodes
	T_{EM}	Circulate through the blood
	T_{RM}	Reside within tissues and organs

cellular cytotoxicity (ADCC) [90–93].

1.7 Functional outcomes of T cell activation

TCR engagement and subsequent intracellular signalling cascades can trigger a range of different effector responses necessary to eliminate pathogens and provide anti-tumour immunity [94, 95].

1.7.1 Cytokine production

T cell activation often results in the secretion of molecules called cytokines that can act as autocrine and paracrine chemical messengers to regulate immunity, inflammation, and proliferation [96, 97]. Different cytokines have different roles in regulating immune responses.

1.7.1.1 IL-2

Interleukin-2 (IL-2) is a key cytokine involved in T cell expansion, survival, and differentiation [98, 99]. Activated $CD4^+$ T cells are the primary producers of IL-2, but several other cell types including dendritic cells and $CD8^+$ T cells can also secrete this cytokine [100, 101].

IL-2 interacts with high and intermediate affinity receptor variants [102–104]. The high-affinity receptor is constitutively expressed on Treg cells, with inducible expression on effector T cells and memory T cells [105].

IL-2 can promote cell killing by stimulating $CD8^+$ T cells to produce effector molecules, such as granzyme and perforin, and cytokines such as IFN-γ [106, 107]. IL-2 signalling can also influence the balance of effector and memory T cells in the periphery [108]. High IL-2 signalling prompts T cells to differentiate into effector cells while low IL-2 signalling supports differentiation into memory T cell phenotypes [109].

1.7.1.2 IFN-γ

IFN-γ is a type II interferon molecule secreted by $CD4^+$ Th1 cells, $CD8^+$ cytotoxic T cells, and NK cells [110]. IFN-γ functions in both an autocrine and paracrine manner, supporting self-activation as well as activation of nearby cells [111].

IFN-γ interacts with the IFN-γ receptor and facilitates intracellular signalling through the JAK/STAT pathway [112]. In macrophages, IFN-γ signalling leads to increased phagocytosis and production of reactive oxygen species and nitric oxide [113, 114]. In T cells, IFN-γ signalling drives $CD4^+$ T cells to differentiate into Th1 cells [115]. In non-hematopoietic cells such as epithelial and stromal cells, IFN-γ signalling leads to an increase in MHC class I expression, improving the chances that infected cells will be recognized by effector T cells [116].

1.7.2 Cell-mediated killing

Cytotoxic $CD8^+$ T lymphocytes (CTLs) are capable of directly killing target cells [117]. They can exert their cytotoxic potential through the release of specialised molecules capable of compromising the membrane integrity of target cells and through direct cell-cell contact [117].

Binding of the TCR to a foreign peptide on MHC class I triggers the release of cytotoxic granules containing perforin and granzyme from the cytosol of a CTL [118]. Perforin molecules will assemble on the target cell membrane and form small channels or "pores" through which granzymes may enter [119]. Granzymes are a family of serine proteases that activate caspase enzymes within the target cell, triggering apoptotic signalling pathways that eventually lead to cell death [120].

CTLs also induce apoptosis through direct cell-cell contacts through ligation of the Fas receptor, present on target cells, with the Fas ligand (Fas L) on cytotoxic T cells [121]. Cross-linking of Fas triggers the activity of intracellular caspases, leading to apoptosis [122]. This process can be enhanced by the activity of surrounding cytokines, including IL-2, which signals T cells to increase the surface expression of Fas ligand [121].

1.7.3 Surface expression of activation markers

T cell activation also leads to changes in the expression of surface receptors including CD69 (a type II C-lectin receptor) and 4-1BB/CD137 (a glycosylated type I membrane protein and member of the tumour necrosis factor receptor superfamily) [123, 124].

CD69 is a marker of early T cell activation, with transcriptional expression detectable 30 min to an hour after stimulation and surface protein expression detectable 2-3 hrs after stimulation [123, 125]. CD69 interacts in *cis* with the sphingo-

sine 1-phosphate receptor 1 (S1P1) protein and the amino acid transporter complex LAT1-CD98 [126, 127].

4-1BB also serves as a marker of T cell activation and can be detected on the cell surface within 24 hours of stimulation [124, 128]. 4-1BB can function as a co-stimulatory molecule through *trans* interactions with its ligand, 4-1BBL [129].

1.8 Accessory Receptors

For productive T cell signalling to occur, the relatively weak and transient TCR/pMHC ligand interaction must be translated into a sustained cascade of biochemical reactions that lead to a robust T cell response [130, 131]. This process of T cell activation must also exhibit an extraordinarily high specificity, balancing sensitivity to foreign ligands with discrimination against self-antigen [132]. This equilibrium is facilitated by co-receptors and accessory molecules that modulate intracellular signalling thresholds [133].

1.8.1 CD28

Signals initiated by the TCR-CD3 complex can be amplified by the engagement of the CD28 T cell surface receptor, a homodimeric glycoprotein found on the majority of human T cells [134, 135]. CD28 engagement with cognate ligands CD80 and CD86 facilitates the recruitment and activation of phosphoinositide 3-kinase (PI3K) which can stimulate transcriptional changes through the action of NF-κB, NFAT, and AP1 [136]. CD28 signalling cascades result in the modulation of multiple T cell processes including survival, proliferation and the production of cytokines IL-2 and IFN-γ [136].

While the intracellular signalling pathways involved in CD28 signalling have been well-characterised, the exact mechanism of CD28 signal transduction remains un-

known [137]. It has been proposed that CD28 triggering follows a mechanism similar to that of the TCR, specifically via the kinetic segregation model [137]. In support of this hypothesis, experimental evidence has indicated that elongation of the CD28/CD80 complex markedly reduces its co-stimulatory effect and impairs segregation of CD80 away from CD45 at the T cell-APC interface [137].

1.8.2 CD2

Both T cells and antigen-presenting cells are known to express a dense network of negatively charged carbohydrates and glycoproteins termed the glycocalyx, which can extend up to hundreds of nanometers out from the cell surface [138]. Because the TCR/pMHC complex spans a short distance of 15 nm, these large glycocalyx molecules can sterically hinder the TCR and prevent the formation and stabilisation of the regions of close-contact between T cells and target cells required for sustained T cell signalling [138].

Close contacts can be stabilised by the activity of CD2, a monomeric transmembrane protein that can act as an adhesion receptor through interactions with its cognate ligand, CD58, although it has also been shown to bind to a second ligand, CD48, albeit with lower affinity [139, 140]. The CD2/CD58 interaction is thought to hold the T cell and the target cell together at an optimal distance for TCR/pMHC engagement [141].

CD2 has two extracellular Ig-like domains (one V-like and one C-like) and a long, proline-rich cytoplasmic tail [141, 142]. CD2 is expressed on almost all mature peripheral T cells, and its CD58 ligand is also highly expressed on nearly all cells in the body [139, 143].

The CD2/CD58 interaction is of low affinity (9-22 μM), but because both CD2 and CD58 are present on the cell surface at high densities, multiple CD2/CD58 binding interactions can occur inside one region of close contact, allowing the collective effect

of multiple interactions to provide stable cell-cell adhesion despite the low affinity of each individual interaction [144]. By holding the T cell and target cell together at an optimal distance for TCR engagement, these CD2/CD58 interactions give the TCR a longer interval of time to scan and recognise potential pMHCs, greatly enhancing T cell sensitivity to low-density antigens [145, 146]. CD2/CD58 binding interactions have been shown to enhance TCR recognition of pMHC in the context of cancer, and the CD58/CD2 axis has been proposed as the primary co-stimulatory pathway for CD8 T cells that lack CD28 [2, 147]. However, despite the significant impact of CD2 on T cell antigen sensitivity, CD2 knockout mice exhibit no defects in either T cell development or the immune response, suggesting redundancy in adhesion receptors [139, 148].

As with CD28, the size of the CD2 receptor/ligand complex has been shown to influence its activity [2]. Elongations of the CD2 receptor were found to decrease T cell antigen sensitivity, supporting the hypothesis that T cell antigen recognition requires size-dependent spatial segregation of cell surface molecules [2].

1.8.3 PD-1

Although both the CD28 and CD2 receptors facilitate activation, T cells also express a variety of inhibitory molecules [133]. Programmed cell death protein-1 (PD-1) is a type I transmembrane receptor that can act as a brake for the immune system, inhibiting T cell proliferation, cytokine release, and cytotoxicity [149]. Upon engagement with its ligand, PD-L1, the intracellular tail of the PD-1 receptor becomes phosphorylated, allowing it to interact with the SH2 (Src homology 2) domains of intracellular phosphatase proteins SHP1 and SHP2 (SH2-containing phosphatases 1 and 2), initiating the process of T cell inactivation through downregulation of the TCR phosphorylation cascade [150].

The mechanism through which this occurs is not completely understood, but recent

studies have suggested that the inhibitory effect of PD-1 involves the dephosphorylation of the cytoplasmic tail of CD28 through the action of PD-1-recruited SHP2 [151]. However, PD-1 engagement has also been shown to inhibit CD2-mediated T cell activation, even though the CD2 receptor does not contain any cytoplasmic tail tyrosines on which SHP2 can act [1]. This data has been used to propose a model of promiscuous PD-1-mediated inhibition through the involvement of PD-1 recruited phosphatases in many different tyrosine phosphorylation-dependent signalling cascades.

As with CD2 and CD28, the extracellular size of the PD-1/PD-L1 complex can impact its effector function. Elongation of the PD-1 receptor leads to a marked decrease in its ability to inhibit T cell activation, again suggesting that the size of these accessory receptor/ligand complexes is in some way integral to their function [2].

1.8.4 SLAM

While some accessory receptors have well-characterised roles as activators (e.g. CD2) or inhibitors (e.g. PD-1), others exhibit more modular activity, capable of both promoting and suppressing the T cell response [133]. The signalling lymphocytic activation molecule (SLAM) family of receptors exemplifies this modularity [152]. SLAM receptors are type I transmembrane proteins with intracellular immunoreceptor tyrosine-based switch motifs (ITSMs) [152]. Upon phosphorylation, these ITSM regions are capable of recruiting adaptor proteins such as SAP (SLAM-associated protein) or inhibitory phosphatases including SHP-1, SHP-2, and SHIP [152]. SAP binding facilitates the recruitment of Src-family kinases including Fyn, which promotes downstream signalling cascades that can enhance T cell activation and cytokine production [153]. In contrast, in the absence of SAP, ITSMs recruit inhibitory phosphatases SHP-1, SHP-2, and SHIP, which act to reduce proximal TCR signalling [154].

1.8.5 Additional accessory molecules

The accessory receptors highlighted above represent only a subset of the multiplicity of surface molecules involved in the complex process of T cell activation. The complete repertoire of T cell co-signalling molecules spans multiple protein families, and these molecules exhibit considerable diversity in their expression patterns, structures, and functions [133].

1.9 Immune-based therapies

The emergence of novel immunotherapies for various malignancies has greatly increased the clinical importance of understanding T cell activity and accessory receptor function [155]. Immunotherapeutic approaches such as adoptive cell transfer (where a patient's own T cells are removed, modified, and re-transfused into the body) and immune checkpoint inhibitor therapy (where inhibitory signals such as the PD-1/PD-L1 axis are blocked by soluble antibodies) have proven efficacy across multiple cancer types [156, 157].

However, these treatments are not universally effective, and understanding the role of accessory receptors in mediating the complex process of antigen recognition and TCR triggering is essential for the development of novel treatment options with enhanced efficacy and minimal off-target effects [156, 157].

1.10 This thesis

This thesis aims to understand the contributions of accessory receptors to T cell activation mediated by both the native TCR and by synthetic CARs. This work is enabled by the recently developed platform for the combinatorial display and titration of cell surface proteins ("CombiCells").

In Chapter 2, we will use CombiCells to explore the role of SLAM family receptors in T cell activation. In Chapter 3, we will use CombiCells to study the contributions of CD2 and PD-1 to CAR-T cell activation. In Chapter 4, we will investigate the limitations of CombiCells and develop ways to improve this platform for cell surface ligand display. The results of this thesis highlight the essential role of accessory receptors in fine-tuning T cell activation by identifying novel candidates within the SLAM family for immunotherapeutic investigation and highlighting the importance of receptor/ligand complex size while supporting the use of the CombiCell system in future T cell activation studies.

2 | The role of SLAM-family co-signalling receptors in T cell antigen recognition

2.0.1 Introduction

T cells exhibit a remarkable ability to respond to extremely low levels of antigen, with studies demonstrating that activation can occur in response to even a single peptide-major histocompatibility complex (pMHC) [158]. This property, known as antigen sensitivity, allows T cells to recognise infected or cancerous cells with high efficiency and is fundamental to effective adaptive immune surveillance [159]. However, this high sensitivity is difficult to reconcile with the intrinsic properties of the T cell receptor (TCR), which binds pMHC with relatively low affinity and rapid dissociation kinetics [160].

As outlined in the introduction, T cells are able to translate weak and transient TCR/pMHC interactions into robust T cell responses while maintaining discrimination towards self-antigens by exploiting a host of additional surface molecules, including proteins such as the CD2 adhesion receptor [133]. CD2 physically stabilises cell-cell interfaces at a distance of around 14 nm, sterically excluding large inhibitory phosphatases from the close contact zone while increasing TCR/pMHC interaction times [139].

CD2 engagement can dramatically lower the concentration of antigen required to trigger T cell activation, in some cases increasing T cell sensitivity by greater than 100-fold [161]. The structurally-related signalling lymphocyte activation molecule (SLAM) family of receptors has also broadly been shown to influence immune responses, playing a role in T cell survival, autoimmunity, and cytotoxicity, although the precise role of these proteins in the complex process of T cell activation remains poorly understood [162].

SLAM receptors are predominantly expressed on haematopoietic cells, including T cells, B cells, natural killer (NK) cells, and antigen-presenting cells [162, 163]. This family consists of nine receptors (SLAMF1-SLAMF9) with a multiplicity of more frequently utilized common names (Table 2.1) [163].

Structurally, SLAM family receptors are type I transmembrane proteins typically characterized by two extracellular immunoglobulin-like domains (except in the case of Ly9, which exhibits four extracellular immunoglobulin-like domains) and a cytoplasmic tail containing conserved signalling motifs [163]. The SLAM family is unique in its ability to transmit both activating and inhibitory signals depending on the availability of intracellular adaptor molecules, allowing SLAM receptors to act as versatile regulators of immune cell activation [153, 163].

Table 2.1: SLAM family naming conventions, structures, and expression patterns.

Common Name	**SLAM Name**	**Structure**	**Expression**
CD150	SLAMF1	V-C2-TM-Y	Mp, DC, B*, T*
CD48	SLAMF2	V-C2-GPI	Mp, DC, B, T, NK
CD229 / Ly9	SLAMF3	V-C2-V-C2-TM-Y	Mp, DC, B, T*
2B4 / CD244	SLAMF4	V-C2-TM-Y	Mp, DC, T, NK
CD84	SLAMF5	V-C2-TM-Y	Mp, DC, B, T, NK
NTB-A	SLAMF6	V-C2-TM-Y	Mp, DC, B, T, NK
CRACC	SLAMF7	V-C2-TM-Y	Mp, DC, B, T*, NK
BLAME	SLAMF8	V-C2-TM	Mp, DC
CD2F-10	SLAMF9	V-C2-TM	Mp, DC, NK

Structure key: immunoglobulin variable domain (V); immunoglobulin constant domain (C2); transmembrane domain (TM); cytoplasmic tyrosine signalling motifs (Y); glycosylphosphatidylinositol anchor (GPI).
Expression key: macrophage (Mp); dendritic cell (DC); B cell (B); T cell (T); natural killer cell (NK). * Indicates expression is upregulated upon activation.
Note: Expression profiles of SLAM-family receptors are subject to literature discordance, with reported expression on lymphocyte subsets often differing across independent studies.

A defining feature of SLAM family receptors is the presence of immunoreceptor tyrosine-based switch motifs (ITSMs) within their cytoplasmic domains [163]. ITSMs are short amino acid sequences typically defined by the consensus motif TxYxxV/I/L, which becomes phosphorylated at the tyrosine residue following SLAM receptor

engagement [153]. When phosphorylated, ITSMs serve as docking sites for SH2 domain-containing adaptor proteins including SLAM-associated protein (SAP) and EWS-FLI1-activated transcript 2 (EAT-2) (Fig 2.1) [153,163]. SAP is a small adaptor protein composed of a single SH2 domain, which binds phosphorylated ITSMs and facilitates the recruitment of Src family kinases including Fyn [153]. This interaction promotes downstream signalling cascades that can enhance T cell activation and cytokine production [153]. In contrast, in the absence of SAP, ITSMs can recruit inhibitory phosphatases SHP-1, SHP-2, and SHIP, resulting in attenuation of signalling (Fig 2.1) [164]. Phosphorylated ITSMs can also recruit EAT-2, which is highly expressed in NK cells [164]. EAT-2 can mediate downstream signalling independently of SAP by recruiting SH2 domain-containing molecules such as PLCγ, Vav1, and SLP-76 (Fig 2.1).

This dual capacity to recruit both activating and inhibitory effector molecules allows SLAM family receptors to function as molecular "switches" to fine-tune immune responses [153]. This phenomenon has been exemplified in the clinic through studies on individuals affected by X-linked lymphoproliferative disease (XLP), a condition involving mutations in SAP that lead to defects in T cell and NK cell function [165]. T cells from XLP patients exhibit enhanced PLCγ activity and increased calcium release (EAT-2 mediated pathways) but decreased VAV phosphorylation and poor IL-2 production (SAP-mediated pathways) [165]. Notably, reintroduction of SAP is sufficient to restore normal signalling [165].

In addition to their intracellular signalling properties, SLAM family receptors exhibit distinctive modes of ligand engagement through their extracellular Ig-like domains. Most SLAM receptors engage in homophilic interactions, whereby identical receptors on opposing cells interact through their membrane-distal IgV domains with low to moderate affinity [166]. However, 2B4 is unique within the SLAM family in that it binds heterophilically to CD48, a glycosylphosphatidylinositol (GPI)-anchored protein highly expressed on multiple haematopoietic cell types [167]. The 2B4/CD48

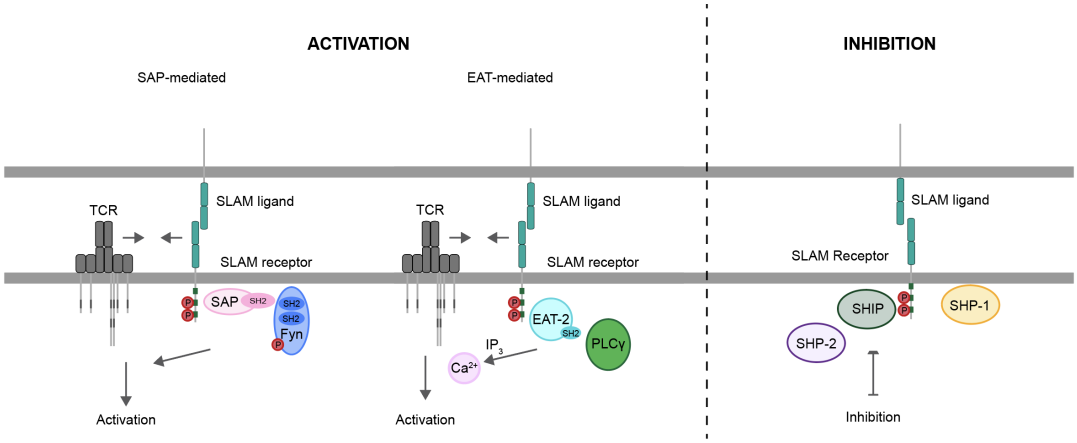

Figure 2.1: SLAM family signalling SLAM family receptors can mediate both activation (left) and inhibition (right) depending on the availability of intracellular adaptor proteins. In the presence of SAP (SLAM-associated protein), SLAM receptor engagement and subsequent phosphorylation of SLAM immunoreceptor tyrosine-based switch motifs (ITSMs) will lead to SAP recruitment, which promotes an interaction between SAP and Src family kinase Fyn. This interaction facilitates activation of Fyn, which will then promote phosphorylation of downstream signalling molecules such as guanine nucleotide exchange factor Vav1, thereby enhancing activation pathways. When EAT-2 is present, as in NK cells, SLAM receptor engagement induces EAT-2 recruitment, which promotes activation of phospholipase PLCγ. This activation contributes to intracellular calcium flux and activation of the ERK pathway. When SAP and EAT-2 are present, their interactions with SLAM family receptors block association of inhibitory phosphatases SHP-1, SHP-2, and SHIP. However, when SAP and EAT-2 are absent, phosphorylated ITSMs will serve as docking sites for SHIP, SHP-1, and SHP-2. These phosphatases will attenuate signalling by dephosphorylating key intermediates in the T cell receptor (TCR) pathway, thereby dampening or terminating TCR-mediated activation.

interaction has been reported to exhibit higher affinity than many homophilic SLAM interactions, and its functional outcome is strongly dependent on the availability of SAP [167].

The SLAM family has emerged as an area of interest in the field of immunotherapy and cancer research. *In vitro* studies have shown that CD3-activated T-cells transfected with SLAMF1 (CD150) exhibit increased cytotoxic activity and IFNγ production in response to human colon cancer cells [168]. Additionally, colorectal cancer patients with high CD150 expression on their tumour-specific innate lymphoid cells exhibited improved survival rates compared to those with low CD150 expression, suggesting that CD150 may serve as a marker of improved anti-tumour activity [169]. In contrast, SLAMF7 (CRACC) is enriched in multiple cancer types including breast cancer and multiple myeloma [170, 171]. Clinical treatments combining the CRACC-targeting monoclonal antibody elotuzumab with lenalidomide and dexamethasone have led to significant improvements in patient survival compared to a lenalidomide/dexamethasone alone treatment control group [171]. These findings highlight the therapeutic potential of SLAM family receptors but also underscore the complexity of their signalling behaviour.

The development of novel SLAM family immunotherapeutics is also complicated by the significant evolutionary divergence in SLAM family function between human and murine models. Although the SLAM gene cluster on Chromosome 1 is conserved between the two species, the functional roles of individual SLAM family members differ markedly [172].

Humans utilize CD58 as the primary ligand for CD2, whereas mice lack CD58 expression and instead use CD48 for CD2 engagement; by contrast, human CD48 serves as the ligand for human 2B4 [173]. Mice also possess an additional intracellular adaptor protein, ERT, which interacts with the ITSMs on the cytoplasmic tails of SLAM receptors; in humans, the SH2D1W (ERT) gene is a non-functional pseudogene [174].

Functional studies using anti-CD150 antibodies further highlight these interspecies differences [175]. In pre-activated human T cells, CD150 engagement can induce proliferation and cytokine production in the absence of TCR re-stimulation, whereas in mice, these T-cell responses require concurrent TCR/pMHC binding [175]. These genomic and functional disparities suggest that human T-cell sensitivities cannot be perfectly modelled in murine systems, necessitating high-fidelity human *in vitro* platforms for the quantitative study of SLAM proteins.

2.0.2 SLAM receptors and the CombiCell system

T cell receptor/ligand interactions have historically been studied using diverse antigen presentation platforms, including genetically modified APCs, solid-phase surfaces, and supported lipid bilayers (SLBs) [176]. While powerful, these systems often face a trade-off between their physiological relevance and their experimental flexibility: cell-based models can require labour-intensive genetic modifications, solid-phase platforms lack biologically-relevant surface stiffness and ligand diffusion, and SLBs are often low throughput and lack the cytoskeletal dynamics of live cells [57,176–178].

To address these limitations, the CombiCell system has emerged as a unique antigen presentation platform that allows for the rapid generation of "designer" APCs [1]. This system bypasses the need for traditional knockouts or viral transductions by leveraging the SpyCatcher/SpyTag binding system, enabling researchers to engineer a standardized cell surface capable of presenting any desired concentration or combination of ligands within minutes (Fig 2.2) [179]. The CombiCell system has been previously utilized to investigate the role of CD2, CD28, and PD-1 in modulating T cell sensitivity [1, 2].

Given that an investigation into SLAM-family function requires the interrogation of multiple distinct receptor/ligand pairs, any systematic study of SLAM-mediated T-cell sensitivity requires a high-throughput and easily tunable antigen presentation

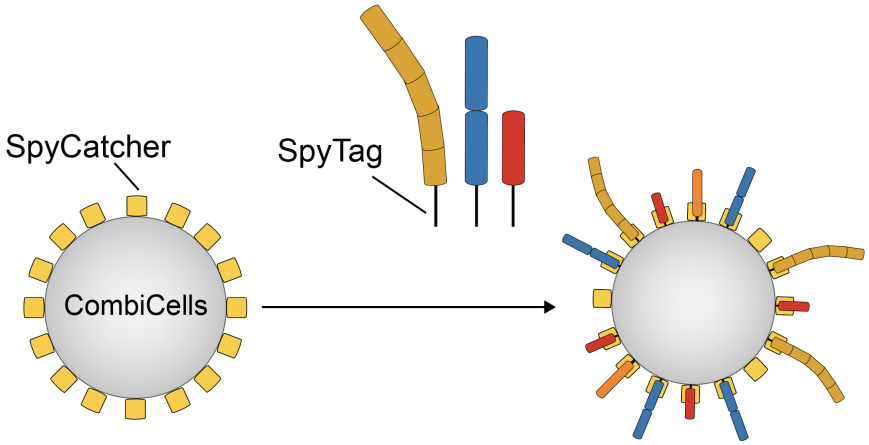

Figure 2.2: Using CombiCells as an artificial antigen presentation platform. Base cell lines engineered to express surface SpyCatcher can form covalent bonds with SpyTagged (ST) proteins to create artificial antigen-presenting cells.

platform. The CombiCell system is uniquely suited for this task; it allows for the precise titration of both SLAM ligands and pMHC, facilitating quantitative mapping of the impact of SLAM engagement on T cell sensitivity.

2.0.3 This chapter

Accessory receptors have been shown to play key roles in the modulation of T cell activation thresholds and have been utilised to develop effective immunotherapy treatments; it is therefore of clinical interest to identify any and all receptor families that may similarly contribute to T cell antigen sensitivity. While the SLAM family has been extensively studied at the molecular level in both humans and mice, and while this work has highlighted their important immune function and led to the development of novel immunotherapeutics, we still do not have an understanding of how these receptors might impact quantitative recognition of antigen, including measures such as antigen sensitivity [180].

In this chapter, we examine the impact of SLAM receptor engagement on T cell activation in both primary human $CD8^+$ T cells and immortalized human Jurkat T

cells. To precisely quantify antigen sensitivities in the presence and absence of SLAM engagement, we employ the novel CombiCell platform, which allows us to maintain precise control over our antigen and accessory ligand densities. Our experimental results suggest that although all SLAM-family receptors are capable of interacting with their cognate ligands within the context of the CombiCell platform, only CD150 and 2B4 receptor engagement leads to phenotypic changes.

2.1 Results

2.1.1 Developing a platform to assess T cell sensitivity to SLAM ligands using CombiCells

To determine whether the presence of SLAM ligands could quantitatively impact T cell sensitivities, we needed to optimise the CombiCell platform for our experimental requirements. This first necessitated the generation of SpyTagged SLAM proteins capable of interacting with SLAM receptors on our effector T cells. In order to maintain assay integrity and limit experimental overload, we utilised only a subset of the nine SLAM family members (Fig 2.3). We excluded the SLAMF8/BLAME and SLAMF9/CD2F-10 receptors, which lack intracellular ITSM regions and are therefore less likely to facilitate changes in intracellular signalling cascades [153]. We also excluded the NTB-A/SLAMF6 receptor due to cloning complications, although additional studies on the role of NTB-A in modulating T cell sensitivity are encouraged.

To create SpyTagged (ST) SLAM ligands for our CombiCell system, we fused the extracellular regions of SLAM proteins CD150, CD48, CD229/Ly9, CD84, and CRACC to a SpyTag (RGVPHIVMVDAYKRYK). To validate these proteins as functional and to ensure effective SpyTag/SpyCatcher coupling, we loaded our SpyTagged proteins onto CombiCells derived from Chinese Hamster Ovary (CHO) cells

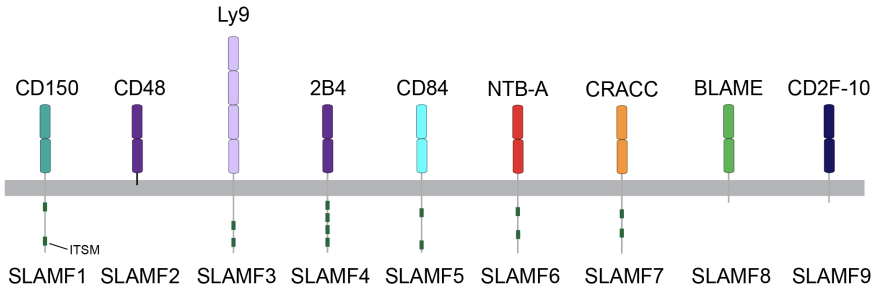

Figure 2.3: SLAM family proteins. Members of the SLAM family with intracellular ITSM regions shown in green. All SLAM family members are type I transmembrane proteins, except CD48/SLAMF2, which is GPI-anchored. SLAM family members CD150, CD48, Ly9, 2B4, CD84, and CRACC will be used in this study.

and used monoclonal antibodies to verify SLAM ligand presentation (Fig 2.4). Our CHO CombiCells had previously been engineered with a CRISPR/Cas9 ICAM-1 KO and transduced with surface SpyCatcher [1].

2.1.2 SLAM ligands have no impact on Jurkat T cell sensitivity

Following validation of the folding and surface presentation of SpyTagged SLAM ligands, we performed an initial screening assay to determine whether SLAM ligand presence could impact T cell sensitivity. For these studies, we utilised Jurkat T cells, an immortalised human T lymphocyte model commonly used to investigate TCR signalling [181]. This cell line has previously been used to study the co-stimulatory functions of several accessory receptors, including CD2, CD28, and SLAM receptors Ly9, NTB-A, and 2B4, making it an ideal model system in which to begin our studies [182–184]. Our Jurkat T cells had previously been transduced to express CD8, CD2, and the model 1G4 TCR [1]. This well-characterized TCR specifically recognises cancer-testes antigen NY-ESO-1 (SLLMWITQC), a 9-mer peptide presented on HLA-A*02:01 [185]. To increase the peptide affinity for MHC, we utilised an NY-ESO-1 variant (SLLMWITQV) with a cysteine to valine substitution in position 9,

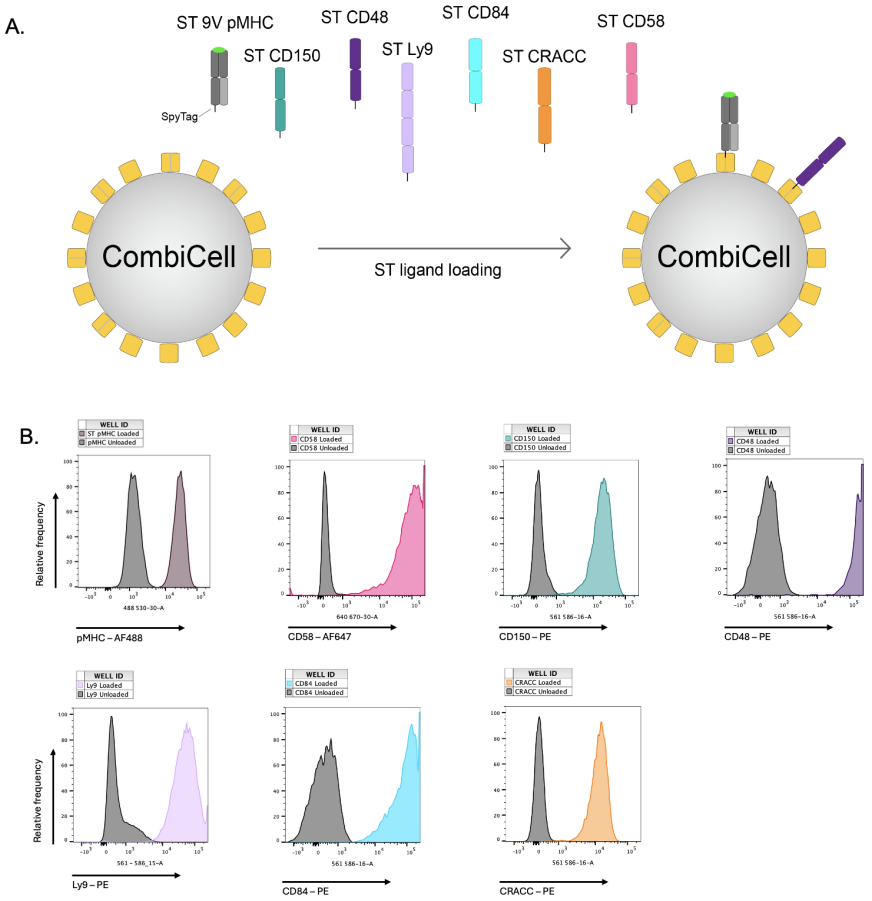

Figure 2.4: Validation of ligand loading on CHO CombiCells. **(A)** Schematic showing loading of SpyTagged ligands (pMHC, CD150, CD48, CD84, CRACC, and CD58) onto Chinese Hamster Ovary (CHO)-based CombiCells expressing surface SpyCatcher (yellow). SpyTagged ligands were added to CombiCells in 60 μL DMEM and incubated for 40 minutes for ligand loading to occur. **(B)** Representative flow cytometry histograms showing loading of each SpyTagged protein. To generate this data, loaded CombiCells were incubated with fluorescently tagged monoclonal antibodies (targeting the functional distal V-domains in the case of SpyTagged SLAM targets) with unloaded controls shown in black.

termed the "9V" NY-ESO-1 variant [186]. The 9V peptide was refolded with the MHC β2m and heavy chain fused to SpyTag, which together composed the trimeric SpyTagged pMHC complex, which could then be titrated on CombiCells for TCR recognition [1].

To assess the impact of SLAM ligand presentation on Jurkat T cell sensitivity, we performed standard CombiCell antigen sensitivity assays using titrations of either antigen alone or antigen alongside a high concentrations of SLAM ligand (CD150, CD48, Ly9, CD84, or CRACC), using the validated co-stimulatory ligand CD58 as a positive control (Fig 2.5 A). Following co-culture, we performed flow cytometry analysis of our T cells to determine the surface expression of activation marker CD69 at each tested pMHC concentration (Fig 2.5 B). This data was then used to generate dose-response curves, with the percentage of CD69-positive T cells used as a measure of percent activation (Fig 2.6 A). For further analysis, we fit these dose-response curves with a Hill function, which we used to extract EC50 values. EC50 values represent the concentration of a compound required to produce a 50% maximal response; in our studies, EC50 values indicated the antigen concentration required for 50% T cell activation (Fig 2.6 B).

We found that the presence of SLAM ligands CD150, CD48, Ly9, CD84, and CRACC had no impact on T cell sensitivity (Fig 2.6). In contrast, addition of known co-stimulatory ligand CD58 led to a 10-fold increase in T cell sensitivity (Fig 2.6).

2.1.3 Overexpression of SLAM receptor 2B4 leads to increased sensitivity in the presence of SLAM ligand CD48

Given the lack of any SLAM-ligand-mediated phenotype in our initial experiments, we decided to assess our Jurkat T cells for endogenous SLAM receptor expression. We found little-to-no surface expression for CRACC, CD150, or 2B4 (Fig 2.7). How-

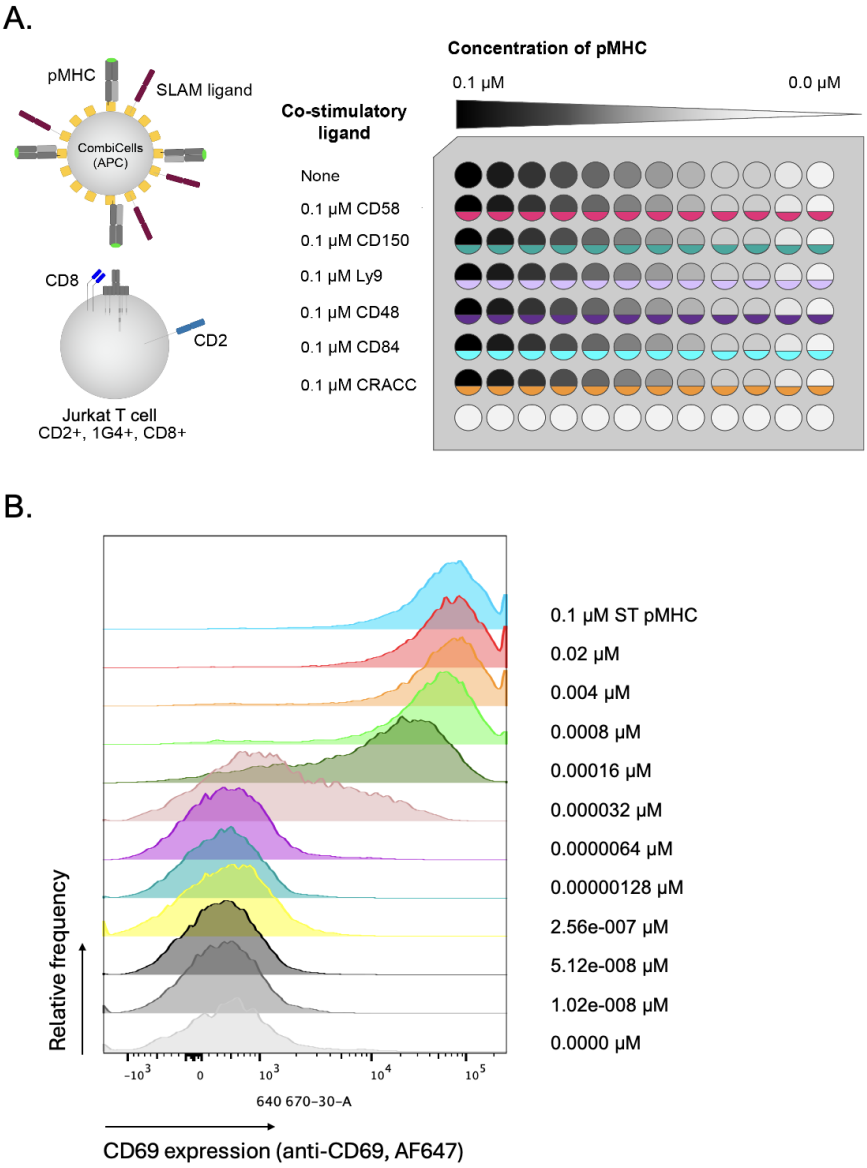

Figure 2.5: SLAM CombiCell assay design and experimental read-out. **(A)** Schematic showing 1G4/CD2/CD8$^+$ Jurkat T cells co-cultured with CHO-K1 CombiCells (left) presenting either a titration of pMHC alone (5-fold down from a maximum concentration of 0.1 μM) or a titration of pMHC alongside a constant concentration (0.1 μM) of SLAM ligand, with CD58 as a positive control (right) **(B)** Representative flow cytometry histograms showing expression of CD69 following staining with a fluorescent human CD69-targeting antibody at each pMHC concentration following co-culture.

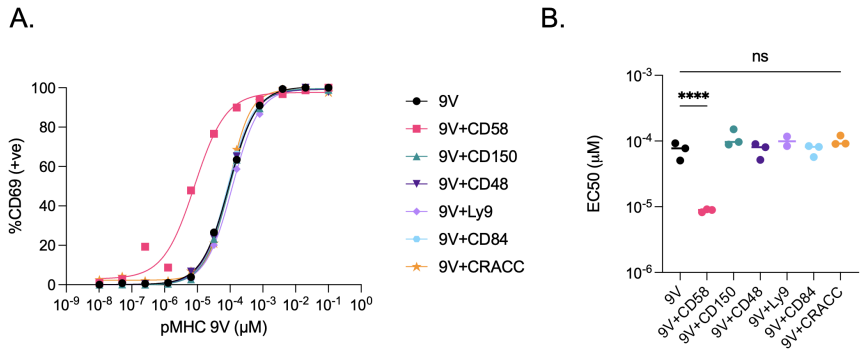

Figure 2.6: SLAM ligands have no impact on Jurkat T cell antigen sensitivity. **(A)** Normalised representative dose-response curves indicating surface expression levels of T cell activation marker CD69 under each condition, at each pMHC concentration. Dose-response curves have been fitted using a four-parameter logistic model (variable slope) equivalent to a Hill function. **(B)** EC50 values extracted using fitted dose-response curves from N=3 independent experiments. Statistical analysis was performed using a repeated-measures one-way ANOVA followed by Holm–Šídák's multiple-comparisons test. Significance thresholds were defined as *=$p \leq 0.05$, **=$p \leq 0.01$, ***=$p \leq 0.001$, and ****=$p \leq 0.0001$.

ever, we found low Ly9 expression and high CD84 expression (Fig 2.7). The poor endogenous expression of SLAM receptors CD150, Ly9, 2B4, and CRACC presented a possible explanation for the lack of phenotype observed in our initial T cell sensitivity assays.

To address the issue of low endogenous SLAM expression, we used lentiviral transduction to generate five novel Jurkat T cells with overexpression of SLAM receptors (Fig 2.8). We then repeated our original antigen sensitivity assays employing our novel Jurkat SLAM lines, again using the CD2/CD58 co-stimulatory receptor/ligand pair as a positive control.

Despite forced overexpression of SLAM receptors, antigen sensitivity was unchanged for all homophilic SLAM receptor/ligand pairs (CRACC, CD150, Ly9, and CD84) when stimulated with high concentrations of their cognate ligands (Fig 2.8). However, overexpression of 2B4 led to a five-fold enhancement in antigen sensitivity upon engagement with cognate ligand, CD48 (Fig 2.8).

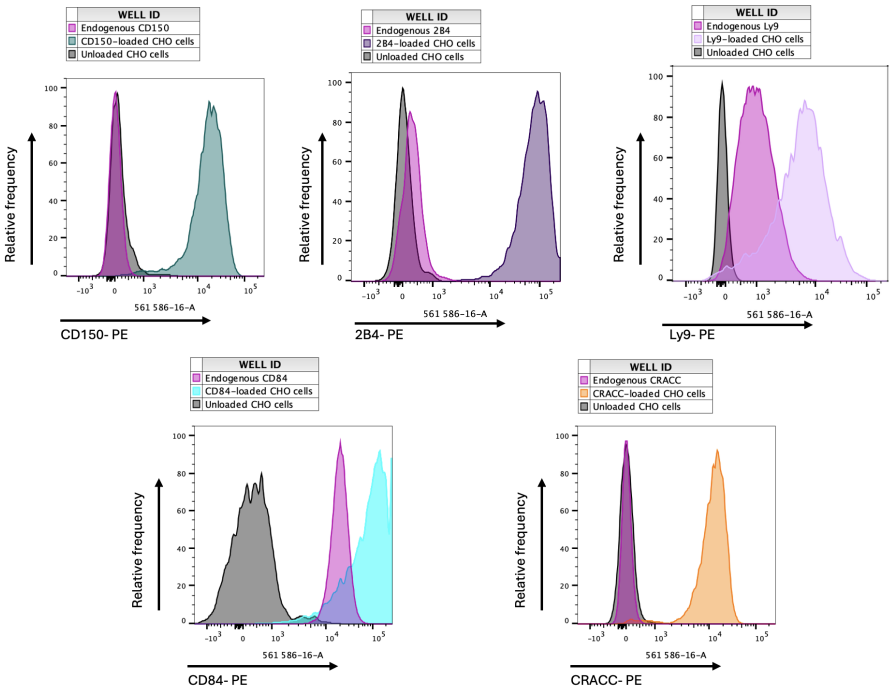

Figure 2.7: Jurkats endogenously express high levels of CD84 and low levels of Ly9, but not 2B4, CRACC, or CD150. Representative flow cytometry histograms showing endogenous Jurkat T cell expression of SLAM receptors (magenta) using CHO cells loaded with CD150 (teal), 2B4 (dark purple), Ly9 (lavender), CD84 (ice blue), and CRACC (orange) as a positive control with stained and unloaded CHO cells (black) as a negative control.

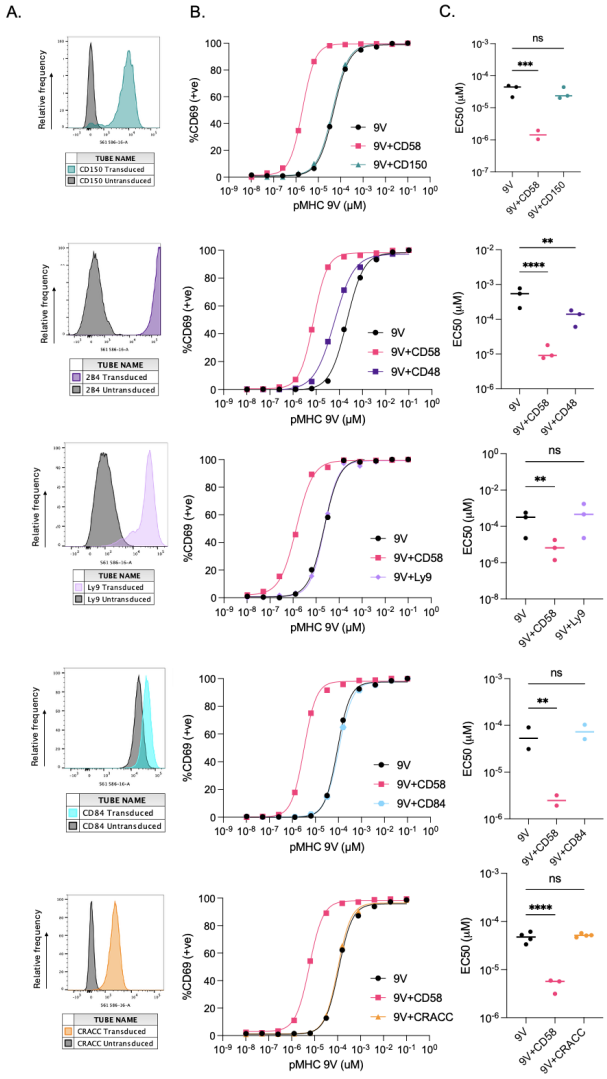

Figure 2.8: Overexpression of 2B4, but not CD150, Ly9, CD84, or CRACC, increases T cell sensitivity. **(A)** Representative flow cytometry histograms showing overexpression of each SLAM receptor following lentiviral transduction and subsequent sorting using untransduced cells (black) as a negative control. **(B)** Representative dose-response curves fitted with a Hill function showing T cell activation in response to a CombiCell sensitivity assay presenting antigen alone (black), antigen with 0.1 μM CD58 (pink), and antigen with 0.1 μM SLAM (CD150 in teal, CD48 in dark purple, Ly9 in lavender, CD84 in ice blue, and CRACC in orange). **(C)** EC50 values extracted from fitted dose-response curves from N=3 independent experiments. Statistical analysis was performed using a repeated-measures one-way ANOVA followed by Holm–Šídák's multiple-comparisons test. Significance thresholds were defined as *=$p \leq 0.05$, **=$p \leq 0.01$, ***=$p \leq 0.001$, and ****=$p \leq 0.0001$.

2.1.4 Further increases in CD48 concentrations do not lead to further increases in T cell antigen sensitivity

CD48 is highly expressed on most haematopoietic cell types and the 2B4/CD48 binding affinity is relatively high (K_D=8μM) compared to what has been observed for homophillic SLAM receptor/ligand interactions (e.g. CD150/CD150 with K_D =200μM); however, the phenotype we observed for the 2B4/CD48 interaction remained mild (5-fold) (Fig 2.8) [140,167,187,188]. Ligand quantification experiments in Jurkats have previously demonstrated that the magnitude of an accessory ligand's impact on T cell sensitivity can in some cases depend on the concentration of ligand used [2]. Therefore, we were interested to see whether increasing the concentration of SpyTagged CD48 in our assay would lead to further T cell sensitivity enhancements. We performed a 2D CombiCell titration assay, varying the concentrations of both our SpyTagged 9V pMHC and our SpyTagged CD48 (Fig 2.9 A). We performed these experiments with both WT Jurkat T cells and 2B4-overexpressing Jurkat T cells (Fig 2.9 A).

In our control WT Jurkat system, CD48 had no effect on antigen sensitivity at any concentration tested (Fig 2.9 B). In our 2B4-overexpressing Jurkat T system, presentation of CD48 led to a five-fold sensitivity enhancement for all CD48 concentrations tested, suggesting that ligand saturation had already been achieved at our original 0.1 μM CD48 concentration (Fig 2.9 C).

Overall, our studies in Jurkat T cells provided compelling evidence to suggest that while the 2B4/CD48 heterophilic SLAM interaction can increase T cell antigen sensitivity in Jurkats, homophilic SLAM interactions with CD150, Ly9, CD84, and CRACC have no sensitivity impact.

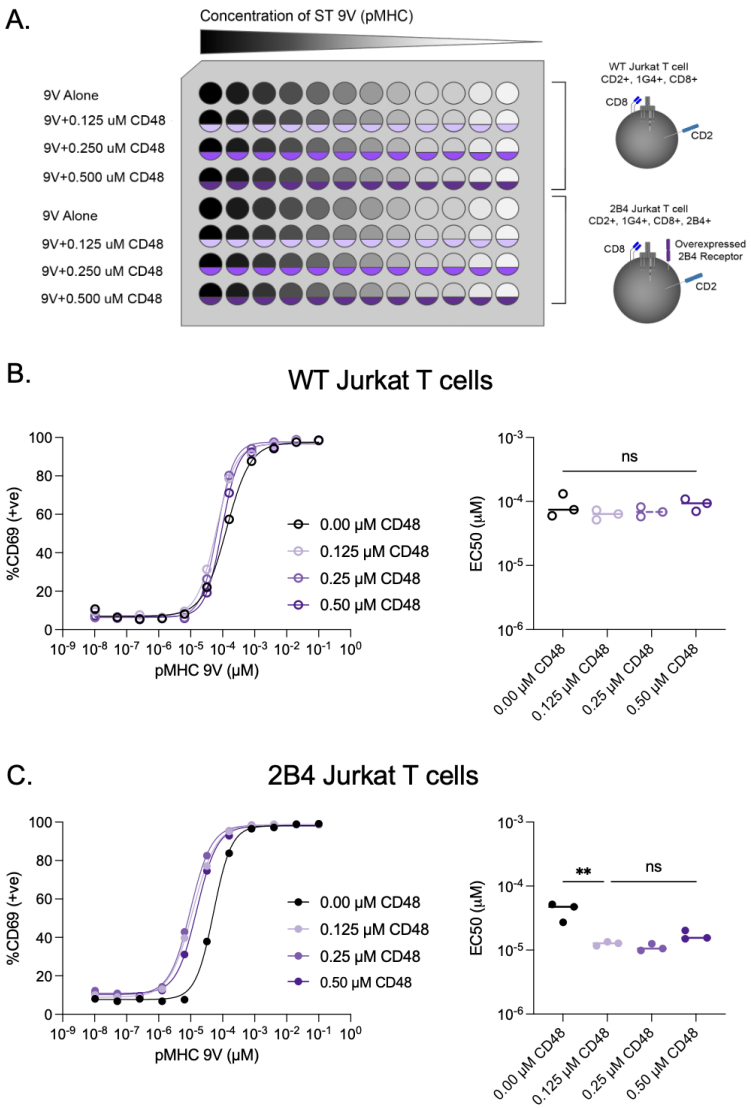

Figure 2.9: CD48 exerts concentration-independent effect on T cell sensitivity. **(A)** Schematic showing 2D titration with antigen titrated along each column of a 96-well plate (5-fold from 0.1 μM) and CD48 ligand titrated along each row (2-fold from 0.5 μM), repeated twice: once for WT Jurkat T cells and once for 2B4 Jurkat T cells. **(B)** WT Jurkat T cell representative dose-response curves (left) fitted with a Hill function using CD69 expression to assess activation. Summative EC50 values extracted from dose-response curves (right) from N=3 independent experiments. **(C)** 2B4 Jurkat T cell representative dose-response curves (left) fitted with a Hill function using CD69 expression to assess activation. Summative EC50 values extracted from dose-response curves (right) from N=3 independent experiments. Statistical analysis was performed using a repeated-measures one-way ANOVA followed by Holm–Šídák's multiple-comparisons test. Significance thresholds were defined as *=$p \leq 0.05$, **=$p \leq 0.01$, ***=$p \leq 0.001$, and ****=$p \leq 0.0001$.

2.1.5 Primary T cells upregulate SLAM expression following stimulation

As aforementioned, the activity of SLAM receptors depends on the presence of intracellular molecules SAP, EAT-2, SHP-1, SHP-2, and SHIP [153]. Although Jurkat T cells are known to express SAP, they do not endogenously express EAT-2 [187]. Additionally, Jurkat T cells are known to exhibit lower expression of SHP-1 and SHIP than what has been observed in primary T cells [189, 190]. Therefore, we developed a pipeline to examine the role of SLAM receptors using primary T cells. We isolated $CD8^+$ T cells from human blood donors and transduced these cells with our model 1G4 TCR (Fig 2.10).

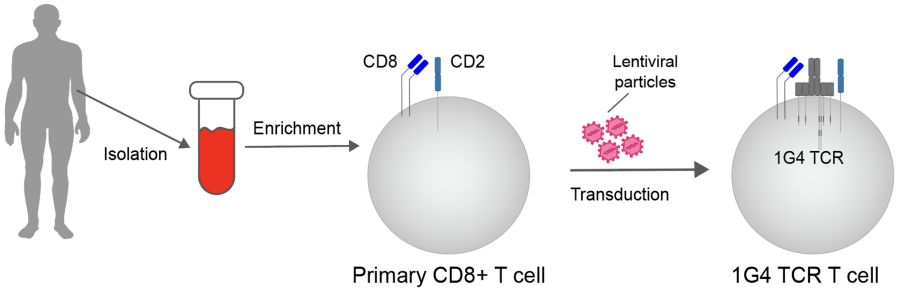

Figure 2.10: Generation of 1G4 TCR Primary T Cells. Schematic showing isolation of $CD8^+$ T cells from blood donors (see Methods) followed by lentiviral transduction with the 1G4 TCR.

Given the low endogenous expression of SLAM receptors observed in Jurkat T cells, we assessed our primary T cells for native SLAM expression. Because previous studies have shown that T cell stimulation induces upregulation of SLAM receptors in primary T cells, we examined native SLAM expression in both resting and activated primaries [191]. We used CombiCells to stimulate our primary T cells with SpyTagged 9V pMHC, verifying that stimulation had occurred by checking for surface expression of primary T cell activation markers 4-1BB and CD69. We then compared the expression levels of SLAM receptors before and after stimulation, using expression of CD45 (which should remain unchanged upon stimulation) as a

negative control and expression of 4-1BB and CD69 as positive controls (Fig 2.11).

We observed a 5-fold increase in the surface expression of CD150 and CRACC and a two-fold increase in the expression of CD84 following stimulation (Fig 2.11 B). No change in the surface expression of Ly9, 2B4, or negative control CD45 was observed (Fig 2.11 B).

2.1.6 T cell antigen sensitivity as assessed by surface 4-1BB and CD69 up-regulation is not impacted by SLAM-family co-signalling

To assess whether SLAM receptor engagement would impact primary T cell sensitivity, we repeated our previous SLAM CombiCell stimulation assay, this time using 1G4/CD8$^+$ primary human T cells as our effectors, again using CD58 as a positive control given that CD8$^+$ primary T cells are known to endogenously express CD2 (Fig 2.12 A) [145]. No SLAM ligand conditions tested had an impact on T cell antigen sensitivity when using surface markers 4-1BB and CD69 as measures of T cell activation (Fig 2.12 B and C). In contrast, engagement of CD2 with CD58 induced a 10-fold enhancement in sensitivity (Fig 2.12 C).

2.1.7 CD150, but not CD48, Ly9, CD84, or CRACC, reduces T cell cytokine production

Although we observed that, across Jurkat T cells and primary T cells, only CD48 could impact antigen sensitivity as measured by surface 4-1BB and CD69 expression, it has previously been suggested that co-signalling receptors can modulate multiple different T cell responses [192]. Therefore, we next investigated the impact of SLAM-family receptor engagement on cytokine production.

We found that engagement of the CD150 receptor led to a 7-fold decrease in maximal

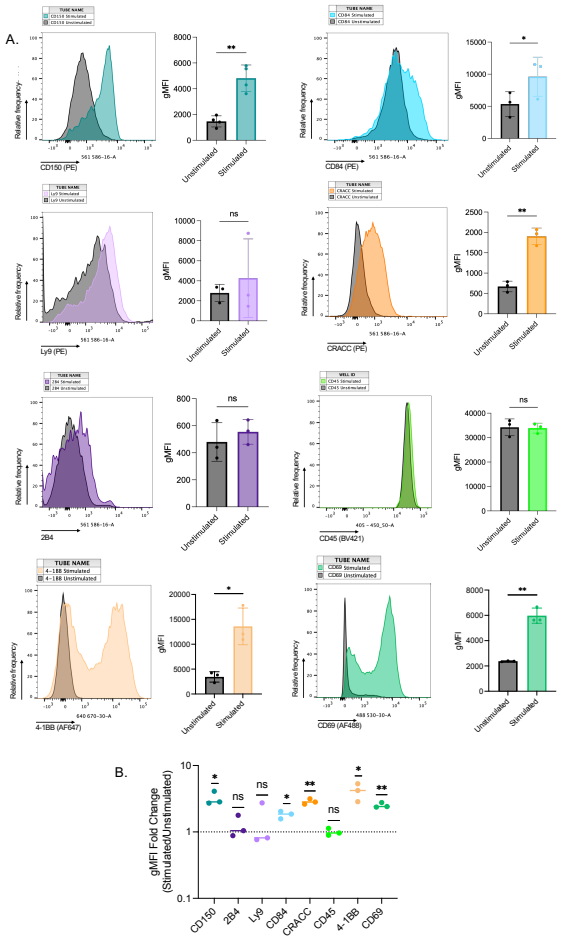

Figure 2.11: Stimulation increases expression of SLAM receptors CD150, CD84, and CRACC. **(A)** Representative histograms and summary gMFI statistics showing SLAM receptor expression before stimulation (black) and after stimulation for CD150 (teal), Ly9 (lavender), 2B4 (dark purple), CD84 (ice blue), and CRACC (orange) with CD45 expression (lime green) as a negative control and 4-1BB (tan) and CD69 (green) as positive controls. **(B)** Summary statistics showing fold-change in gMFI (calculated as gMFI of stimulated cells/gMFI of unstimulated cells) for N=3 independent experiments with 3 different blood donors. A one-sample t-test was used to determine whether the fold-change in EC50 values differed significantly from a theoretical value of 1. Significance thresholds were defined as *=$p \leq 0.05$, **=$p \leq 0.01$, ***=$p \leq 0.001$, and ****=$p \leq 0.0001$.

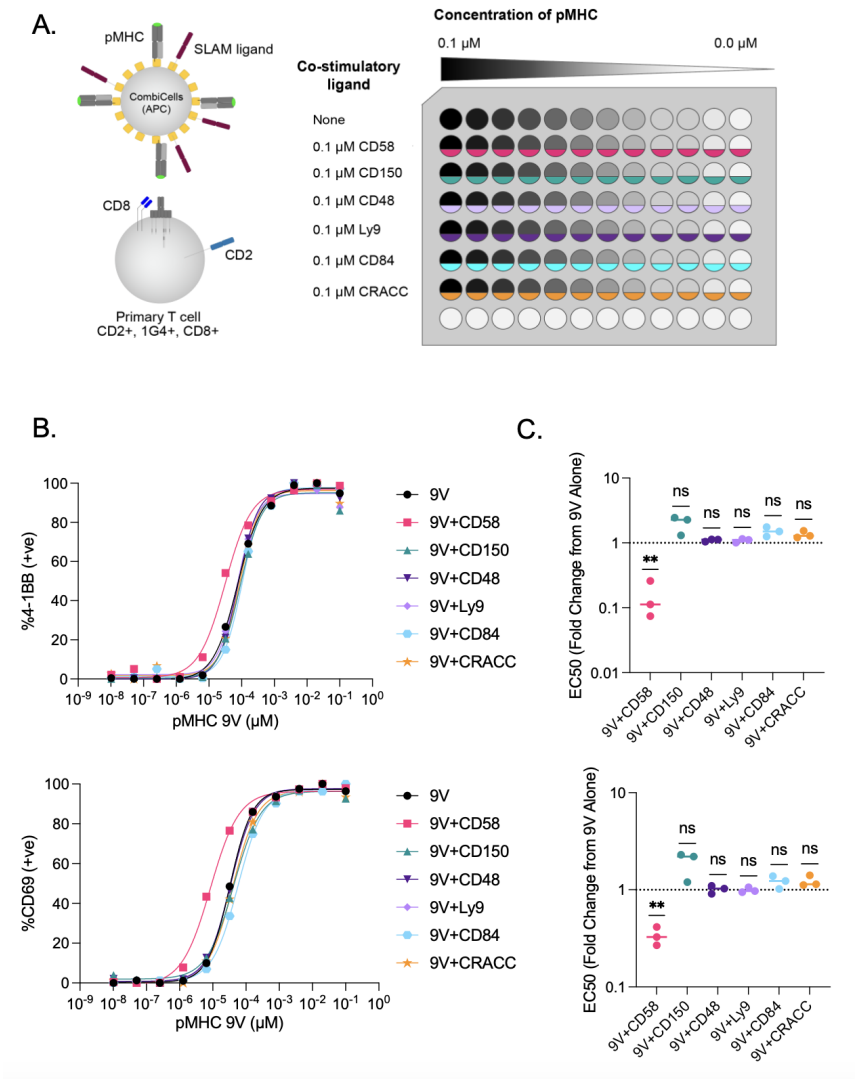

Figure 2.12: SLAM ligands have no impact on primary T cell antigen sensitivity as assessed by expression of surface activation markers. **(A)** Schematic showing CombiCell sensitivity assay with titration of ST pMHC (5-fold down from a maximum concentration of 0.1 μM) in the presence and absence of different ST SLAM ligands (0.1 μM) using ST CD58 (0.1 μM) as a positive control. **(B)** Representative normalized dose-response curves indicating surface expression of T cell activation marker 4-1BB (top) and CD69 (bottom), fitted with a Hill function. **(C)** Fold-change of EC50 values from N=3 independent experiments with 3 different blood donors. EC50s were extracted using fitted dose-response curves from 4-1BB (top) and CD69 (bottom). Fold-change was calculated through comparison of each SLAM condition to the peptide-alone condition. A one-sample t-test was used to determine whether the fold-change in EC50 values differed significantly from a theoretical value of 1. Significance thresholds were defined as *=$p \leq 0.05$, **=$p \leq 0.01$, ***=$p \leq 0.001$, and ****=$p \leq 0.0001$.

IL-2 production (Fig 2.13). We also observed a 3-fold decrease in sensitivity upon addition of the CRACC ligand, suggesting that CRACC engagement impacts the antigen threshold for IL-2 production, despite having no impact on the antigen threshold for CD69 or 4-1BB surface expression (Fig 2.13).

2.2 Discussion

Previous data from the literature suggests that accessory receptor engagement can profoundly impact T cell antigen sensitivity [1, 2, 161]. In particular, CD2 has been shown in some experimental contexts to enhance T cell sensitivity by more than 100-fold, highlighting the potential for members of this receptor family to act as potent T cell activation modulators [2, 161]. Based on these observations, we sought to determine whether members of the structurally-related SLAM family might exert a similar influence on T cell sensitivity.

We began our experiments using the established immortal Jurkat T cell line. Analysis of endogenous Jurkat SLAM expression revealed that SLAM family receptors were not uniformly expressed, with several family members showing low or undetectable surface expression (Fig 2.7). Consistent with this finding, initial functional assays did not reveal any SLAM-dependent enhancements in T cell sensitivity, when assessed using surface expression of CD69 as a measure of activation (Fig 2.6).

Given the limited endogenous expression of SLAM receptors on Jurkat T cells, we next tested whether forced overexpression of SLAM receptors could induce a phenotype. To this end, Jurkat T cells were transduced with lentiviral constructs encoding individual SLAM family receptors (Fig 2.8). Overexpression of the homophilic SLAM receptors (CD150, Ly9, CRACC, CD84) had no effect on T cell sensitivity (Fig 2.8). In contrast, overexpression of 2B4 (SLAMF4) resulted in a 5-fold sensitivity enhancement when cells were stimulated with its heterophilic binding partner, CD48 (Fig 2.8). Additional sensitivity assays utilising CD48 concentrations greater

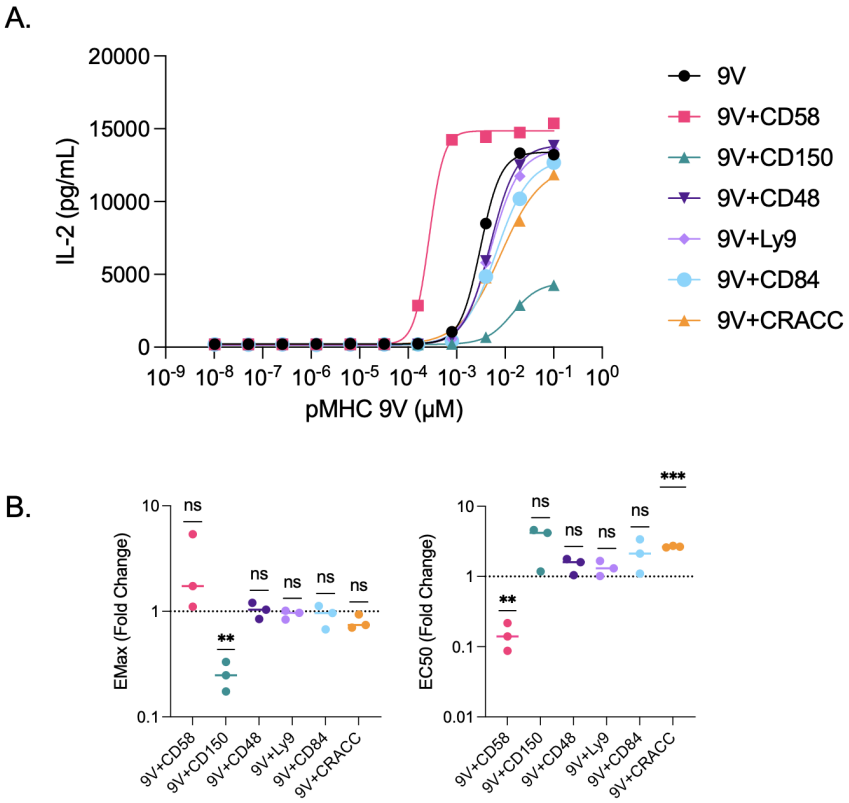

Figure 2.13: CD150 ligand addition leads to decrease in IL-2 production. **(A)** Representative dose-response curves showing IL-2 production following standard CombiCell titration experiment with either a titration of ST 9V peptide alone or a titration of 9V peptide alongside a constant concentration (0.1 μM) of ST accessory ligand. **(B)** Fold-change in EMax (left) and EC50 (right) values from N=3 independent experiments with 3 different blood donors. EMax values were determined as the maximum concentration of IL-2 produced (pg/mL). EC50s were extracted using fitted IL-2 production dose-response curves. Fold-change was calculated through comparison of each SLAM condition to the peptide-alone condition. A one-sample t-test was used to determine whether the fold-change in EC50 and EMax values differed significantly from a theoretical value of 1. Significance thresholds were defined as *=$p \leq 0.05$, **=$p \leq 0.01$, ***=$p \leq 0.001$, and ****=$p \leq 0.0001$.

than 0.1 μM did not lead to further enhancements in T cell sensitivity (Fig 2.9). Notably, the 2B4/CD48 pairing is the only receptor-ligand interaction within the SLAM family that exhibits heterophilic binding and is reported to exhibit a substantially higher affinity than what has been observed for homophilic SLAM receptors (K_Ds of around 8 μM and 200 μM, respectively) [153, 188]. 2B4 is also distinct within the SLAM family in that it has four immunoreceptor tyrosine-based switch motifs (ITSMs) within its cytoplasmic tail [193]. Most other SLAM family members have only two ITSMs, which may limit the magnitude of the downstream signalling events that can be initiated following their engagement [193].

The sensitivity enhancement observed with 2B4 engagement was found to be lower than that which was observed following CD2 engagement under the same experimental conditions (5-fold vs 10-fold). The CD2/CD58 and 2B4/CD48 receptor/ligand pairs reportedly exhibit similar binding affinities (K_Ds of around 9-22 μM and 8 μM, respectively), suggesting that this difference in effect size is most likely not driven by differences in binding strength [53, 187]. The higher sensitivity effect observed with CD2 engagement could potentially be explained by differences in intracellular signalling architectures of the two receptors. CD2 possesses a specialized, proline-rich cytoplasmic tail capable of direct Lck and Fyn recruitment, whereas 2B4 signalling utilises SAP recruitment for downstream effects [139, 153]. Consequently, the sensitivity of the 2B4 response may be limited by the stoichiometric availability of SAP. This theory is supported by the saturation effect observed at 0.1 μM CD48, which provides evidence to suggest that 2B4-mediated signalling in Jurkats may exhibit a distinct ceiling due to a limited availability of intracellular adaptors (Fig 2.9). Further studies quantifying Jurkat SAP concentrations and/or inhibiting SAP to determine whether this abolishes the 2B4/CD48-mediated sensitivity enhancement could provide additional information on the mechanism of action involved.

We also note that the physical geometry of the CD2/CD58 complex has the potential to play a role in its enhanced sensitivity effects. Structural studies indicate

that the CD2-CD58 interaction exhibits substantial conformational plasticity and rotational flexibility [194, 195]. This flexibility could allow the CD2/CD58 complex to tilt or rotate in order to maintain ligand-binding interactions during the dynamic process of immunological synapse formation, facilitating consistent exclusion of CD45 and robust T cell sensitivity enhancement [55]. There is less data to support a flexible 2B4-CD48 binding interaction, and if this complex is more geometrically constrained, it could fail to accommodate small topographic changes in the plasma membrane, potentially leading to less efficient exclusion of large inhibitory molecules such as CD45. Studies comparing the geometric constraints of the 2B4/CD48 and CD2/CD58 receptor/ligand complexes could therefore provide further evidence on the observed differences in antigen sensitivity effect size.

Of note, our experimental design had several limitations. Jurkat T cells, while a useful model for understanding T cell sensitivity, exhibit low endogenous expression of EAT-2, SHIP, and SHP-1, all of which have been implicated in SLAM-mediated signal cascades [189, 190]. Therefore, it is possible that our Jurkat T cells lacked the intracellular infrastructure required for SLAM-mediated inhibition. For this reason, we continued our SLAM studies in primary human $CD8^+$ T cells. Primary $CD8^+$ T cells provide several advantages over Jurkat T cells including more robust expression of essential intracellular signalling molecules and the ability to secrete multiple cytokines and chemokines [196].

In primary T cells, we found that stimulation with pMHC led to upregulation of SLAM receptors CD150, CRACC, and CD84 (Fig 2.11). However, no sensitivity changes were observed upon SLAM receptor engagement when using CD69 and 4-1BB as a measure of activation (Fig 2.12). We found a 7-fold decrease in maximal IL-2 production upon CD150 receptor engagement, but this same effect was not seen with 2B4, CRACC, Ly9, or CD84 (Fig 2.13). We also found that engagement of the CRACC receptor resulted in a 3-fold increase in the antigen sensitivity threshold required for IL-2 production, although no changes in maximal IL-2 production were

observed following CRACC binding (Fig 2.13).

CD150 participates in homophilic binding interactions through its membrane-distal IgV-like domain. The affinity of CD150's self-association is under debate. Early studies using surface plasmon resonance (SPR) reported a K_D of approximately 200 μM, suggesting a low-affinity binding interaction; however, more recent solution-phase studies using sedimentation velocity analytical ultracentrifugation (SV-AUC) have reported a significantly stronger monomer-dimer equilibrium constant of 0.48 μM [188,197]. In our functional studies, we observed upregulation of CD150 upon T cell activation as well as a 7-fold reduction in maximal IL-2 production following homophilic CD150 engagement, but we saw no CD150-engagement-mediated changes in the expression of early activation markers CD69 or 4-1BB at the 20-hour timepoint (Figs 2.11, 2.12, and 2.13).

The upregulation of CD69 and 4-1BB is mediated by Ras-MAPK and NF-κB signalling pathways, whereas IL-2 production exhibits a higher activation threshold and requires the coordinated activity of the transcription factors NFAT, AP-1, and NF-κB [123, 198, 199]. NFAT activity in particular is highly sensitive to calcium flux [200]. In a resting state, NFAT is sequestered in the cytoplasm in a hyperphosphorylated form [200]. TCR engagement and subsequent intracellular signalling cascades lead to sustained increases in intracellular calcium levels, which activate the phosphatase calcineurin to dephosphorylate NFAT [200]. Dephosphorylated NFAT then translocates to the nucleus, where it associates with additional proteins such as AP-1 and interacts with the IL-2 promoter to initiate transcription [200].

To prevent re-phosphorylation and nuclear export of NFAT, intracellular calcium levels must remain high [201]. Therefore, the threshold required for sustained IL-2 production could potentially be higher than what is needed for CD69/4-1BB expression. We propose a mechanism of action wherein CD150 engagement and subsequent recruitment of inhibitory phosphatases such as SHP-2 leads to attenuation of the

calcium flux, causing NFAT to exit the nucleus and thereby reducing IL-2 production without affecting expression of early activation markers such as CD69 and 4-1BB. Additional studies measuring calcium flux with and without CD150 engagement, or further studies looking at additional high-threshold T cell effector responses also subject to fluxtuations in calcium levels could help to inform our hypothesis regarding this subtle CD150/SHP-2-mediated dampening effect.

Stimulation of $CD8^+$ primary T cells also led to CRACC upregulation. A 3-fold decrease in antigen sensitivity for the production of IL-2 was observed, although no change in maximal IL-2 production was detected. As with CD150, CRACC upregulation following T cell stimulation has been previously reported in the literature, but few studies have directly examined the impact of CRACC expression on T cell sensitivities and effector functions [202]. Notably, while the cytoplasmic tail of CRACC contains two ITSM regions, biochemical studies using pull-down assays indicate negligible SAP binding [203,204]. Instead, CRACC's intracellular signalling is mainly thought to be facilitated by EAT-2, which, while present in NK cells, is not constitutively expressed in cytotoxic $CD8^+$ T cells [203, 204]. Consequently, the inhibitory effect on IL-2 production seen with CRACC-engagement on our primary $CD8^+$ T cells could be the result of forced SHP recruitment in the absence of EAT-2. Further studies involving CRACC engagement on NK cells, which endogenously express EAT-2, could help to elucidate the precise mechanism responsible for the observed phenomenon. It is, however, notable that there exist subsets of cells (e.g. $CD4^+$ T cells) with reported CRACC expression but no detectable EAT-2 protein, which further indicates that CRACC signalling is likely to lead to different functional outcomes in distinct cell types [204].

We did not observe any 2B4-mediated sensitivity effects in our primary T cell studies, despite the 5-fold sensitivity enhancement observed when using the Jurkat system. We hypothesise that this lack of a phenotype in primary T cells is the result of low endogenous 2B4 expression; the Jurkat T cell phenotype was only observed following

overexpression of the 2B4 receptor.

Primary T cell data often exhibits higher inter-experimental variation compared to Jurkat T cell data as a result of high inter-donor variation in the expression of key surface and intracellular signalling proteins [205]. Given that SLAM-ligand-mediated effects are highly dependent on the concentration of SLAM receptors expressed on the effector T cells, we employed fold-change measurements to compare primary T cell experiments from different donors.

Of note, SLAM receptors are differentially expressed across multiple different haematopoietic cell types, and their surface expression is often dynamically regulated during activation [153, 172, 202]. The significant heterogeneity in SLAM expression across different T cell subsets somewhat limits the physiological relevance of our studies, as we investigate their role in the activation of $CD8^+$ primary T cells and $CD8^+/CD2^+$ Jurkat T cells alone. Given the importance of intracellular effector molecules SAP, EAT-2, SHP-1, SHP-2, and SHIP in moderating the SLAM-mediated balance between activation and inhibition, additional studies looking at SLAM-mediated phenotypes in other T cell subsets could be essential in understanding how this balance is achieved.

Despite these limitations in the physiological relevance of our findings, the results of these experiments underscore the utility of the CombiCell system as an experimental platform for quantitatively assessing T cell sensitivities and provide further information on the rheostat-like function of SLAM family receptors. The modularity and precision of the CombiCell system enabled us to perform this large-scale, parallel screening of multiple SLAM family receptors.

3 | The role of extracellular size in TCR and CAR-T cell antigen recognition

3.1 Introduction

Chimeric antigen receptor (CAR) T cell therapies have emerged as a leading treatment for B and T cell malignancies, exhibiting efficacy against diseases such as multiple myeloma, chronic lymphocytic leukaemia, and acute myeloid leukaemia [206–209].

To administer these therapies, a patient's T cells are isolated and transduced with a synthetic molecule called a chimeric antigen receptor (CAR) designed to target the antigen of interest. These CAR-T cells are expanded *ex vivo*, and then reintroduced into the patient, now finely tuned to identify and destroy malignant cells (Fig 3.1) [210, 211].

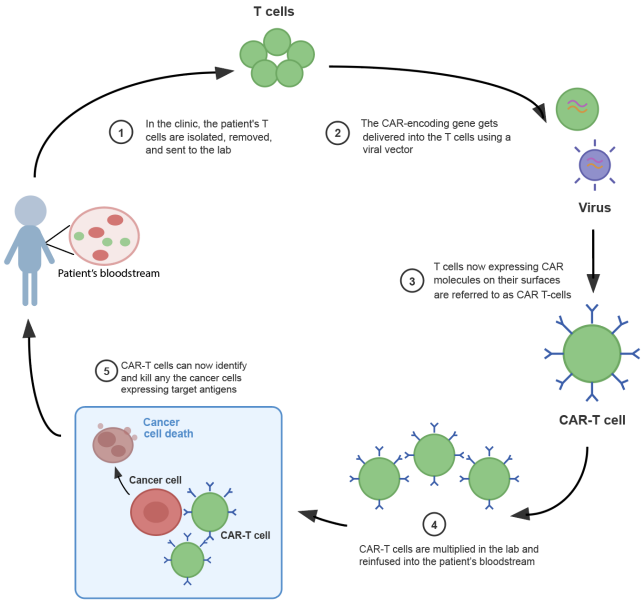

Figure 3.1: Production and administration of CAR-T cells

3.1.1 CAR structure

Chimeric antigen receptors are composed of four domains: the antigen recognition domain, the hinge domain, the transmembrane domain, and the intracellular signalling domain (Fig 3.2) [211].

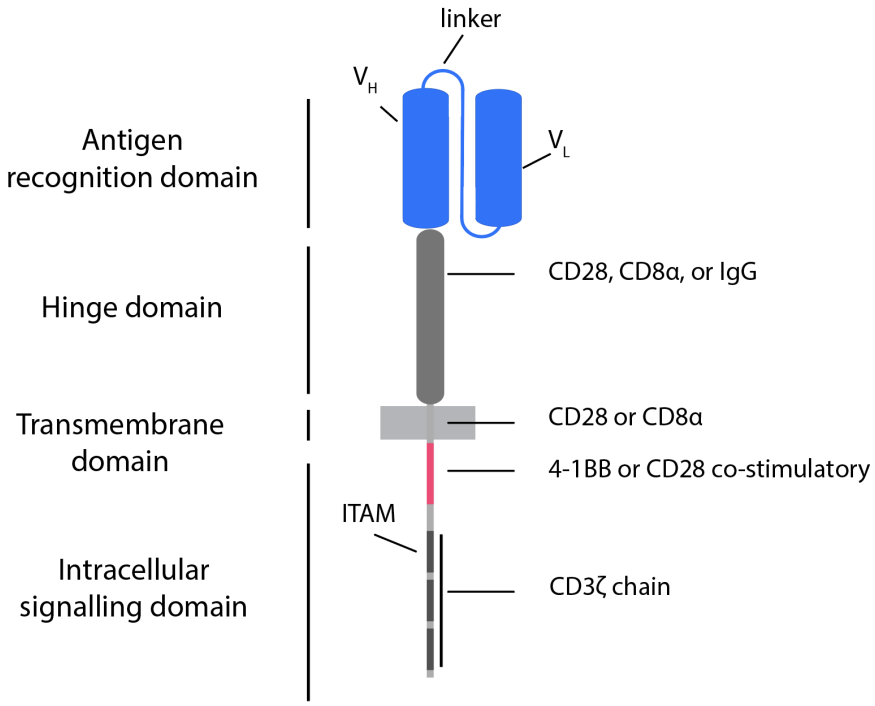

Figure 3.2: Second-generation CAR structure

The antigen recognition domain binds to an epitope on the antigen of interest and is derived from the variable domain of a monoclonal antibody. This domain is typically composed of a single chain of variable fragments (scFv) consisting of light (V_L) and heavy (V_H) chains from the antibody [212]. The light and heavy chains are connected by a short linker, typically composed of serine, glycine, glutamine, or lysine [212].

The hinge region connects the antigen recognition domain to the transmembrane domain and can serve as a spacer and/or to increase flexibility. The most commonly used hinge regions are derived from CD28 and CD8α [213].

Hinge regions differ between CARs, with the ideal spacer length depending on the position and size of the target antigen [214]. Longer and more flexible hinge regions are optimal for membrane-proximal, sterically hindered, or glycocalyx-embedded antigens [214, 215]. In these cases, the flexible and elongated hinge can extend the scFv away from the T-cell surface and limit steric clashes between the CAR and the target cell membrane, allowing for more effective immunological synapse formation [214, 215]. Shorter and stiffer hinge regions are preferable for membrane-distal and highly accessible antigens, as they exclude large phosphatases such as CD45 and promote tighter synapse geometry, allowing for more efficient CAR triggering [214, 216].

The transmembrane domain sits between the hinge and intracellular domains and is typically derived from either CD8α or CD28 [217]. *In vitro* studies using two CD19-targeting CARs with either CD8α hinge/transmembrane domains or CD28 hinge/transmembrane domains found that the CD8α CAR produced lower levels of cytokines and exhibited less activation-induced cell death (AICD) compared to the CD28 CAR [218]. This result is also supported by clinical data suggesting that CARs with CD8α hinge/transmembrane domains exhibit fewer neurologic toxicities and lower serum cytokine levels than CARs with CD28 hinge/transmembrane domains, potentially making the CD8α CAR advantageous in cases where minimising T cell exhaustion and improving long-term persistence are a priority [206, 218, 219]. Overall, advantages and disadvantages have been identified for both CD8α and CD28-based CARs, and, as a result, both are in clinical use [220].

The intracellular domain controls downstream signalling cascades required for T cell activation. For second-generation constructs, this region is comprised of either a CD28 or 4-1BB co-stimulatory domain followed by a CD3ζ activation domain. The co-stimulatory region determines signal strength, kinetics, and metabolic programming [221]. For rapid effector differentiation and potent early cytotoxicity, CD28-containing CARs are typically preferred [222–224]. For more sustained sig-

nalling and enhanced persistence, 4-1BB-based constructs are utilised [222,223,225]. The CD3ζ domain provides the primary activation signal. Phosphorylation of its immunoreceptor tyrosine-based activation motifs (ITAMs) leads to recruitment of ZAP-70 and the initiation of downstream signalling cascades [226].

3.1.2 CAR-T cell successes

The clinical success of CAR-T cell therapy has been demonstrated most clearly for B-cell malignancies, where CD19-targeting products have achieved high response rates in relapsed and refractory patient populations. For B-cell acute lymphoblastic leukaemia (B-ALL), CD19-directed CAR-T cells have produced remission rates of approximately 80–90%, with many patients achieving complete remission [227]. Similarly, for aggressive B-cell lymphomas, including diffuse large B-cell lymphoma (DLBCL), CD19 CAR-T cell therapies have resulted in overall response rates of over 50%, with durable remissions in patients refractory to multiple prior treatments [228,229]. Together, these outcomes highlight the significant impact of CAR-T cell therapies on B-cell cancers.

3.1.3 CAR-T cell limitations

Despite the strong clinical responses seen for many haematological malignancies, a substantial proportion of CAR-T-treated patients ultimately experience relapse. Reported relapse rates can range from 30–70% depending on disease type and duration of follow-up [230]. A major relapse risk factor is antigen escape, a process through which tumour cells downregulate expression of the target antigen to a level below the activation threshold for CAR engagement [231]. This reflects an inherent limitation of CAR-T cell sensitivity: CARs are unable to activate effectively against low-density antigens [232].

This phenomenon has been further demonstrated *in vitro*, where CAR-T cells can

require 100-fold more antigen than the TCR for activation [161]. The precise reason for this difference in sensitivity between the CAR and the TCR has yet to be elucidated.

3.1.4 Sensitivity differences between the CAR and the TCR

Many recent efforts to improve the function of the chimeric antigen receptor (CAR) have focused on optimising intracellular signalling. While these modifications have enhanced CAR effector function against high-density antigens, they have not led to substantial improvements in CAR sensitivity to low-density antigens [233].

Notably, the canonical TCR can respond to even a single peptide MHC (pMHC), whereas the standard CAR can require up to 100-fold more antigen for activation [158, 161, 232]. This difference in sensitivity persists even for CARs with higher baseline affinities than their corresponding TCRs, suggesting that this phenomenon cannot be explained through receptor-ligand binding strength alone [234, 235]. Additionally, when the TCR and CAR are assessed in reductionist *in vitro* systems lacking accessory receptor interactions, TCR sensitivity decreases dramatically, becoming indistinguishable from that of the CAR [161]. Therefore, the defect in CAR sensitivity may involve differences in the immune context in which it acts, specifically in its inability to exploit co-signalling receptors [2, 161].

3.1.5 The impact of accessory ligands on CAR and TCR sensitivities

The idea that immune context could influence differences in CAR and TCR sensitivities is further supported by evidence that co-stimulation dramatically enhances the sensitivity of TCR-T cells, yet has only modest impacts on activation thresholds for CAR-T cells [161]. When engagement of the CD2/CD58 accessory receptor-ligand complex is incorporated into TCR-T cell activation assays, sensitivity increases by

greater than 100-fold [161]. In contrast, inclusion of the same co-stimulatory interaction when using CAR-T cells results in a less than 5-fold sensitivity enhancement [161].

CD2 is hypothesized to function in both signalling and adhesive capacities. CD2 forms numerous low-affinity bonds (K_D = 9-22 μM) with its high-density binding partner, CD58 [144]. These interactions collectively create a strong intercellular adhesive effect. The CD2-CD58 complex spans approximately 14 nm, matching the dimensions of the TCR-pMHC complex and facilitating the alignment of opposing membranes at an optimal distance for antigen recognition [59,236]. CD2-CD58 adhesion thereby promotes formation and stabilization of close-contact zones, enhancing the likelihood of productive TCR-pMHC engagements [139].

In addition to its mechanical role, CD2 contributes directly to intracellular signalling. Ligation of CD2 leads to recruitment of Src-family kinases Lck and Fyn, which can amplify proximal TCR signalling pathways by enhancing the phosphorylation of CD3ζ and ZAP-70 [139]. Thus, CD2 engagement not only stabilizes the immunological synapse but also lowers the threshold for TCR activation by reinforcing downstream signalling cascades.

3.1.6 The size-matching hypothesis

Unlike the TCR, which typically spans an extracellular distance of 7 nm, CARs can be quite large, ranging in size from 10 to 13 nm (Table 3.1) [2]. It has been proposed that the increased extracellular size of the CAR could prevent simultaneous engagement of both the CD2-CD58 complex and CAR-antigen complex, thereby reducing the co-stimulatory effect of the CD2 receptor (Figure 3.3) [2]. In support of this hypothesis, the CD28 CAR exhibits a higher sensitivity to low-density antigens than the CD8α CAR, correlated with the CD28 CAR exhibiting a smaller extracellular size than the CD8α CAR (10.9 vs 13.2 nm) (Table 3.1) [2, 161, 233].

Table 3.1: TCR and CAR Dimensions

Receptor	Receptor size (nm)
1G4 TCR	7.8
CD28 CAR (D52N scFv)	10.9
CD8α CAR (D52N scFv)	13.2

Previous studies have attempted to size-match the CAR–antigen complex with the CD2/CD58 receptor–ligand pair through the use of elongated CD2 variants. For conventional TCR-T cells, elongation of CD2 was found to reduce overall signalling sensitivity [2]. In contrast, for CAR-T cells, the introduction of elongated CD2 variants resulted in an increase in overall sensitivity, suggesting that optimal spatial alignment between receptor–ligand pairs may differ for TCR- and CAR-mediated signalling [2].

The elongated CD2 variants were generated using sequences derived from the extracellular domain of CD43. CD43 is a mucin-type glycoprotein known to adopt a highly extended conformation lacking tertiary structure [237]. Given these structural properties, inserted segments from CD43 were assumed to function as relatively rigid spacers, thereby enabling precise modulation of CD2 length. Following extensive screening of multiple variants, a 40–amino acid CD2 extension (CD2-CD43(40)) was identified as optimal for the CD8α CAR, while an 8–amino acid extension (CD2-CD43(8)) was optimal for the CD28 CAR [2].

Importantly, the CD2/CD58 receptor–ligand complex is not unique in requiring an intermembrane distance of $\sim$14 nm for optimal engagement. Structural studies of the PD-1/PD-L1 interaction indicate that this complex is mediated through an IgV–IgV extracellular domain interaction, producing a receptor–ligand pair of comparable length ($\sim$14 nm) to the CD2/CD58 and TCR/pMHC close contact interactions [238, 239]. Previous work has shown that elongation of PD-1 reduces its ability to inhibit the TCR but enhances its ability to inhibit the CAR [2].

Together, these results suggest that maintaining a consistent size across receptor/li-

gand pairs at the close contact can enhance the tunability of both the TCR and the CAR, strengthening the size-matching hypothesis and its relation to the kinetic segregation model.

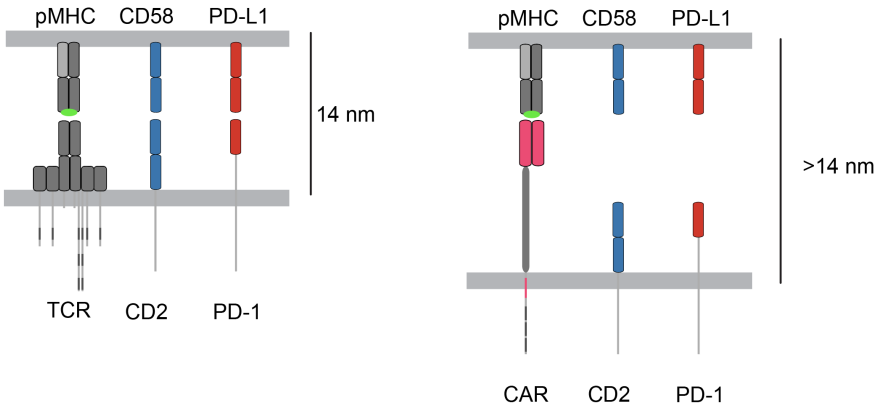

Figure 3.3: Size mismatch between CAR and accessory molecules prevents protein engagement

3.1.7 This chapter

We have shown in the previous chapter that engagement of accessory receptors can both enhance and impair TCR-T cell activation thresholds. It has been hypothesised that CAR-T cells are unable to effectively exploit these same accessory receptors, potentially due to size discrepancies between the CAR and the TCR. To resolve these issues and investigate the impact of accessory receptors on CAR-T cell sensitivity, we again employ the CombiCell system to precisely quantify CAR-T cell antigen sensitivities in the presence and absence of co-signalling molecules CD2 and PD-1.

We expand upon previous work indicating that elongation of PD-1 can improve its activity on a CAR, precisely quantifying the potency of both WT and elongated PD-1 receptor variants [2]. We further demonstrate that variations in the structure of the CAR itself can optimise its sensitivity without the need for additional accessory receptor modifications. Based on our observations from these experiments,

we incorporate the size-matching hypothesis into our CAR-T cell design and test truncated variants of the standard CAR in an effort to better understand the impact of accessory receptor exploitation on CAR-T cell sensitivity.

3.2 Results

3.2.1 Developing a platform to study PD-1/PD-L1 mediated CAR-T cell inhibition

To investigate the impact of the PD-1/PD-L1 interaction on TCR-T cell and CAR-T cell sensitivities, we developed an experimental platform that would allow us to titrate antigen, CD58, and PD-L1 in a size-matched system.

For this platform, we again utilized Jurkat T cells previously engineered through CRISPR/Cas9 knockouts to be CD2 and TCR negative [2]. We transduced these CD2/TCR$^-$ Jurkat T cells with the PD-1 receptor and either the 1G4 TCR or the CD8α CAR. We then further transduced these cells with a CD2 variant size-optimised for their respective TCR or CAR receptor (CD2 WT for the 1G4 TCR and CD2-CD43(40) for the CD8α CAR) (Fig 3.4 A and B).

We performed a pilot experiment to validate this platform and verify the ability of the PD-1/PD-L1 receptor/ligand complex to mediate inhibition. To this end, we performed a standard CombiCell titration assay, co-culturing our PD-1-expressing TCR and CAR-T cells with CombiCells presenting PD-L1, CD58, and a titration of antigen (Fig 3.5 A). We found that addition of PD-L1 led to inhibition of both TCR-T cells and CAR-T cells (Fig 3.5 B and C). We observed a nearly 100-fold decrease in sensitivity for the TCR, but only a 10-fold decrease in sensitivity for the CAR. This difference in the effect size of PD-1/PD-L1-mediated inhibition between the TCR and the CAR further supports the hypothesis that CAR-T cells are unable to effectively exploit PD-1/PD-L1 interactions.

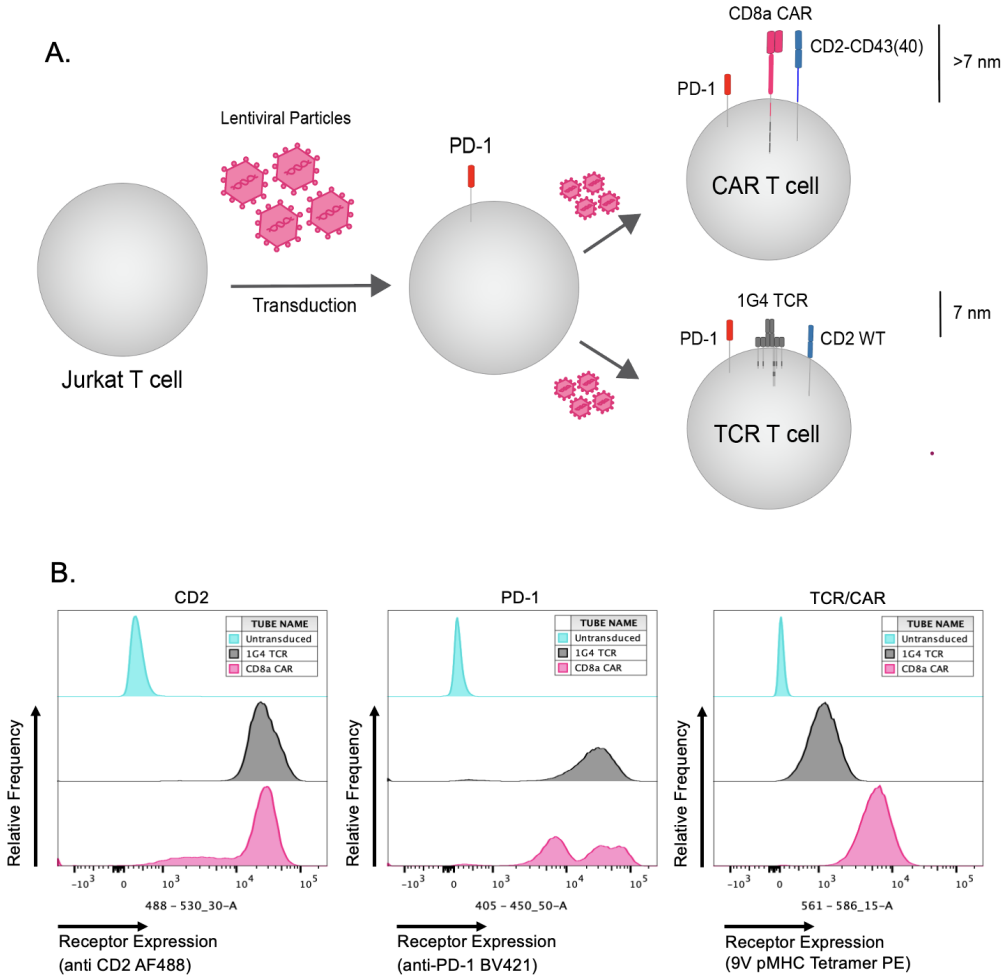

Figure 3.4: Generating TCR and CAR Jurkat T cells with size-optimised CD2. **(A)** Schematic showing the generation of Jurkat T cells expressing PD-1, either the CD8α CAR or the 1G4 TCR, and a size-matched CD2 receptor (CD2 WT for the 1G4 TCR and CD2-CD43(40) for the CAR). **(B)** Flow cytometry histograms showing surface expression of CD2 variants (left), PD-1 WT (centre), and the CAR/TCR (right) for TCR-T cells (black) and CD8α CAR-T cells (pink), using untransduced cells as a negative control (blue).

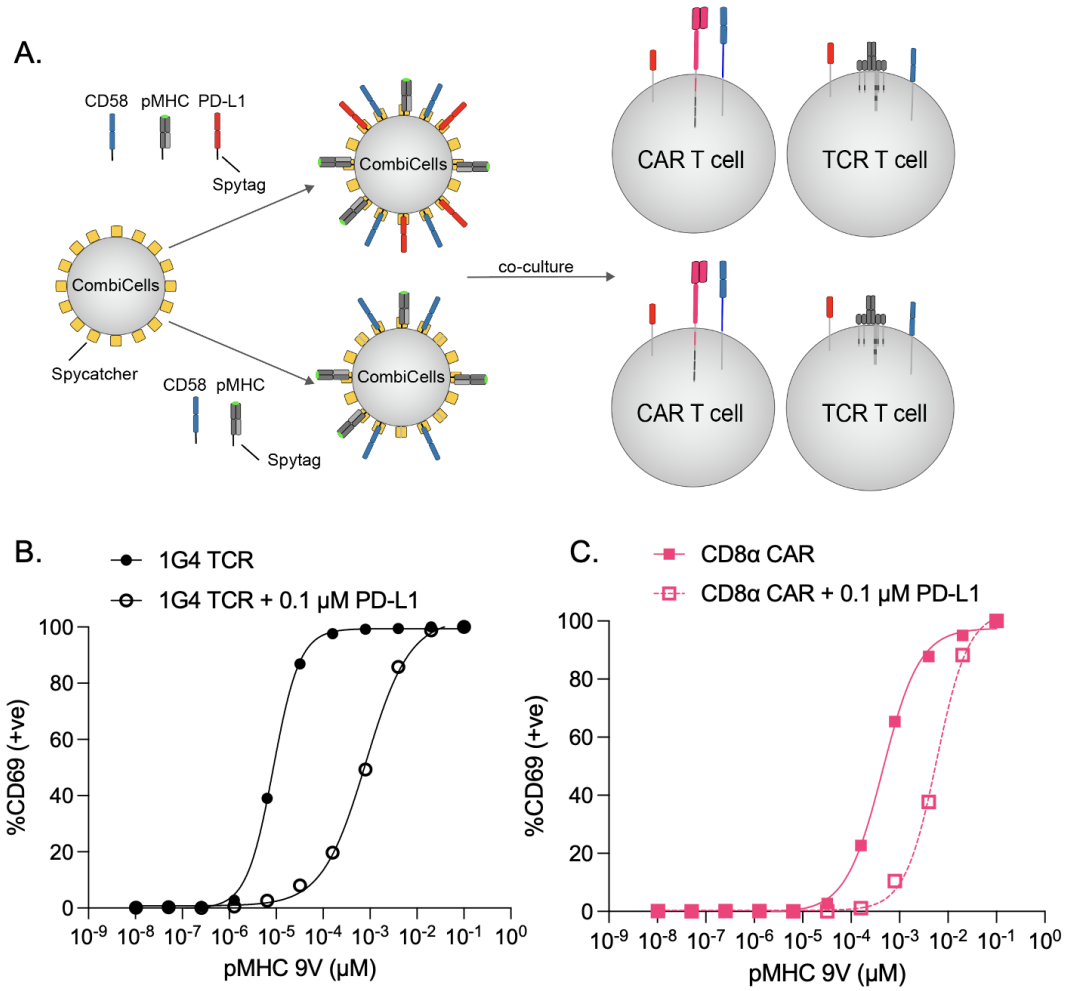

Figure 3.5: Engagement of PD-1 by PD-L1 inhibits TCR-T cell and CAR-T cell activation.. **(A)** Schematic showing CHO CombiCell sensitivity assay using TCR Jurkat T cells (PD-1, CD2 WT) and CAR Jurkat T cells (PD-1, CD2-CD43(40)). Jurkats were co-cultured with CombiCells presenting 0.1 μM ST CD58 and a titration of ST pMHC 9V (5-fold titration with a maximum concentration of 0.1 μM), with or without 0.1 μM ST PD-L1. **(B)** Normalised dose-response curves indicating surface expression of T cell activation marker CD69 for TCR-T cells (black) and **(C)** CAR-T cells (pink). Solid lines and solid shapes indicate absence of PD-L1. Dashed lines and open shapes indicate presence of PD-L1. Dose-response curves were fitted using a four-parameter logistic model (variable slope), equivalent to a Hill function.

3.2.2 CAR sensitivity to PD-L1 inhibition can be improved through elongation of PD-1

Having validated our CombiCell inhibition assay platform, we next sought to quantify the potency of PD-1 in both size-matched and size-mismatched inhibition systems. For this, we needed to generate CAR-T cells expressing either PD-1 WT or elongated PD-1. We chose to use PD-1-CD43(40), previously demonstrated to be size-optimised for the CD8α CAR, for our elongated receptor (Fig 3.6 A and B). To ensure that differences in receptor transduction efficiencies would not impact our sensitivity assessment, we sorted the cells for matched expression (Fig 3.6 B).

To test the impact of size-optimising PD-1 on CAR sensitivity, we titrated both antigen and PD-L1 on CombiCells. We then used these CombiCells to stimulate our PD-1 WT and PD-1 elongated CAR-T cells (Fig 3.7 A and B).

We found that elongation of the PD-1 receptor increased the potency of PD-1/PD-L1-mediated inhibition (Fig 3.7 A and B). To translate these μM ligand concentrations into molecular densities, we performed quantitative calibration followed by brightfield microscopy to determine the average number of PD-L1 molecules per cell at each loading condition and the total cell surface area, which together allowed us to estimate the loaded ligand surface density (Fig 3.7 C and D). We found that to achieve a 10-fold inhibition effect, the elongated receptor required 2.8-fold less ligand than PD-1 WT (Fig 3.7 E), and, more quantitatively, that PD-1-CD43(40) requires a PD-L1 density of 187 molecules of PD-L1/ μM^2 to achieve a 10-fold inhibition effect while PD-1 WT requires a density of 524 molecules of PD-L1/ μM^2 to achieve the same (Fig 3.7 E).

These results further support the hypothesis that size complementarity between receptors is essential for effective signal integration and that size mismatches may limit the ability of CAR-T cells to exploit endogenous accessory receptors.

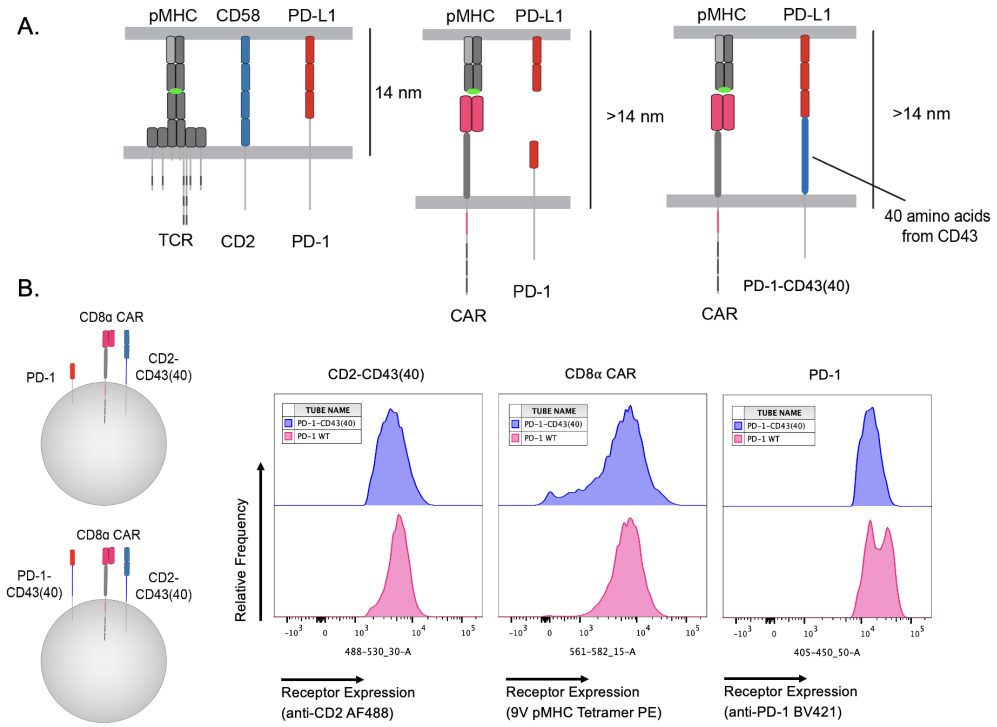

Figure 3.6: Generation of CAR-T cells with size-optimised PD-1. **(A)** Schematic showing matched sizes of the CD2/CD58, PD-1/PD-L1, and TCR/pMHC complexes in TCR-mediated close contacts (far left) alongside mismatched sizes for CAR-mediated close contacts (centre) and re-matched sizes for CAR-mediated close contacts with elongated PD-1 (PD-1-CD43(40)) (far right).**(B)** Schematic (far left) and flow cytometry histograms showing surface expression of CD2-CD43(40) (left), CD8α CAR (centre), and PD-1 variants for CAR PD-1 WT T cells (pink) and CAR PD-1-CD43(40) T cells (blue).

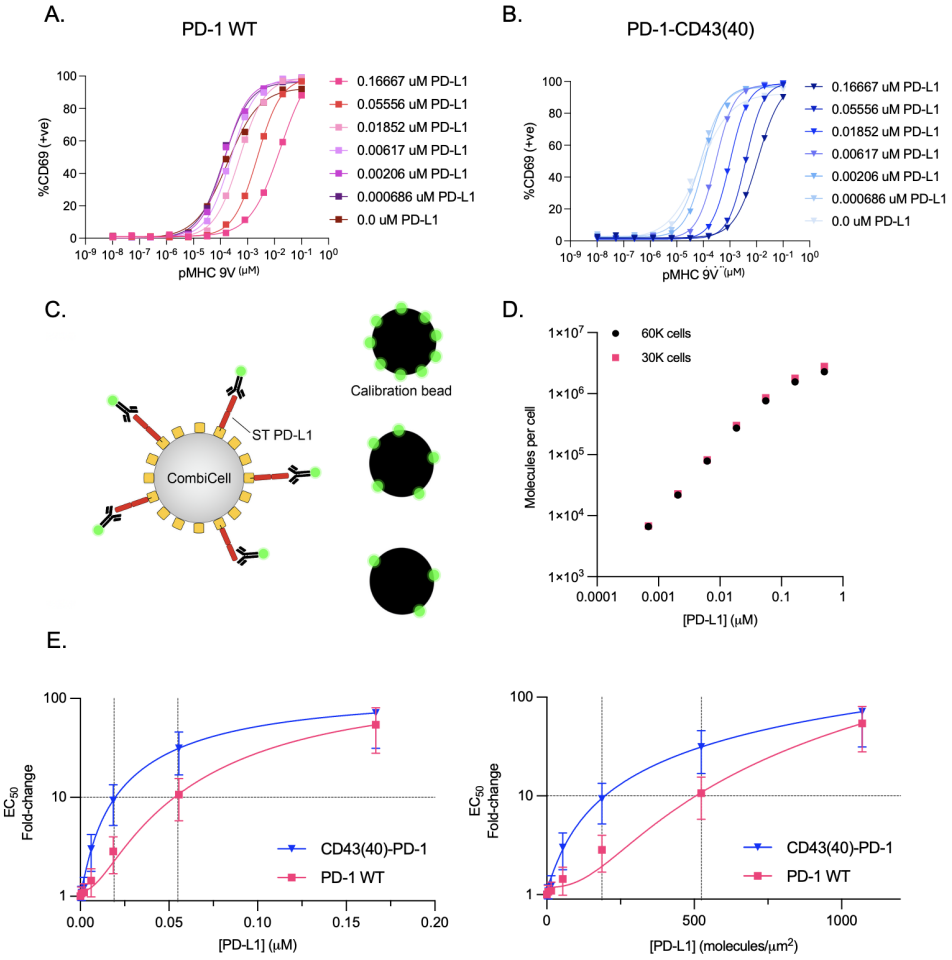

Figure 3.7: Elongation of PD-1 improves CAR sensitivity to inhibition. **(A)** Representative 2D titration dose-response curves for CAR-T cells expressing WT PD-1 (left, squares, pink) and PD-1-CD43(40) (right, inverted triangles, blue). CAR-T cells were co-cultured with CHO CombiCells expressing 0.1 μM ST CD58, a ST 9V titration (5-fold from a maximum concentration of 0.1 μM), and a ST PD-L1 titration (3-fold from a maximum concentration of 0.16667 μM). Dose-response curves were fitted using a four-parameter logistic model (variable slope), equivalent to a Hill function. **(C)** Schematic showing surface levels of ST PD-L1 loaded on CHO CombiCells and fluorescent calibration beads used for **(D)** quantitative calibration of PD-L1 used to translate μM concentrations into molecules of PD-L1 per cell for each indicated ligand concentration. **(E)** Fold-change of EC50 values for PD-1 WT (squares, pink) and PD-1-CD43(40)(inverted triangles, blue) plotted against PD-L1 μM concentration (left) and PD-L1 density (right). Error bars represent data from N=3 independent experiments. Dashed lines represent concentrations of PD-L1 required for a 10-fold increase in EC50. Flow cytometry calibration data and microscopy measurements used to generate panels D and E were collected by Tommy Dam and are represented here and in [2] with permission from Tommy Dam.

3.2.3 "Compact" CAR demonstrates enhanced sensitivity

As established above, CAR sensitivity to both activation and inhibition can be enhanced through elongation of accessory receptors (e.g. CD2 and PD-1). However, we wanted to determine whether we could generate a CAR variant capable of exploiting native CD2/CD58 interactions. We therefore designed a novel CAR engineered to match the extracellular dimensions of the TCR: the Compact CAR.

The Compact CAR is composed of Fab heavy and light chains fused to a CD28-derived transmembrane and cytoplasmic domain with intracellular CD28 co-stimulation domains and a CD3 ζ chain (Fig 3.8 A) [2]. With this structure, the Compact CAR maintains the cytoplasmic signalling of traditional second-generation CARs while matching the extracellular size of the TCR.

To test the sensitivity of the Compact CAR, we transduced primary T cells with the TCR, the CD8α CAR, and the Compact CAR. The Compact CAR showed no differences in transduction efficiency or surface expression compared to the standard CD8α CAR (Fig 3.8 B and D). Notably, the standard and Compact CARs exhibited an approximately 2-fold increase in surface expression compared to the TCR (Fig 3.8 C). This difference likely reflects TCR competition for limited endogenous CD3 molecules essential for TCR but not CAR expression (Fig 3.8 B).

To assess the activity of the Compact CAR, we performed a CombiCell sensitivity experiment using 1G4, CD8α CAR, and Compact CAR primary T cells in an assay against CombiCells derived from a B cell leukaemia (NALM6 cells), which endogenously expresses CD58 (Fig 3.9 A) [240]. The Compact CAR exhibited a nearly 100-fold increase in sensitivity relative to the standard CD8α CAR (Fig 3.9 B an C). Additionally, we found no differences between the antigen sensitivities of TCR-T cells and Compact CAR-T cells (Fig 3.9 B and C).

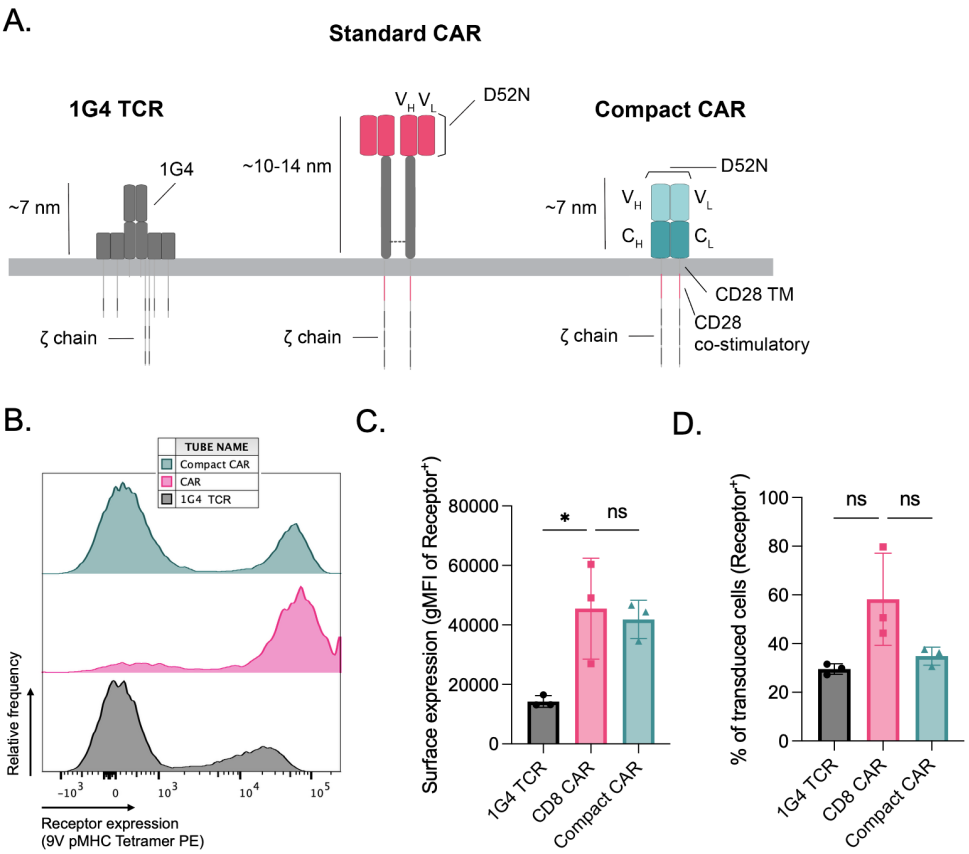

Figure 3.8: Compact CAR exhibits surface expression on primary T cells **(A)** Schematic showing structures of 1G4 TCR (black), D52N CD8α H/TM-28ζ CAR (pink), and D52N Compact CAR (teal). **(B)** Flow cytometry histograms showing surface expression of the TCR, CAR, and Compact CAR on virally transduced CD8$^+$ primary T cells following a 9V tetramer binding assay, used to determine **(C)** surface expression levels for each construct, measured using the gMFIs of receptor$^+$ T cells, and **(D)** transduction efficiencies for each construct, assessed as percentage of receptor$^+$ T cells out of the total T cell population. Data represents N=3 independent experiments from 3 different blood donors. Statistical analysis was performed using a repeated-measures one-way ANOVA, followed by Holm–Šídák's multiple-comparisons test. Significance thresholds were defined as *=$p \leq 0.05$, **=$p \leq 0.01$, ***=$p \leq 0.001$, and ****=$p \leq 0.0001$.

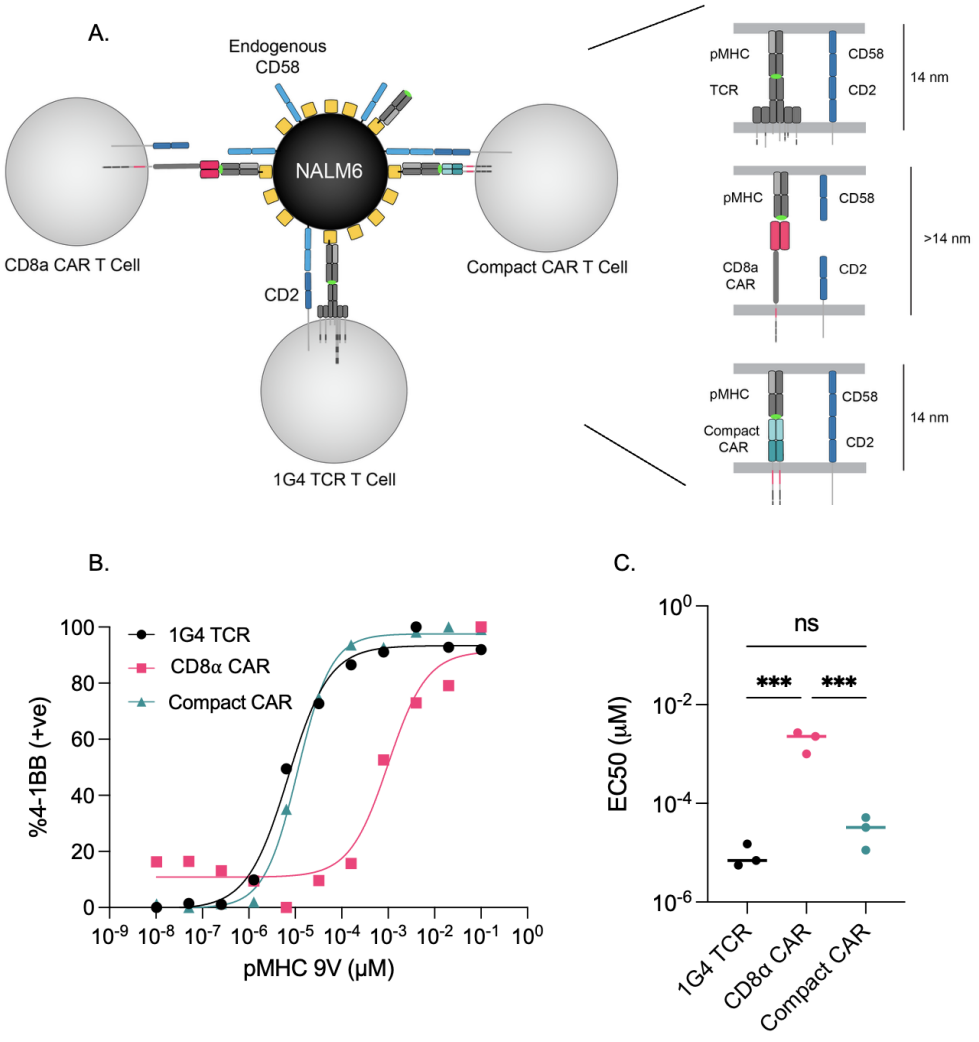

Figure 3.9: Size-matched Compact CAR demonstrates enhanced sensitivity to endogenous ligands (A) Schematic showing NALM6 CombiCell assay (left) and hypothesized close contact interactions (right). NALM6 CombiCells endogenously expressing CD58 were pulsed with a titration of 9V peptide (5-fold from a maximum concentration of 0.1 μM) and co-cultured with primary CD8+ T cells expressing the 1G4 TCR, the CD8α CAR, or the Compact CAR. T cell sensitivity was determined through flow cytometry, using surface expression of T cell activation marker 4-1BB. **(B)** Normalized representative dose-response curves showing 4-1BB expression fitted using a four-parameter logistic model (variable slope), equivalent to a Hill function. **(C)** EC50 values extracted using fitted dose-response curves from N=3 independent experiments with 3 different blood donors. Statistical analysis was performed using a repeated-measures one-way ANOVA, followed by Holm–Šídák's multiple-comparisons test. Significance thresholds were defined as *=$p \leq 0.05$, **=$p \leq 0.01$, ***=$p \leq 0.001$, and ****=$p \leq 0.0001$.

3.2.4 Compact CAR exhibits improved cell killing to the Standard CAR

Having shown using the CombiCell system that the Compact CAR exhibits improved antigen sensitivity relative to the standard CAR, we desired to determine whether this enhanced activity could be seen in a more physiologically relevant context. We wanted to assess Compact CAR performance at different E:T ratios in longitudinal cell killing assays. We therefore performed an Incucyte assay to directly compare the cell killing abilities of the TCR, the standard CAR, and the Compact CAR (Fig 3.10 A).

At effector-to-target ratios of 1:1, 1:2, and 1:4, the Compact CAR exhibited a cell killing ability comparable to that of the 1G4 TCR and superior to that of the standard CAR (Fig 3.10 B).

Taken together, these results (Figs 3.9 and 3.10) suggest that the Compact CAR structure not only exhibits improved antigen sensitivity relative to the standard CAR but also maintains this improved performance at different E:T ratios across long-term killing assays.

3.2.5 CAR size-matching fails to achieve TCR-level sensitivities

Given the promising results from the Compact CAR, we wanted to test whether similar sensitivity and killing improvements could be made by shortening the stalk of a standard CAR. The design of the Compact CAR included significant differences from the hinge region of the standard CAR, utilising IgG1-CH1 in the place of a CD8α or CD28 stalk. We therefore aimed to distinguish whether the enhanced sensitivity of the Compact CAR arose from these fundamental structural alterations or whether extracellular size-matching alone could account for the observed improvements.

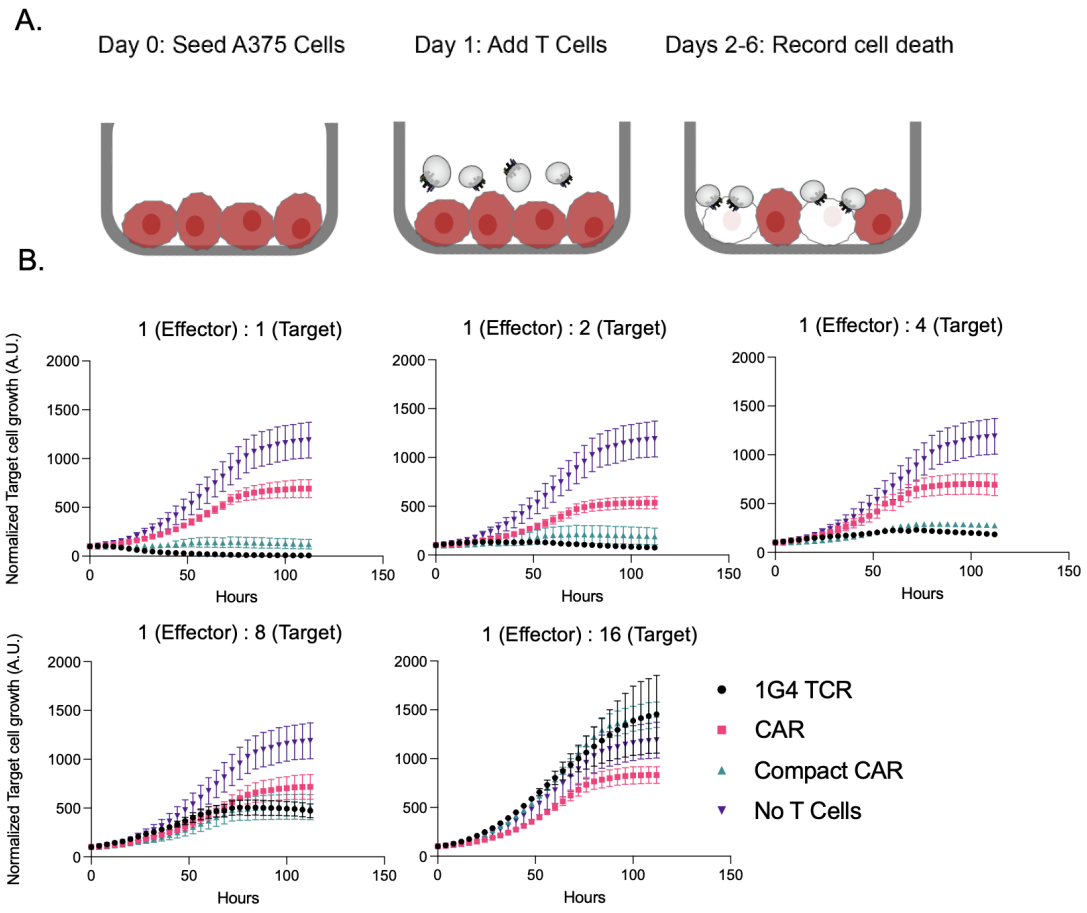

Figure 3.10: Compact CAR exhibits enhanced killing relative to the standard CAR (A) Schematic showing longitudinal killing assay workflow. Red cells indicate live, fluorescent targets while white cells indicate cell death. **(B)** Representative growth curves from longitudinal killing assays. 12,000 A375 cells expressing nuclear mCherry and HLA-A*02:01/NY-ESO-1 peptide were seeded and allowed to double overnight. At t=0, primary human $CD8^+$ T cells expressing the 1G4 TCR (black, circles), the CD8α standard CAR (pink, squares), or the Compact CAR (teal, triangles) were added at varying effector-to-target ratios (1:1, 1:2, 1:4, 1:8, 1:16), with a no-T cell condition as a control (purple, inverted triangles). A375 growth was recorded every two hours, with mCherry fluorescence indicating tumour cell growth and survival. Data is shown as mean ± SD of technical triplicates.

To test this, we generated a series of novel CAR constructs with truncated extracellular stalks. We selected the CD28-derived CAR rather than the CD8α-derived CAR as the base for these truncations because we wanted to maintain structural consistency with the Compact CAR, which utilises CD28-derived transmembrane and cytoplasmic domains.

The CD28-derived standard CAR hinge comprises 40 amino acids (H(40), pink) (Fig 3.11 A). To investigate the impact of hinge length, we progressively truncated the membrane-distal region to generate novel constructs with a 25-amino-acid stalk (H(25), ice blue) and a 21-amino-acid stalk (H(21), lavender) (Fig 3.11 A). We transduced these novel constructs into $CD8^+$ primary T cells, using the 1G4 TCR as a control. There were no differences in the transduction efficiencies of the TCR, the standard CD28 CAR, or the novel truncated CD28 CAR constructs (Fig 3.11 B and C). Overall surface expression of the TCR was again lower than that of all CAR variants, likely due to CD3 availability, but no differences in surface expression were observed between the original (H(40)) and novel (H(25), H(21)) CAR variants (Fig 3.11 D).

To simultaneously assess sensitivity and cell-killing, we pulsed the 9V peptide on a human U87 gliblastoma cell line that had been stably transduced with NanoLuc luciferase (NLuc). Upon loss of membrane integrity during cytotoxicity, intracellular NLuc is released into the supernatant, where luminescence can be quantified to assess target cell death. We then compared TCR-T cell and CAR-T cell sensitivities using both expression of surface activation markers and cell killing ability as readouts. For both activation marker expression and target cell killing assays, the standard CAR exhibited poorer sensitivity than the TCR (Fig 3.12 A and B). However, there were no differences in sensitivity observed between the full-length CAR and the truncated CAR variants (Fig 3.12 A and B).

For both activation marker expression and target cell killing assays, the standard

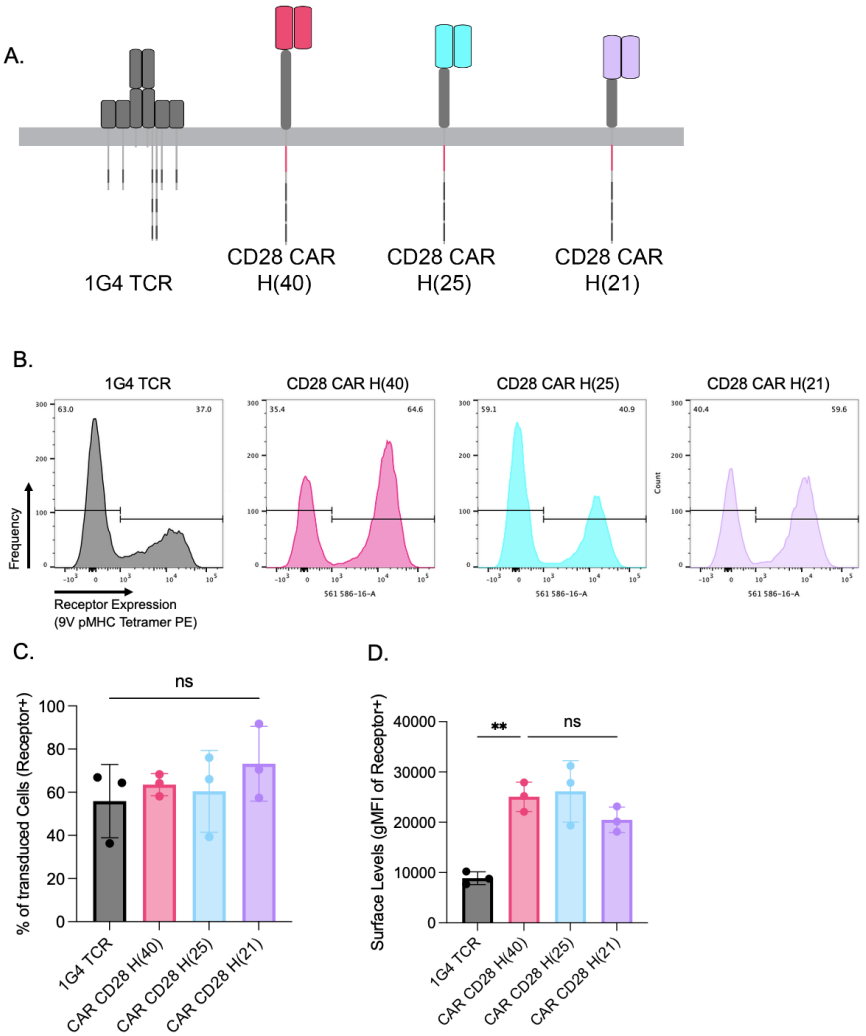

Figure 3.11: Truncated CD28 CAR variants exhibit comparable transduction efficiencies and surface expression levels to the standard CAR. **(A)** Schematic showing CD28 CAR variants with hinges containing 40 (pink), 25 (ice blue), and 21 (lavender) amino acids respectively. **(B)** Flow cytometry histograms showing surface expression of TCR and CAR variants following a 9V tetramer binding assay, used to determine **(C)** transduction efficiencies for each construct, assessed as percentage of receptor$^+$ T cells and **(D)** surface expression levels for each construct, measured using the gMFI of the subset of receptor$^+$ T cells. Data represents N=3 independent experiments from 3 different blood donors. Statistical analysis was performed using a repeated-measures one-way ANOVA, followed by Holm–Šídák's multiple-comparisons test. Significance thresholds were defined as *=$p \leq 0.05$, **=$p \leq 0.01$, ***=$p \leq 0.001$, and ****=$p \leq 0.0001$.

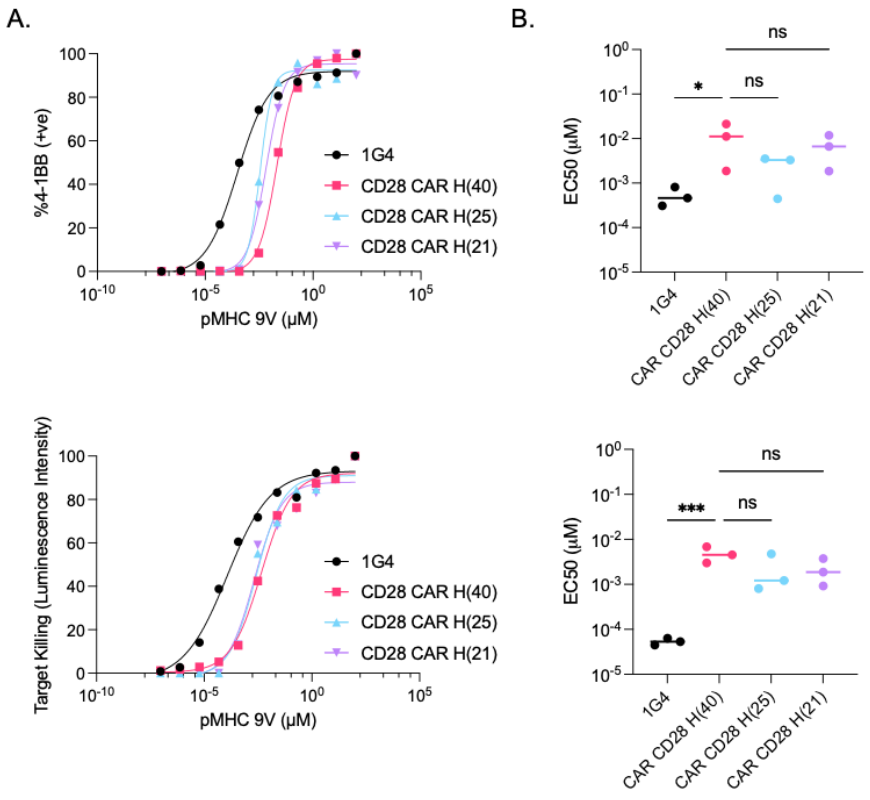

Figure 3.12: Reducing the length of the extracellular hinge of a CAR has no impact on antigen sensitivity. (A) Representative dose-response curves from peptide pulsing experiments using NLuciferase U87 target cells and primary human $CD8^+$ T cells expressing 1G4 TCR (black), CD28 CAR H(40) (pink), CD28 CAR H(25) (ice blue), and CD28 CAR H(21) (lavender) using 4-1BB surface expression (top) and target killing luminescence (bottom) to assess sensitivity. Dose-response curves have been fitted with a Hill function. **(B)** Summary statistics showing EC50 values from N=3 independent experiments with three different blood donors for 4-1BB expression (top) and target killing (bottom). EC50 values were extracted from fitted dose-response curves. Statistical analysis was performed using a repeated-measures one-way ANOVA, followed by Holm–Šídák's multiple-comparisons test. Significance thresholds were defined as *=$p \leq 0.05$, **=$p \leq 0.01$, ***=$p \leq 0.001$, and ****=$p \leq 0.0001$.

CAR exhibited poorer sensitivity than the TCR (Fig 3.12 A and B). However, there were also no differences in sensitivity observed between the full-length CAR and the truncated CAR variants (Fig 3.12 A and B).

3.3 Discussion

CAR-T cells are characterized by low antigen sensitivity, which limits their efficacy against tumours expressing low levels of target antigen and increases the probability of antigen-escape driven disease relapse [241, 242]. Recent modifications to CARs have primarily focused on modifying intracellular signalling domains, leading to improved efficacy against high-density antigens, but these strategies have failed to improve CAR activity towards low-density antigens [233, 243].

The native TCR requires nearly 100-fold less antigen for activation than the standard CAR [158, 161, 232]. This high sensitivity has been suggested to be dependent on exploitation of co-signaling receptors (e.g. CD2), which amplify sensitivity to low antigen densities through adhesion and signal integration at the close contact, a synaptic connection spanning roughly 14 nm between the T cell and the antigen presenting cell. Several integral receptor/ligand complexes appear to interact inside this close contact (e.g. TCR/pMHC, PD-1/PD-L1, and CD2/CD58), all of which span a distance of roughly 14 nm [2, 161, 236].

The CAR may be physically constrained from exploiting these accessory receptors effectively due to its extended extracellular size. Standard CAR designs, including those with CD8α or CD28 stalk regions, have been reported to exhibit larger extracellular dimensions than the native TCR (7.8 nm for TCR versus 10-13 nm for CARs), potentially preventing spatial alignment with accessory receptor-ligand pairs at immune synapse close contacts [2]. This misalignment could limit co-stimulatory input and contribute to the low sensitivity of standard CARs.

In this chapter, we have shown that changes in the extracellular sizes of surface proteins such as CARs, CD2, and PD-1 can impact their ability to integrate their intracellular signalling processes, resulting in changes to antigen sensitivity. We first show that elongation of the PD-1 receptor to the size-optimised PD-1-CD43(40) variant increases its potency by nearly 3-fold, requiring significantly less ligand (187 vs 524 molecules/ μM^2) to achieve a 10-fold inhibition effect (Fig 3.7). We then introduce the truncated "Compact" CAR, which demonstrates enhanced sensitivity compared to the standard CAR and equal sensitivity to the TCR in both sensitivity assays and longitudinal cell killing assays (Fig 3.9 and 3.10). We hypothesize that this improvement in Compact CAR ability is the result of its matched extracellular size with the TCR and therefore its ability to exploit endogenous accessory receptors.

However, the Compact CAR exhibits some structural differences from the standard CAR: it utilises IgG1-CH1 and IgG1-CL regions instead of conventional CD8α or CD28 stalks, thereby exhibiting both a reduction in extracellular size and a modification in structural geometry. In order to test whether the observed enhancement in sensitivity could be solely attributed to size-optimisation, we generated two truncations of a CD28-based standard CAR with the goal of creating standard CAR constructs size-matched to the Compact CAR and the TCR (Fig 3.11). Notably, truncations of the standard CAR did not produce the same increase in sensitivity observed for the Compact CAR (Fig 3.12). Several mechanistic explanations may account for this outcome. First, precise size matching may not have been achieved for the two CAR variants tested. Even small deviations in extracellular length or orientation can disrupt optimal receptor-ligand engagement at the synapse, and it is possible that none of our novel CAR constructs perfectly mimicked the Compact CAR and TCR dimensions. Therefore, testing additional truncations could improve sensitivity results. Second, given its fundamental structural differences from the standard CD28 CAR, the flexibility and steric constraints of the Compact CAR may differ from those of the standard CAR, such that truncation alone would be

insufficient to restore sensitivity. Additional studies could help to elucidate potential causes of the differences in truncated standard CAR and Compact CAR sensitivities. A systematic exploration and screening of all possible CAR lengths using single-amino acid mutations to remove each subsequent amino acid (thereby testing all possible CAR lengths) could help to elucidate whether CAR size modifications alone are sufficient to restore sensitivity. In the event that no tested CAR length has the ability to match TCR or Compact CAR sensitivities, further investigations into the flexibility and steric constraints of the TCR, the Compact CAR, and the standard CAR would be necessary to fully characterise the mechanism behind the enhanced sensitivity of the Compact CAR.

Overall, these findings underscore the importance of spatial considerations in CAR design. Although intracellular signalling modifications can improve CAR potency once engagement occurs, restoring CAR sensitivity to low-density antigens may require changes to CAR extracellular architecture to enhance accessory receptor exploitation. Notably, our studies indicate that the size-matched Compact CAR can recapitulate the sensitivity of native TCRs, highlighting a complementary design principle that could improve CAR efficacy in clinically relevant low-antigen contexts.

4 | Refining CombiCells by size-matching native and SpyCatcher-coupled surface ligands

4.1 Introduction

As shown in previous chapters, accessory receptors can profoundly impact the antigen sensitivities of both TCR-T cells and CAR-T cells [161]. However, understanding the individual and combinatorial contributions of these receptors has proved challenging due to their diversity and variability [130]. Multiple antigen presentation platforms exist to study these interactions, each offering their own distinct advantages and limitations [176].

4.1.1 Traditional Antigen Presentation Systems

4.1.1.1 Genetically Manipulated Antigen Presenting Cells

Genetically engineered APCs have been widely utilised to study accessory receptors [151, 244]. With this system, immortalized cell lines undergo genetic modifications (e.g. CRISPR/Cas9 knockouts or viral transductions) to overexpress, delete, or alter the expression of individual ligands [161]. T cell activation assays comparing modified APCs to unmodified parental lines have been used to investigate how individual accessory receptors, including PD-1 and BTLA, contribute to the complex process of T cell activation [244, 245].

Notably, genetically modified APCs exhibit significant limitations in antigen density characterisation, scalability, and reproducibility. Because these cells are often generated through viral transduction, ligand concentrations cannot be titrated, and the expression of low-density ligands can be challenging to quantify [246]. T cells can respond to even a single pMHC complex on an antigen-presenting cell, a concentra-

tion well below the detection limit of flow cytometry [1,246]. As a result, genetically modified APCs are not the ideal platform for quantifying T cell activation thresholds. Additionally, genetically modified APCs require continuous *in vitro* culture, which introduces the risk of genetic drift. Genetic drift can introduce changes to the expression profiles of surface receptors and intracellular signalling molecules, which can have significant impacts on experimental measurements and potentially compromise the reproducibility of experimental results [178]. Finally, genetically modified APCs require the simultaneous maintenance of multiple cell lines: for each additional accessory ligand studied, several novel APC lines must be generated and cultured in parallel in order to evaluate the ligand's activity under different immune contexts (Fig 4.1) [176,247].

Therefore, while traditional APC systems preserve the structural and contextual features of the immunological synapse, they are often impractical for large-scale studies that depend on precise antigen concentrations and precise ligand combinations.

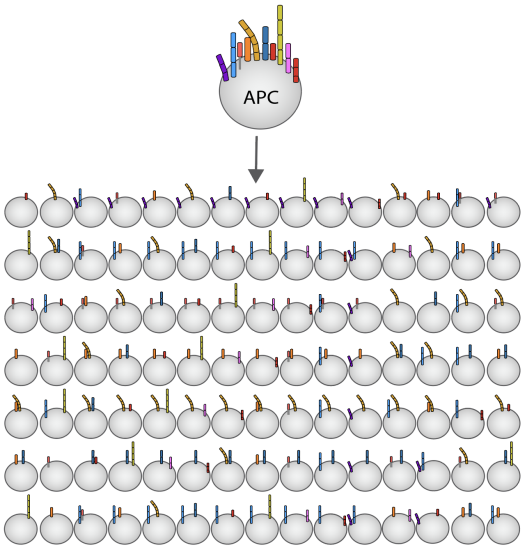

Figure 4.1: Genetically modified antigen-presenting cells

4.1.1.2 Artificial platforms: plates and supported lipid bilayers

Artificial platforms including solid-phase surfaces (plastic and glass plates) and fluid-phase surfaces (supported lipid bilayers/SLBs) have also been widely deployed to study the activity of accessory receptors [248]. For these platforms, the purified extracellular domain of an accessory ligand is coupled to the platform surface through chemical conjugation, affinity tags, or lipid tail insertion in the case of SLBs [249, 250]. This methodology provides a distinct advantage over genetically modified APCs, as ligand combinations and densities can be precisely titrated without the need for verification through flow cytometry.

Solid-phase surfaces have been used to investigate key principles of TCR triggering, including activation thresholds, the influence of ligand spatial organization, and cooperative contributions of accessory receptors [160, 232, 251, 252]. SLBs have been utilised to study the impact of antigen concentration and antigen affinity on T cell responses as well as the role of accessory receptors CD28, PD-1, CD2, and LFA-1 in T cell activation [253–255].

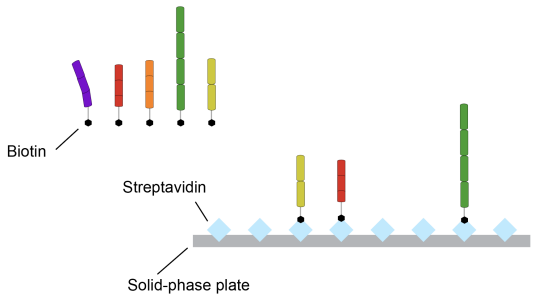

Figure 4.2: Solid-phase antigen presentation platform

Unfortunately, these platforms are limited in their physiological relevance. For solid-phase surfaces, immobilized ligands lack lateral mobility, a parameter central to the kinetic segregation model [177, 256]. SLBs have improved biological relevance compared to their solid-phase counterparts; they allow ligands to retain lateral mobility and exhibit biologically relevant surface stiffness [177]. However, SLB systems are

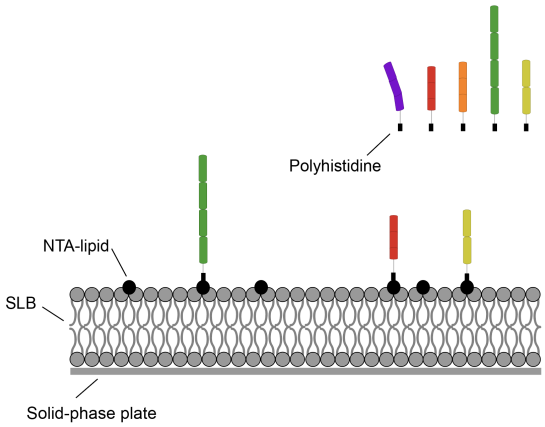

Figure 4.3: Supported lipid bilayer presentation platform

often not high-throughput and therefore lack the necessary scalability required to study all of the receptor/ligand interactions required to fully characterize the immune synapse [176].

4.1.2 The CombiCell System

The CombiCell system was developed to address these shortcomings, offering an antigen presentation platform that enables precise ligand titration under physiologically relevant conditions (Table 4.1) [1, 176].

Table 4.1: Comparison of experimental platforms for ligand presentation and control

	Modified APCs	Solid-Phase	SLBs	CombiCells
Ligand combination studies	✗	✓	✓	✓
Ligand concentration studies	✗	✓	✓	✓
Ligand size conservation	✓	✓	✓	✗
Ligand mobility conservation	✓	✗	✓	✓
Surface stiffness conservation	✓	✗	✓	✓
High-throughput	✗	✓	✗	✓

Because the CombiCell system uses SpyCatcher/SpyTag technology to couple ligands of interest directly to the cell surface, researchers can precisely control the concentrations and combinations of ligands presented [1]. Additionally, because

this platform is cell-based, it supports biologically relevant ligand diffusion kinetics [1, 176].

The CombiCell platform has been used to investigate the impacts of receptor/ligand pairings such as CD2/CD58, PD-1/PD-L1, and LFA/LFA-1 on T cell signalling [1,2]. Its utility has also been demonstrated in the previous two chapters to examine the role of the SLAM family in TCR T cell activation and to quantify the potency of the PD-1/PD-L1 interaction on CAR T cell sensitivity [2].

When utilising a novel platform to investigate T cell activation, it is essential to fully characterize the system and identify any potential limitations or platform artifacts. Notably, the CombiCell system requires that proteins of interest be fused with a SpyTag (ST), which covalently bonds to a SpyCatcher on the CombiCell surface [1]. This SpyTag/SpyCatcher interaction has the potential to increase the extracellular size of the presented ligand.

The SpyTag is a chain of 16 amino acids (RGVPHIVMVDAYKRYK) with no defined secondary structure [1, 257]. SpyCatcher is a 13 kDa globular protein (Fig 4.4) [179, 258,259]. To generate the surface-displayed SpyCatcher required for CombiCells, the globular SpyCatcher protein is fused via a flexible GSSGSGGS linker to a 16-amino-acid hinge region derived from human CD52 (hCD52) (Fig 4.4) [1]. The hCD52-derived hinge is then anchored to the cell surface through a GPI-lipid [260, 261].

Each of these added extracellular domains (the SpyCatcher itself, the flexible linker, and the CD52-derived hinge) has the potential to contribute to the overall size of surface SpyCatcher and, therefore, to the perceived size of the SpyTagged ligand (Fig 4.4). The precise change in size attributable to surface SpyCatcher is difficult to determine, as it can adopt multiple orientations due to the flexibility of the GSSGSGGS linker [262]. However, *in silico* modelling suggests that surface SpyCatcher has the potential to contribute up to 4.6 nm to the overall size of presented ligands (Fig 4.4 B) [49, 263].

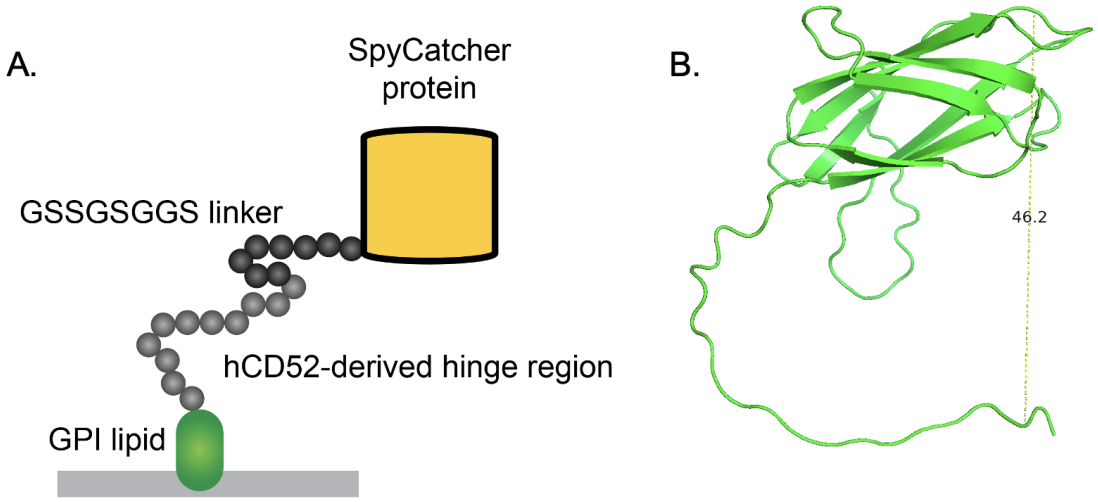

Figure 4.4: Surface SpyCatcher structure representations (A) Stylised and annotated schematic of surface SpyCatcher (not to scale). **(B)** PyMol representation of surface SpyCatcher structure taken from AlphaFold structure prediction model, with end-to-end distances determined using the built-in PyMol distance measurement tool. Surface SpyCatcher size measurements represent an estimate, dependent on hinge stretching and flexibility.

The impact of the size increase resulting from surface SpyCatcher depends on the manner in which the SpyCatcher system is used (Fig 4.5). Under conditions where all ligands of interest are presented on SpyCatcher, as demonstrated in Chapter 2 (The role of SLAM-family co-signalling receptors in T cell antigen recognition), any theoretical increase in size would be universally applied to all ligands, therefore ensuring a size-matched system even while the overall close contact size may exceed that of the endogenous close contact (Fig 4.5, right panel). However, under conditions where one or more of the ligands under investigation are natively expressed on the CombiCell, as demonstrated in Chapter 3 (The role of extracellular size in TCR and CAR-T cell antigen recognition), a potential size mismatch between the SpyCatcher presented antigen and the native co-signalling ligand could exist (Fig 4.5, middle panel). Therefore, it is of interest to thoroughly analyze the CombiCell platform for differences in the activity of SpyTagged and natively presented/endogenous

ligands.

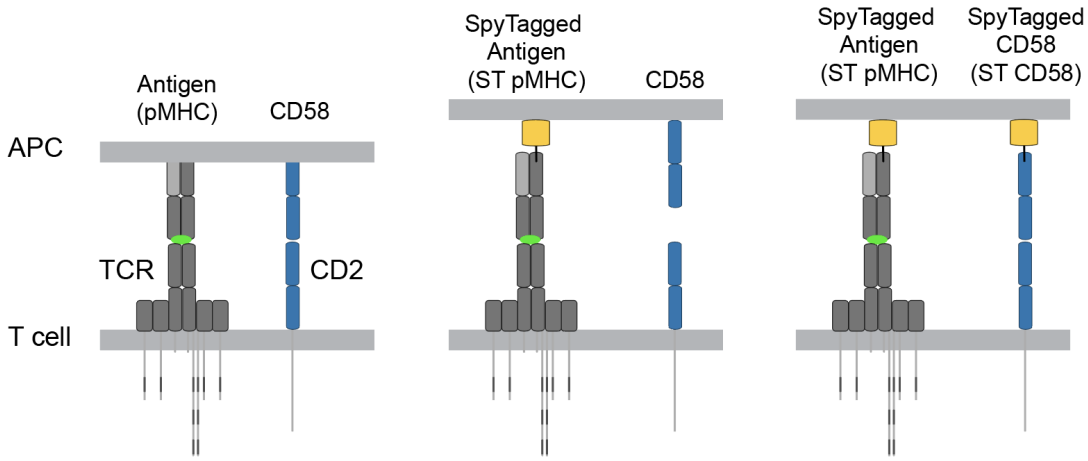

Figure 4.5: Surface SpyCatcher may alter size matching at the close contact. Schematic showing TCR/endogenous pMHC and CD2/endogenous CD58 receptor/ligand pairs (left), TCR/ST pMHC and CD2/endogenous CD58 receptor/ligand pairs (centre), and TCR/ST pMHC, CD2/ST CD58 receptor/ligand pairs.

4.1.3 This Chapter

In this chapter, we compare the potency of SpyTagged and endogenous ligands using the CD2/CD58 receptor/ligand pair as a model system. We then introduce a platform to evaluate CombiCell size matching using elongated CD2 receptor variants. Based on evidence suggesting size discrepancies between endogenous and SpyTagged ligands, we introduce novel surface SpyCatcher variants with truncated hinge regions in an effort to improve SpyCatcher size-matching, testing both transmembrane and GPI-anchored forms.

4.2 Results

4.2.1 SpyTagged ligands may increase TCR sensitivity

In order to investigate the ways in which SpyTagged (ST) ligands might differ from their endogenous counterparts, we utilised the well-characterized CD2/CD58 receptor ligand pair and engineered a platform to assess their relative activities. For this platform, we developed two complementary CombiCell lines: one with endogenous expression of CD58 and one without (Fig 4.6).

We selected human U87 glioblastoma cells as the CombiCell base for this platform due to their endogenous expression of CD58 [161]. However, these cells required several modifications to be suitable for the CombiCell platform (Fig 4.6).

Unlike CHO cells, which are of hamster origin and lack human HLA expression, U87 cells express HLA class I molecules that have the potential to interact with the TCR on Jurkat T cells [264]. To prepare our U87 cells for a CombiCell assay, which titrates a defined pMHC (9V NY-ESO-1), we performed an HLA knockout by using CRISPR/Cas9 to disrupt the β2M gene encoding the β2 microglobulin protein essential for the formation of MHC class I (Fig 4.6) [265]. We verified the knockout using flow cytometry (Fig 4.7 A).

Given that our study design required a direct comparison between the activities of endogenous and SpyTagged CD58, we introduced an additional CRISPR/Cas9 knockout targeting CD58 into the β2M-deficient U87 line, generating double-knockout cells (Fig 4.7 A). Both the β2M single-knockout and β2M/CD58 double-knockout lines were subsequently transduced with surface SpyCatcher and sorted for matched expression (Fig 4.7 B and C).

To look for functional differences in the activity of SpyTagged and endogenous CD58 ligands, we performed an antigen titration assay and compared the sensitivities of

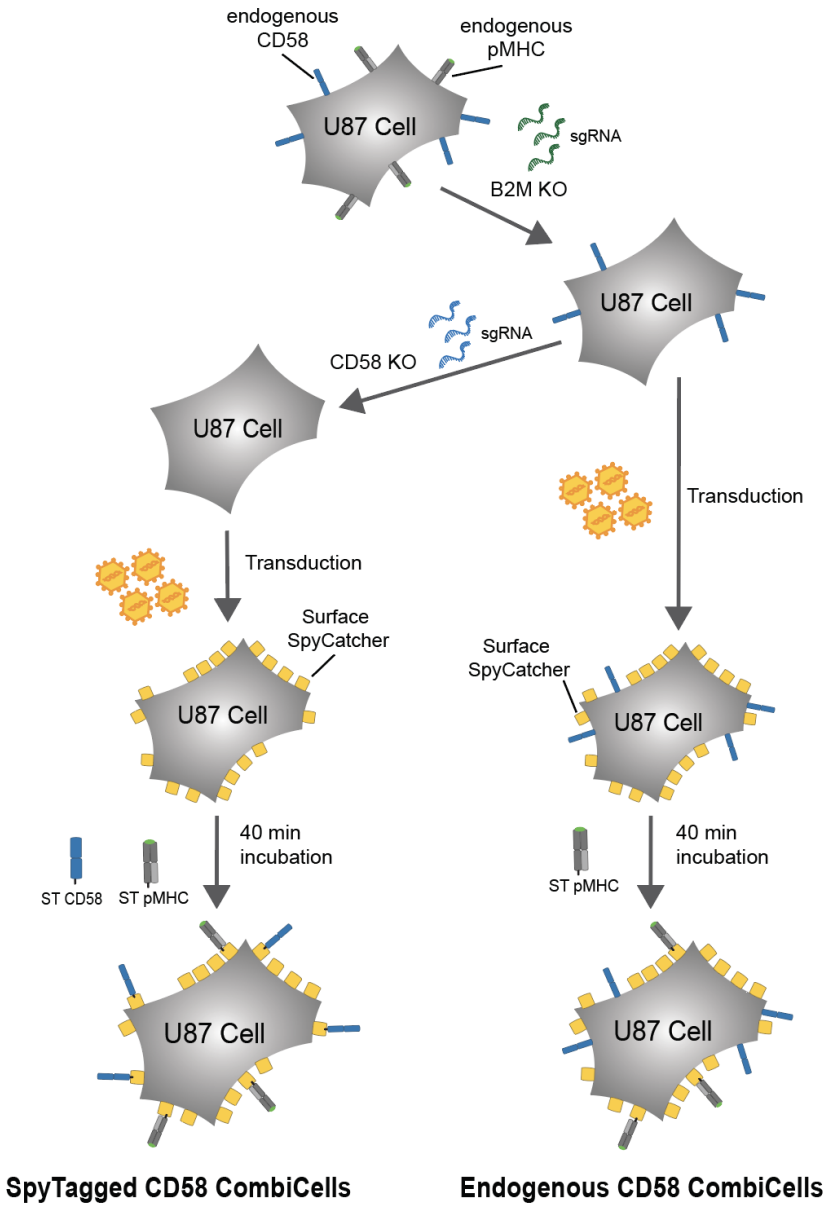

Figure 4.6: Generation of U87 CombiCells A parental U87 cell line underwent either a CRISPR/Cas9-mediated β2M single-KO (right) or a CRISPR/Cas9-mediated β2M/CD58 double-knockout (left). Both cell lines were then transduced with surface SpyCatcher using lentiviral vectors to generate a single-KO (β2M) CombiCell line and a double-KO (β2M/CD58) CombiCell line. The single-KO cells, which endogenously express CD58, could be titrated with the 9V NY-ESO-1 pMHC to generate "Endogenous CD58 CombiCells" while the double-KO cells could be titrated with the 9V NY-ESO-1 pMHC and a constant concentration of ST CD58 to generate "ST CD58 CombiCells."

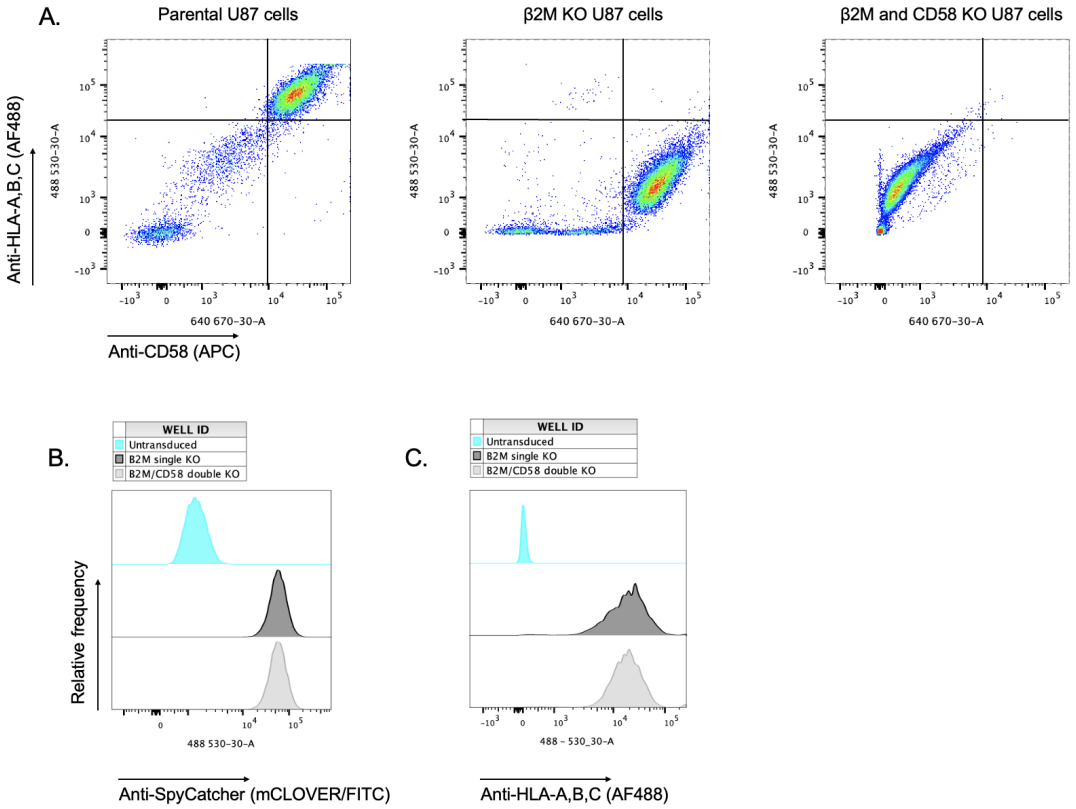

Figure 4.7: Verification of U87 knockout efficacy, SpyCatcher transduction, and ligand loading. **(A)** Flow cytometery dot plots showing expression of CD58 and HLA on parental U87 cells (left), β2M KO U87 cells (centre), and β2M/CD58 KO U87 cells (right). **(B)** Flow cytometry data showing expression levels of surface SpyCatcher following lentiviral transduction and sorting of β2M single-KO U87 cells (black) and β2M/CD58 double-KO U87 cells (grey) with untransduced β2M/CD58 double-KO U87 cells as a control (blue). **(C)** Flow cytometry data showing presentation levels of SpyTagged (ST) 9V pMHC following loading and incubation of 0.1 μM ST 9V pMHC onto β2M single KO U87 cells (black) and β2M/CD58 double-KO U87 cells (grey) with untransduced β2M/CD58 double-KO U87 cells as a control (blue).

1G4/CD2$^+$ Jurkat T cells when presented with either SpyTagged pMHC and endogenous CD58 (presented on β2M single-knockout CombiCells) or SpyTagged pMHC and SpyTagged CD58 (presented on β2M/CD58 double-knockout CombiCells) (Fig 4.8 A). When directly compared, Jurkat T cells presented with SpyTagged CD58 exhibited a 20-fold increase in sensitivity compared to those presented with endogenous CD58 (Fig 4.8 B and C).

4.2.2 Developing a platform to assess size-matching in CombiCells

To look for potential differences in the extracellular sizes of endogenous and SpyTagged CD58 ligands, we developed a platform to assess how receptor and ligand size affects T cell sensitivity.

We transduced CD2 knockout Jurkat T cells with three variants of the CD2 receptor, each of a different size (Fig 4.9 A). For these receptor constructs, we again utilised the mucin CD43 to perform the elongation, generating CD2-CD43(40) and CD2-CD43(234) variants containing 40 or 234 amino acid extensions respectively derived from CD43. These extensions were attached to the extracellular region of CD2 through a short, flexible linker (GSSSS) connecting the C terminus of CD2 to the N terminus of CD43 (Fig 4.9 A) [2]. After transduction, we verified similar receptor expression levels for all CD2 constructs and 1G4 TCRs to ensure that sensitivity changes could not be attributed to differential receptor expression (Fig 4.9 B).

Data from electron microscopy studies suggests that CD43 adopts an extended conformation, with each amino acid contributing on average 0.2 nm to the overall protein size [237]. The flexible linker is estimated to contribute an additional 0.85 nm [2]. Therefore, we theorized a size increase of around 8 nm for the CD2-CD43(40) construct and 47 nm for the CD2-CD43(234) construct. Notably, these estimates assume a fully extended polypeptide backbone [161,237]. However, lengthy polypep-

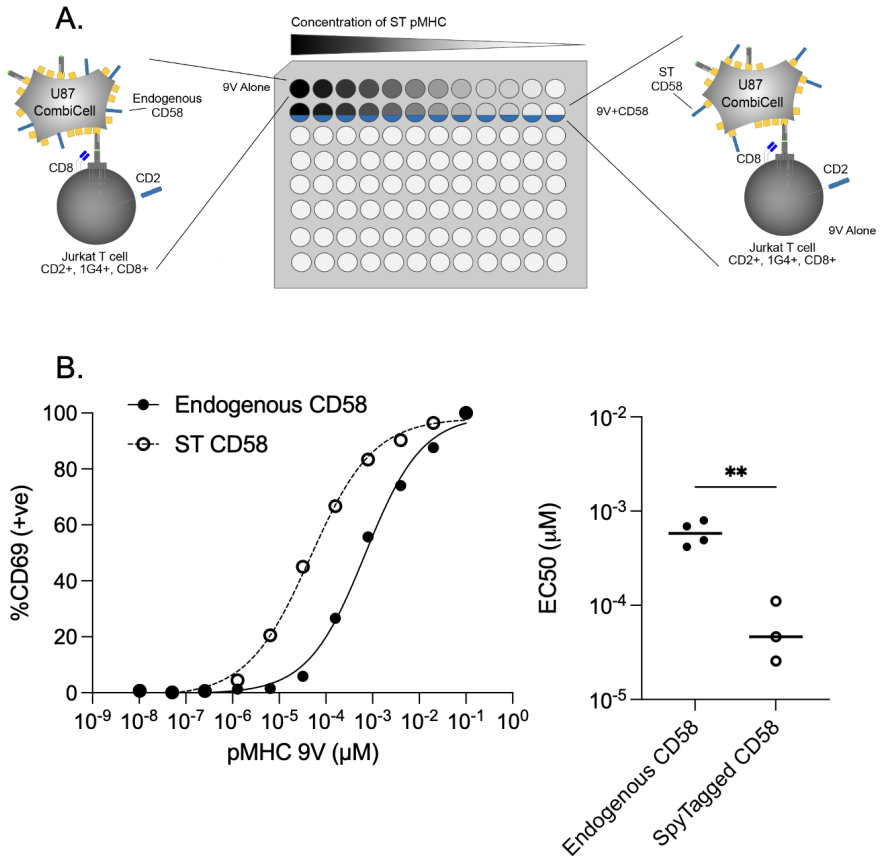

Figure 4.8: SpyTagged CD58 exhibits a higher potency than endogenous CD58. **(A)** Schematic showing titration of 9V NY-ESO-1 peptide (5-fold titration from a maximum concentration of 0.1 μM) on Endogenous CD58 CombiCells (solid circles) and titration of 9V NY-ESO-1 peptide (5-fold titration from a maximum concentration of 0.1 μM) alongside a constant concentration of 0.1 μM ST CD58 on ST CD58 CombiCells (open circles). **(B)** Normalised dose-response curve fitted with a Hill function showing expression of T cell activation marker CD69 (left) and summary statistics showing EC50 values extracted from dose-response curves (right). Statistical analysis was performed using a one-way ANOVA, followed by Holm–Šídák's multiple-comparisons test. Significance thresholds were defined as *=$p \leq 0.05$, **=$p \leq 0.01$, ***=$p \leq 0.001$, and ****=$p \leq 0.0001$.

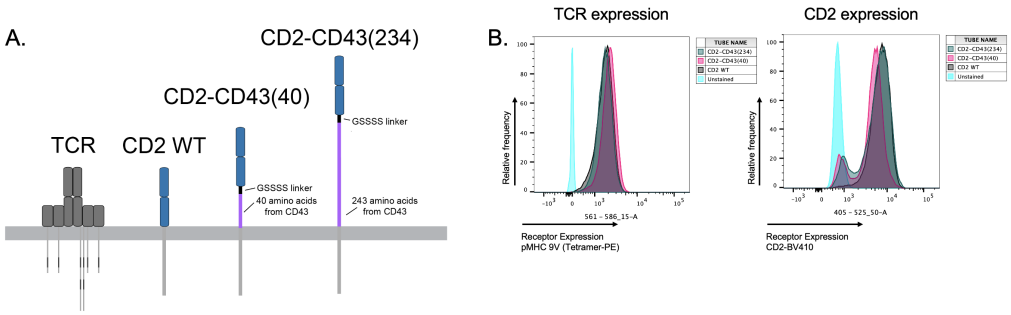

Figure 4.9: Generation of 1G4 Jurkat T cells with elongated CD2 receptors. **(A)** Schematic showing an artistic rendering of the extracellular regions of the TCR, CD2 WT, CD2-CD43(40), and CD2-CD43(234), not to scale. Linker region shown in black, with CD43 amino acid extensions shown in purple. **(B)** Representative flow cytometry histograms showing expression of the 1G4 TCR (left) and CD2 variants (right) for the CD2 WT Jurkat T cell line (black), the CD2-CD43(40) Jurkat T cell line (pink) and the CD2-CD43(234) Jurkat T cell line (teal).

tide chains such as CD2-CD43(234) are unlikely to conform exactly to such a structure [266]. Consequently, the effective molecular extension for CD2-CD43(234) may exhibit a more variable size than the predicted length.

4.2.3 Testing the effect of CD2 variants on Jurkat T cell sensitivity to endogenous CD58 and SpyTagged CD58

To assess the impact of CD2 elongation on T cell sensitivities to endogenous and SpyTagged CD58, we repeated our previous activation assays, titrating peptide to stimulate each of our three Jurkat T cell lines.

Under endogenous CD58 conditions, CD2 WT Jurkats and elongated CD2-CD43(40) Jurkats exhibited equivalent sensitivities (Fig 4.10). However, under SpyTagged CD58 conditions, the elongated CD2-CD43(40) construct exhibited a 30-fold decrease in sensitivity compared to CD2 WT (Fig 4.10). The CD2-CD43(234) Jurkat T cells exhibited significantly decreased antigen sensitivities compared to CD2 WT under both endogenous and SpyTagged CD58 conditions (Fig 4.10).

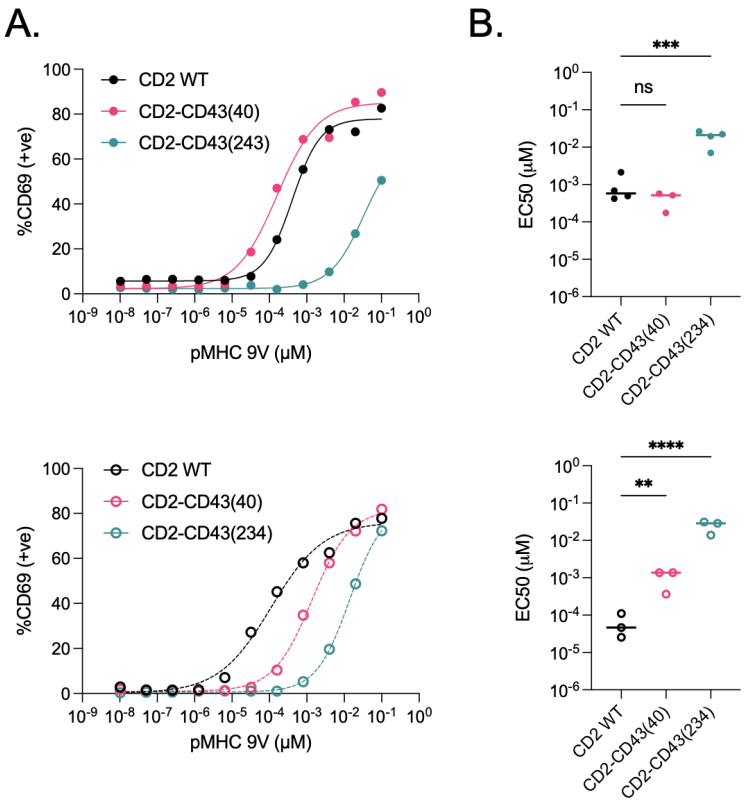

Figure 4.10: WT and elongated CD2 receptors exhibit equivalent sensitivity to native CD58 in CombiCell assays (A) U87 CombiCells expressing either endogenous CD58 (top, closed circles) or ST CD58 (0.1 μM) (bottom, open circles) and presenting a titration of ST 9V NY-ESO-1 pMHC (5-fold titration from a maximum concentration of 0.1 μM) were co-cultured with CD2 WT Jurkats (black), CD2-CD43(40) Jurkats (pink), or CD2-CD43(234) Jurkats (teal). Representative dose-response curves showing changes in expression of T cell surface activation marker CD69 have been fitted with a Hill function. **(B)** EC50 values extracted from dose response curves represent summary statistics from N=3 independent experiments for endogenous CD58 CombiCells (top, closed circles) and ST CD58 CombiCells (bottom, open circles). Statistical analysis was performed using a repeated-measures one-way ANOVA followed by Holm–Šídák's multiple-comparisons test. Significance thresholds were defined as *=$p \leq 0.05$, **=$p \leq 0.01$, ***=$p \leq 0.001$, and ****=$p \leq 0.0001$.

Data from previous studies, as well as earlier chapters in this thesis, suggest that even modest changes in the extracellular dimensions of close-contact accessory receptors can significantly alter T cell sensitivities [2]. However, no measurable sensitivity differences were observed between the CD2 WT and CD2-CD43(40) variants when interacting with endogenously presented CD58, despite the estimated 8 nm difference in the lengths of these receptors. We therefore hypothesised that the lack of a phenotype following CD2 elongation in the context of the CombiCell assay could have arisen from size discrepancies in the mode of antigen presentation: in the endogenous CD58 CombiCell assay, pMHC was presented on surface SpyCatcher whereas CD58 was natively presented. Supporting this, in the SpyTagged CD58 CombiCell assay where both pMHC and CD58 were presented on surface SpyCatcher, the CD2-CD43(40) variant exhibited functional defects.

Taken together, these findings are consistent with a size-mismatch phenotype, wherein the relative dimensions of receptor/ligand pairs, rather than absolute receptor lengths, help govern T cell sensitivities (Fig 4.11). When both CD58 and pMHC are presented via SpyCatcher, TCR/ST pMHC and CD2/ST CD58 interactions can occur in parallel, allowing CD2 engagement to enhance antigen sensitivity. Elongation of CD2 in this context is hypothesised to disrupt the simultaneous engagement of these receptor-ligand pairs, thereby reducing antigen sensitivity relative to WT CD2. In contrast, when only pMHC is SpyCatcher-presented, TCR/ST pMHC and CD2/endogenous CD58 interactions are unlikely to occur in parallel due to a size mismatch, preventing coordinated engagement. Under these conditions, elongation of CD2 has no measurable effect on antigen sensitivity relative to WT CD2 (Fig 4.11).

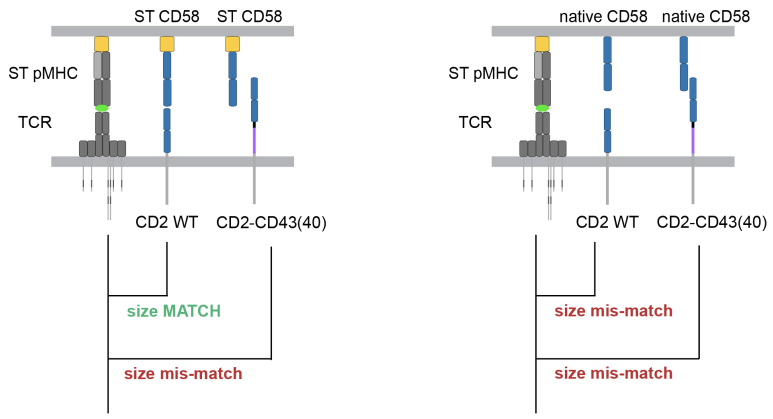

Figure 4.11: Schematic of hypothesized receptor size matching. Schematic showing TCR/ST pMHC interactions under ST CD58 (left) and native CD58 (right) conditions

4.2.4 Truncated SpyCatchers improve T cell sensitivity to endogenous CD58

We have estimated that surface SpyCatcher could contribute an up to 4.6 nm increase in the extracellular size of CombiCell-presented proteins due to the inherent bulk of SpyCatcher itself and the flexible CD52-derived hinge (Fig 4.4).

To test whether truncating the surface SpyCatcher hinge could improve the potency of endogenous CD58, we generated two novel surface SpyCatcher variants: SpyCatcher Δ8 and SpyCatcher Δ15. For the Δ8 construct, we removed the GSS-GSGGS linker. For the Δ15 construct, we removed the linker and all but the GPI-anchoring serine from the CD52 hinge, which is required for surface expression (Fig 4.12 A).

We used lentiviral transduction to introduce these variants into single and double-knockout U87 cells to generate new CombiCell lines. We confirmed using flow cytometry that truncation had no impact on surface SpyCatcher expression or pMHC loading ability, finding that transduction efficiency and expression levels of surface SpyCatcher were matched for all constructs, and that pMHC loading remained con-

sistent despite changes in structure (Fig 4.12 B and C).

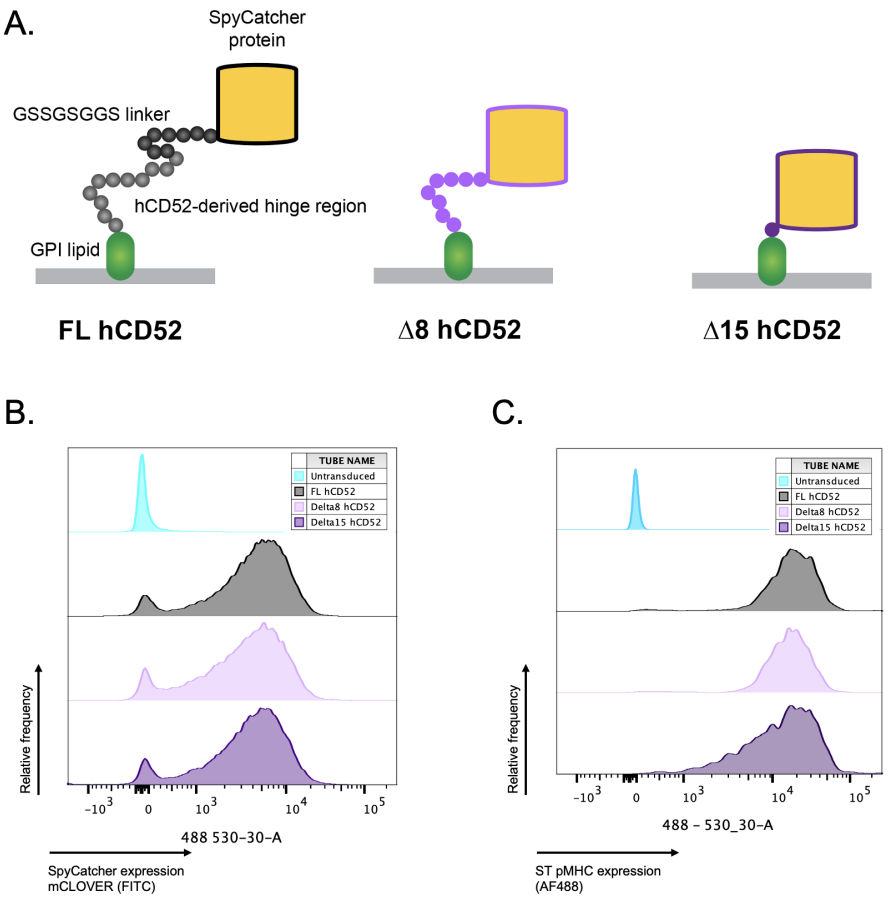

Figure 4.12: Truncated hCD52 surface SpyCatcher variants exhibit no change in transduction efficiency, surface expression, or peptide presentation ability. **(A)** Schematic representations of full-length and novel CD52-derived surface SpyCatcher variants. **(B)** Flow cytometry data showing surface expression levels of FL (black), Δ8 (lavender), and Δ15 (dark purple) CD52-derived surface SpyCatchers on β2M KO CombiCells following sorting. **(C)** Flow cytometry data showing presentation of 9V-pMHC levels for FL (black), Δ8 (lavender), and Δ15 (dark purple) CD52-derived surface SpyCatchers on β2M KO CombiCells after loading with 0.1 μM ST 9V pMHC.

To assess the functionality of these novel CombiCell lines, we utilised our previously derived size-matching platform and performed antigen titration assays using Jurkat T cells expressing CD2 WT, CD2-CD43(40), or CD2-CD43(234) receptors under endogenous and SpyTagged CD58 conditions (Fig 4.13).

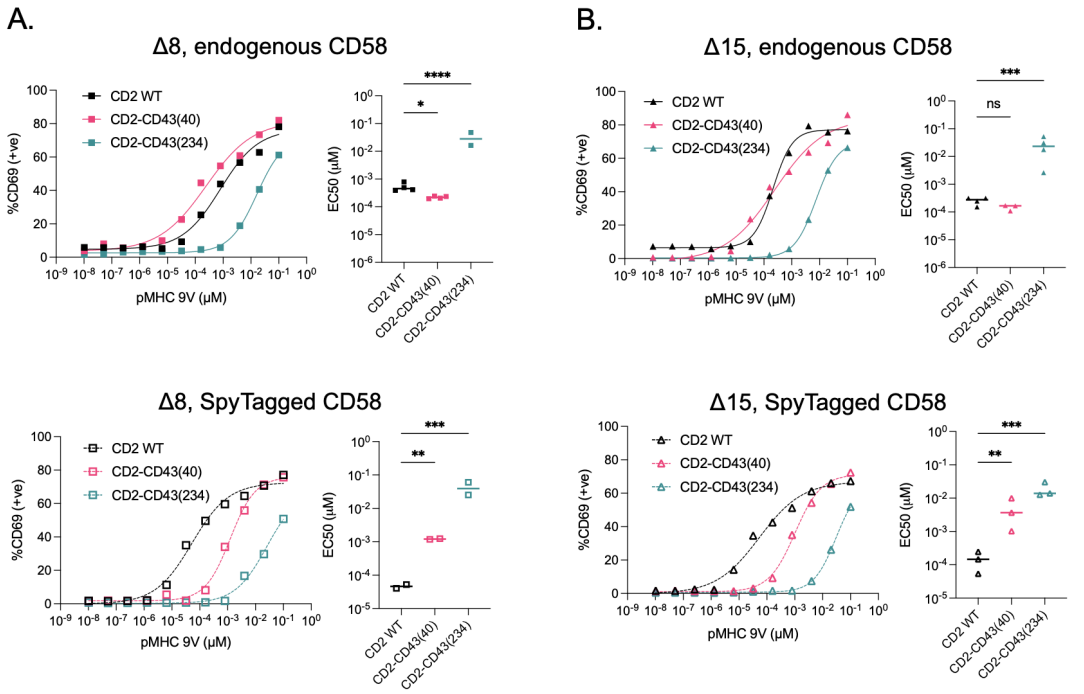

Figure 4.13: Elongation of CD2 does not decrease T cell antigen sensitivity to endogenous CD58, despite truncation of surface SpyCatcher. **(A)** Representative dose-response curves (left) fitted with a Hill function for Δ8 surface SpyCatcher CombiCells under endogenous CD58 (top, closed squares) and SpyTagged CD58 (bottom, open squares) conditions with summary statistics (right) showing EC50 values extracted from dose-response curves. **(B)** Representative dose-response curves (left) fitted with a Hill function for Δ15 surface SpyCatcher CombiCells under endogenous CD58 (top, closed triangles) and SpyTagged CD58 (bottom, open triangles) conditions with summary statistics (right) showing EC50 values extracted from dose-response curves. Statistical analysis was performed using a repeated-measures one-way ANOVA followed by Holm–Šídák's multiple-comparisons test. Significance thresholds were defined as *=$p \leq 0.05$, **=$p \leq 0.01$, ***=$p \leq 0.001$, and ****=$p \leq 0.0001$.

We again found that elongation of CD2 did not lead to a decrease in T cell antigen sensitivity. However, when we performed additional analyses to directly compare the baseline sensitivities to CD2 WT Jurkat T cells for all three novel constructs, we found a two-fold sensitivity enhancement for the Δ15 variant compared to the FL variant (Fig 4.14 A). No statistically significant differences in sensitivity to Spy-Tagged CD58 were observed for any of the constructs tested (Fig 4.14 B).

The elongated CD2 variant is not perfectly size-matched to the CombiCell system - it presents a hypothesised 8 nm size increase relative to CD2 WT whereas SpyCatcher is only hypothesised to induce around a 4.6 nm size change (Fig 4.4 and Fig 4.11). This could serve as one potential explanation for why the Δ15 SpyCatcher variant exhibits enhanced exploitation of natively-presented CD58, as evidenced by its increased sensitivity to CD2 WT compared to FL SpyCatcher, but still exhibits equivalent CD2 WT and CD2-CD43(40) sensitivities (Fig 4.14). Additional testing using other CD2 receptor size variants more closely matched to the hypothesized 4.6 nm SpyCatcher size increase could provide further insight into the relative functionality of the hCD52-derived FL and Δ15 surface SpyCatchers.

4.2.5 Transmembrane SpyCatchers lead to further improvements to endogenous CD58 sensitivities

Having truncated our GPI-anchored SpyCatcher to the maximum extent, we investigated alternative SpyCatcher hinges derived from transmembrane proteins. CD52-derived SpyCatcher expresses by attaching directly to a GPI lipid on the outer leaflet of the plasma membrane, which may itself protrude out from the cell surface. Therefore, a transmembrane hinge SpyCatcher has higher truncation potential, as it integrates directly into the membrane. Furthermore, GPI-anchored proteins and transmembrane proteins can differ in their diffusion behaviours, with GPI-anchored proteins often exhibiting faster lateral diffusion kinetics [267,268]. Therefore, having

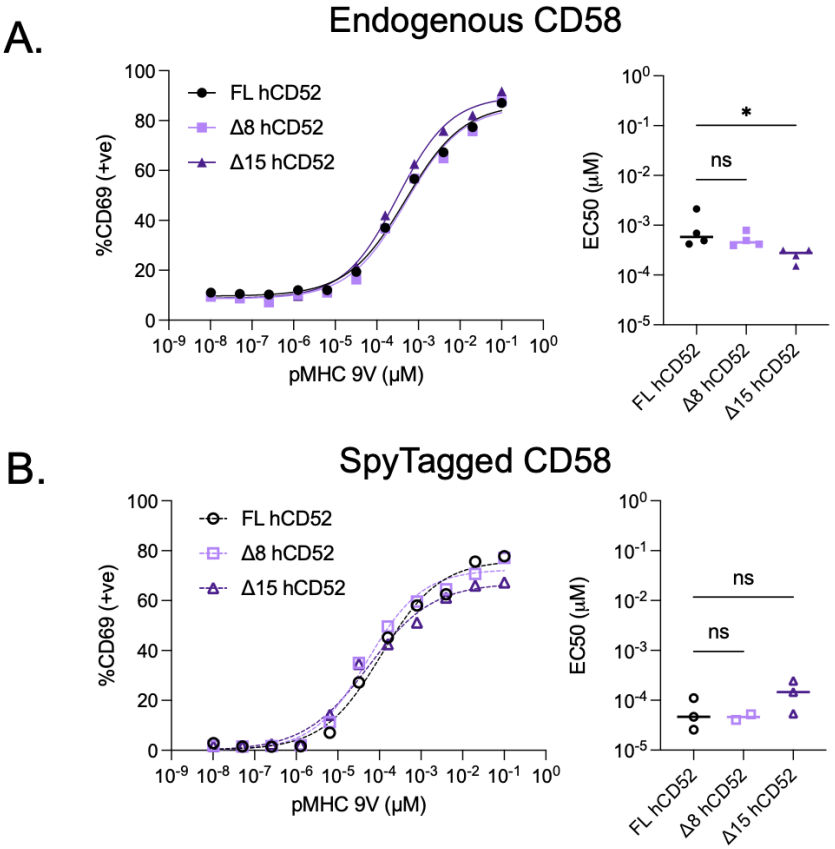

Figure 4.14: CD2 WT Jurkat T cells show enhanced sensitivity to antigen presented on Δ15 SpyCatcher under endogenous CD58 conditions. **(A)** Representative dose-response curves (left) and summary statistics (right) directly comparing CD2 WT Jurkat T cell sensitivities to ST pMHC presented by FL SpyCatcher (black), Δ8 SpyCatcher (lavender), and Δ15 SpyCatcher (dark purple) under endogenous CD58 conditions. **(B)** Representative dose-response curves (left) and summary statistics (right) directly comparing CD2 WT Jurkat T cell sensitivities to ST pMHC presented by FL SpyCatcher (black), Δ8 SpyCatcher (lavender), and Δ15 SpyCatcher (dark purple) under 0.1 μM SpyTagged CD58 conditions. Statistical analysis was performed using a repeated-measures one-way ANOVA followed by Holm–Šídák's multiple-comparisons test. Significance thresholds were defined as *=$p \leq 0.05$, **=$p \leq 0.01$, ***=$p \leq 0.001$, and ****=$p \leq 0.0001$.

two SpyCatcher hinge options could be of benefit in the event that the SpyTagged ligands under investigation differ in their endogenous surface expression mechanisms.

We initialised a screening process to characterise the activity of transmembrane candidates derived from human CD28 (hCD28), human CD86 (hCD86), and mouse CD80 (mCD80) proteins. Unlike GPI-anchored hinges, transmembrane hinges contain both intracellular and extracellular domains. Consequently, we needed to truncate both regions during our screening process in order to prevent surface SpyCatcher itself from contributing to intracellular signalling within the CombiCell. We found that excess truncation of either the intracellular or extracellular domain led to poor surface expression, so we completed an iterative screening process during which we tested the surface expression of multiple size variants for each construct (hCD28, hCD86, mCD80) in an effort to create the shortest hinge possible without impacting SpyCatcher surface expression. Following our screening process, we identified one truncated candidate per parental construct (Δ3 CD28, Δ10 CD86, and Δ14 CD80) and transduced our single-KO U87 cells with these constructs. We sorted for matched expression of surface SpyCatcher and performed a loading control experiment to ensure that all novel constructs could load SpyTagged proteins (Fig 4.15 A and B). Having validated the functionality of our novel CombiCell lines, we again performed our standard antigen sensitivity titration assay using CD2 WT Jurkat T cells as our effectors. We compared the sensitivities of CD2 WT Jurkat T cells to pMHC presented on parental full-length transmembrane hinges and truncated transmembrane hinges, using the Δ15 hCD52-derived GPI variant as a control (Fig 4.16 A, B, and C).

For CD86-derived and CD80-derived surface SpyCatchers, the full-length variants exhibited poorer antigen sensitivities than the truncated variants (Fig 4.16 B, and C). This same phenomenon was not observed for the CD28 variant (Fig 4.16 A); however, the CD28 variant was given the smallest overall truncation (removal of 3 amino acids as opposed to removal of 10 and 14 amino acids for CD86 and CD80

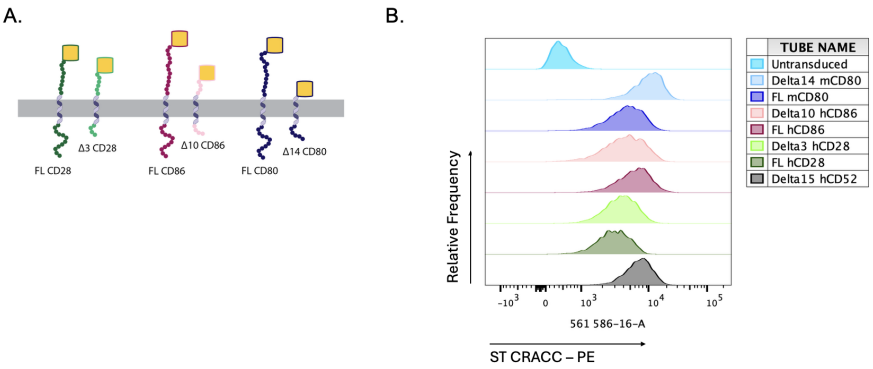

Figure 4.15: Transmembrane surface SpyCatchers have similar loading capacities to GPI-anchored surface SpyCatchers (A) Schematic representation of full-length and truncated transmembrane surface SpyCatcher candidates derived from CD28 (green family), CD86 (red family), and CD80 (blue family). **(B)** Flow cytometry data showing loading capabilities of each novel surface SpyCatcher construct. Single-KO U87 CombiCell lines transduced with novel surface SpyCatchers and sorted for matched expression were incubated with 0.1 μM of ST CRACC, washed, and stained with a fluorescently-conjugated monoclonal antibody targeting CRACC (PE) to test loading capabilities. The Δ15 hCD52 SpyCatcher (bottom, black) was used as a positive control for loading. Untransduced U87 lines were used as a negative control for loading (top, light blue).

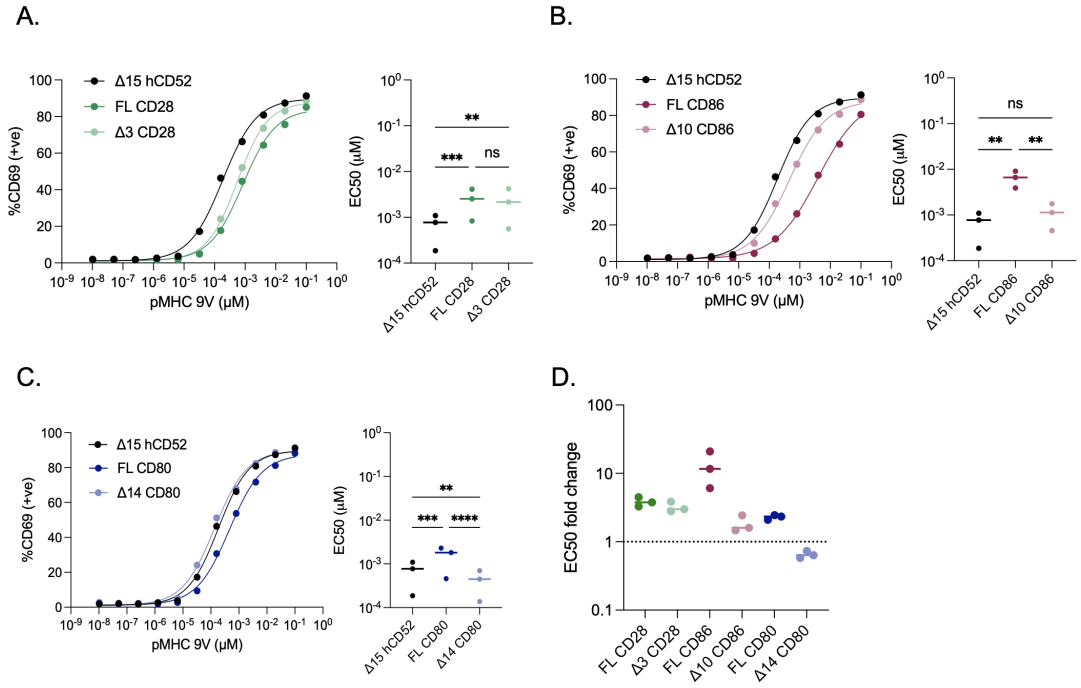

Figure 4.16: Truncated CD80 transmembrane surface SpyCatcher exhibits improved sensitivity compared to truncated GPI-anchored surface SpyCatcher (A) Representative dose-response curves showing CD69 expression fitted using a four-parameter logistic model (variable slope), equivalent to a Hill function (right) and summary statistics representing EC50 values extracted from fitted dose-response curves from N=3 independent experiments. Data was collected from CombiCell antigen titration experiments using CD2 WT Jurkat T cells co-cultured with CombiCells presenting a titration of the 9V NY-ESO-1 peptide (5-fold down from a maximum concentration of 0.1 μM) presented on **(A)** hCD28-derived surface SpyCatchers, **(B)** hCD86-derived surface SpyCatchers, and **(C)** mCD80-derived surface SpyCatchers using the Δ15 CD52-derived surface SpyCatcher (black) as a control. Statistical analysis was performed using a repeated-measures one-way ANOVA followed by Holm–Šídák's multiple-comparisons test. Significance thresholds were defined as *=$p \leq 0.05$, **=$p \leq 0.01$, ***=$p \leq 0.001$, and ****=$p \leq 0.0001$. **(D)** Fold-change in EC50 values comparing each construct to the Δ15 CD52 control within each independent experiment.

respectively).

The Δ14 CD80 hinge exhibited a two-fold decrease in sensitivity relative to even the Δ15 hCD52 hinge, suggesting this variant as a potential candidate for additional studies (Fig 4.16).

Notably, this study design utilised a high concentration of SpyTagged CD58 (0.1 μM). High ligand concentrations are typically used in CombiCell stimulation assays in an effort to achieve ligand saturation and maximize the likelihood of observing a phenotype [1, 2]. However, differences in the expression levels of endogenous and SpyTagged CD58 molecules could induce changes in T cell sensitivity, as increased CD58 concentrations could lead to an increased frequency of CD2/CD58 interaction. To determine whether the observed sensitivity changes could be attributed to changes in CD58 surface abundance as opposed to being an artifact of the SpyTag/SpyCatcher system, we used flow cytometry to compare the expression levels of SpyTagged and endogenous CD58 (Fig 4.17).

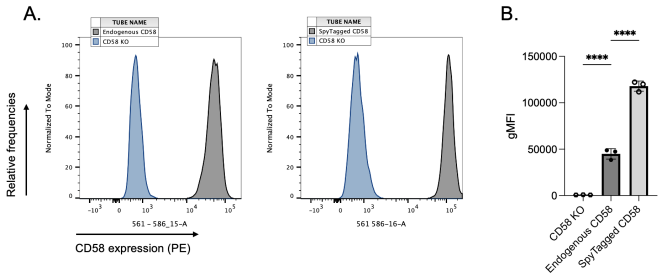

Figure 4.17: SpyTagged CD58 at a concentration of 0.1 μM exhibits higher surface expression than endogenous CD58. **(A)** Representative flow cytometry histograms showing surface expression of endogenous CD58 (left) and 0.1 μM SpyTagged CD58 (right) in black, using U87 CD58 KO cells as a negative control (blue). **(B)** Summary statistics using gMFI to compare CD58 surface expression levels. Statistical analysis was performed using a repeated-measures one-way ANOVA, followed by Holm–Šídák's multiple-comparisons test. Significance thresholds were defined as *=$p \leq 0.05$, **=$p \leq 0.01$, ***=$p \leq 0.001$, and ****=$p \leq 0.0001$.

We found a three-fold increase in the surface expression of 0.1 μM SpyTagged CD58

as compared to the surface expression of endogenous CD58 (Fig 4.17 B). This difference in CD58 surface density could help explain the increased potency of SpyTagged CD58. Additional sensitivity studies with matched expression of endogenous and SpyTagged CD58 ligands are required to provide further insight into any definitive potency differences between SpyTagged and endogenous CD58.

4.3 Discussion

CombiCells have recently emerged as a novel antigen presentation platform capable of overcoming many of the common technical pitfalls of other systems utilised previously to investigate the contributions of accessory receptors and ligands to T cell activation [1, 2, 176]. By leveraging SpyCatcher/SpyTag technology, CombiCells allow researchers to present ligands of interest at any desired concentration or combination on a surface that preserves biologically relevant stiffness and ligand diffusion kinetics [1, 179]. However, the inherent bulk of the 13 kDa SpyCatcher protein and its CD52-derived hinge has the potential to increase the size of ligands, potentially introducing a mismatch in receptor/ligand pairs in experiments where only one ligand is presented on SpyCatcher [179, 258]. In this chapter, we endeavoured to investigate the potential for any size discrepancies between endogenous and SpyTagged CD58 ligands using T cell sensitivity assays with CD2 receptors of varying lengths. We found that elongated and WT CD2 receptors exhibit equivalent sensitivities when presented with the endogenous CD58/SpyTagged pMHC pairing, counter to what we would expect if the SpyCatcher system had no effect on extracellular ligand sizes. This same phenomenon was not observed with the SpyTagged CD58/SpyTagged pMHC pairing (Fig 4.10).

In order to improve the exploitation of endogenous CD58, we developed two novel CD52-derived surface SpyCatchers, removing either the flexible linker region alone (Δ8 variant) or both the flexible linker and the majority of the CD52-derived hinge

(Δ15 variant). Truncation had no impact on either the surface expression of SpyCatcher or the loading of SpyTagged peptides (Fig 4.12). We found that, under endogenous CD58 conditions, presenting pMHC on the Δ15 hCD52-derived surface SpyCatcher instead of the full-length hCD52 variant led to a two-fold enhancement in antigen sensitivity (Fig 4.14).

Having truncated our CD52-derived, GPI-anchored surface SpyCatcher to the maximum extent, we then transitioned to testing transmembrane SpyCatcher hinges in the hopes that these hinge variants would allow ligand presentation to occur closer to the cell surface than what would be possible with a GPI-anchored hinge. Additionally, given differences in the behaviour and diffusion kinetics of native transmembrane and GPI-linked ligands, we wanted to ensure that we developed both a transmembrane surface SpyCatcher and a GPI-linked surface SpyCatcher to allow CombiCell users the option of selecting a surface SpyCatcher variant capable of mimicking native ligand activity to the greatest extent possible [1, 267].

We developed a truncated transmembrane hinge derived from a mouse CD80 protein capable of providing a two-fold enhancement (relative to the truncated CD52-derived hinge) in antigen sensitivity under endogenous CD58 conditions (Fig 4.16). Other transmembrane hinges tested did not yield such significant sensitivity enhancements, but we did observe a correlation between the extent of the truncation and the resultant improvement in sensitivity, with larger truncations leading to more significant changes in antigen sensitivities (Fig 4.16).

Notably, our study has several limitations that warrant further investigation to strengthen our conclusions. First, the concentration of SpyTagged CD58 used (0.1 μM) produced significantly higher surface expression than what was observed with endogenous CD58 (Fig 4.17). While such high ligand levels are useful for assessing overall phenotypes, the discrepancy in expression prevents direct activity comparisons between endogenous and SpyTagged ligands [1, 2]. Follow-up studies

comparing the activity of SpyTagged CD58 at a concentration matching that of endogenous CD58 would provide further insight into any artifacts contributed by the SpyCatcher/SpyTag system. These studies could either involve overexpression of CD58 on base U87 cells or a titration of SpyTagged CD58 to determine the optimal concentration for comparison.

Additionally, the platform used to assess the impacts of receptor and ligand sizes on T cell sensitivity lacked exact size matching. While the CD2 elongation experiments showed that a modest increase in CD2 receptor size was insufficient to induce a sensitivity change under conditions with SpyCatcher-presented antigen but native co-stimulatory ligand, this effect remained consistent even when we truncated surface SpyCatcher. Because our CD2 elongation was not matched in size to the FL hinge or the truncated hinge, we were unable to use this assay to further highlight any potential sensitivity improvements induced by the Δ15 hinge. Additional experiments with a CD2 hinge elongated by 4.6 nm (size-matched to the hypothesised surface SpyCatcher size) would be expected to exhibit improved sensitivity compared to CD2 WT within the FL CD52-derived CombiCell system but poorer sensitivity than the CD2 WT within the Δ15-derived system.

Finally, our experimental design could benefit from the addition of additional controls including a CD58-negative condition and an endogenous CD58 condition involving native antigen presentation. The former would provide further information on the activity of T cells in the absence of CD58-mediated co-stimulation while the latter would provide a baseline for the activity of T cells under fully endogenous conditions, with the SpyTag/SpyCatcher system playing no role (Fig 4.18).

Together, our data indicate a potential size discrepancy between endogenous CD58 and SpyTagged CD58 and suggest that truncation of both GPI-anchored and transmembrane surface SpyCatcher hinges can enhance exploitation of endogenous CD58.

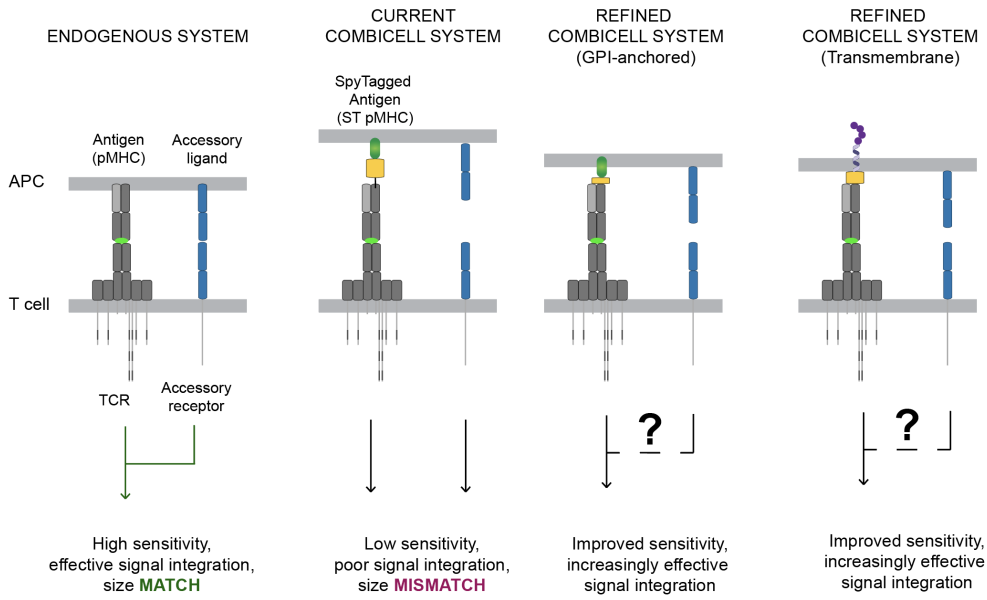

Figure 4.18: Summary schematic of surface SpyCatcher truncations and their effects on the extracellular sizes of presented ligands Schematic showing TCR/ST pMHC interactions under endogenous conditions (far left) and CombiCell conditions with ST pMHC presented on either full-length hCD52-derived surface SpyCatcher (left), truncated hCD52-derived surface SpyCatcher (right), or truncated mCD80-derived surface SpyCatcher (far right).

5 | Discussion

5.1 Contextual relevance

T cell accessory receptors play an integral role in T cell activation, helping to determine the functional outcomes of TCR signalling [130, 133]. These receptors exhibit great diversity in their expression, structure and function, with co-stimulatory receptors (e.g. CD2 and 4-1BB) capable of amplifying the T-cell response while co-inhibitory receptors (e.g. PD-1 and BTLA) can suppress it [133]. Achieving this balance between activating and inhibitory inputs is critical for fine-tuning the immune response, and co-signalling receptors have therefore become highly attractive targets for the development of novel immunotherapeutics [269]. The clinical importance of these molecules is underscored by their successful exploitation in checkpoint blockade therapies (e.g. PD-1 inhibition) and in the design of synthetic CAR-T cells, where intracellular domains from receptors such as CD28 and 4-1BB have been incorporated into the receptor design in order to enhance T cell function [270].

While there are many studies focusing on the role of the intracellular signalling pathways involved in T cell co-stimulation and co-inhibition, few investigations have focused on quantifying the impact of accessory receptors on quantitative T cell responses, such as antigen sensitivity [2, 133, 161]. This is likely due in part to the significant technical limitations of conventional APC-based systems, in which generating different combinations of surface proteins requires repeated knockouts or transductions [176]. These approaches are time-consuming and necessitate the generation of multiple cell lines, which are susceptible to genetic drift during prolonged culture [178]. Such constraints have limited our ability to systematically examine the impacts of accessory receptors on T cell activation.

Artificial platforms including solid-phase surfaces such as plastic and glass plates and

fluid-phase surfaces such as SLBs have also been used previously to quantitatively assess accessory receptor contributions to T cell antigen sensitivities [43, 131, 253]. However, while these systems do allow researchers to maintain control over ligand combinations and antigen densities, they also have significant limitations: solid-phase surfaces prevent lateral ligand mobility and SLBs often are not sufficiently high-throughput to perform the large-scale investigations required to fully characterise the immunological synapse [176].

Systematic investigations into the individual and combinatorial roles of accessory receptors require an experimental approach that is biologically relevant, high-throughput, and highly modular [176]. The CombiCell system was specifically developed to address these shortcomings, offering an antigen presentation platform enabling precise and high-throughput ligand titration capabilities while maintaining physiologically relevance [1, 176]. The CombiCell system has been widely utilised to investigate the impacts of receptor/ligand pairings (including CD2/CD58, PD-1/PD-L1, and LFA/LFA-1) on T cell signalling. This platform has also been utilised alongside SLBs to assess the impact of the physical anchoring of the ICAM1 receptor on downstream signalling pathways, providing a direct comparison point between the two antigen presentation systems [271].

5.2 Thesis aims

In this thesis, we employ the CombiCell system to quantitatively investigate the role of SLAM-family receptors in T cell antigen recognition. We further utilise the system to quantify the potencies of accessory receptors in the context of CAR-T cells, with an emphasis on understanding the role of extracellular sizes in the processes of TCR and CAR-T cell antigen recognition. Finally, we focus on assessing the system itself and understanding its advantages and limitations, as well as considerations required for future use.

5.3 Essential findings, future work, and limitations

5.3.1 Investigating the contributions of SLAM-family receptors in antigen recognition

5.3.1.1 Essential findings

In Chapter 2, we utilised the CombiCell system to systematically assess the impact of SLAM receptor family engagement on T cell sensitivity. When using Jurkat T cells as our effector cells, we found that engagement of homophilic SLAM receptors CD150, CD84, Ly9, and CRACC had no impact on T cell sensitivity. However, using this same model system, we observed a 5-fold increase in T cell sensitivity upon engagement of the 2B4 receptor with its cognate ligand, CD48. We noted that the 2B4-mediated sensitivity enhancement was lower than what was observed upon engagement of the structurally similar CD2 receptor (which contributed a 10-fold sensitivity increase under the same experimental conditions), and hypothesized that this difference in effect size could be the result of either differences in intracellular signalling processes or differences in receptor/ligand complex flexibility.

Following our Jurkat T cell investigations, we moved to studying SLAM receptor activity in primary $CD8^+$ human T cells, in the hopes that this model system would increase the number of experimental read-outs and allow us to assess SLAM-mediated effects on diverse T cell effector responses. We found that pMHC stimulation of primary $CD8^+$ T cells led to upregulation of SLAM receptors CD150, CRACC, and CD84, but no sensitivity changes were observed when these receptors were presented with their cognate ligands, as assessed when using CD69 and 4-1BB as a measure of activation. However, when using IL-2 production as a T cell response marker, we found a 7-fold decrease in maximal IL-2 production upon CD150 engagement and a 3-fold decrease in antigen sensitivity upon CRACC engagement.

5.3.1.2 Significance, future work, and limitations

Our studies exhibited several limitations in experimental design and scope; we therefore recommend additional experiments to further investigate these concepts.

Within the context of the SLAM system, the diversity of expression of these receptors across multiple haematological cell types (e.g. NK cells, T cells, dendritic cells, monocytes) and the variety of intracellular adaptor molecules they can recruit prevents one single model system from accurately capturing all potential SLAM-mediated effector functions [182]. Although using $CD8^+$ primary human T cells as effector cells did elucidate some SLAM-mediated functions not revealed through Jurkat studies (e.g. changes in IL-2 production), this model system is still unlikely to be able to recapitulate all potential SLAM-mediated signalling pathways, in particular due to the lower expression of EAT-2 in $CD8^+$ T cells relative to NK cells [204, 272]. To increase our understanding of SLAM-receptor functions across different haematological cell types, additional studies on NK cells, which have been used previously to study CRACC-mediated EAT-2 recruitment, are merited [204]. NK cells are also known to express 2B4 and NTB-A; therefore NK-derived effector cells could provide essential data on the activity of several different SLAM family members [273].

In addition, the scope of this thesis includes only a small subset of potential readouts (e.g. flow cytometry analysis of CD69 and 4-1BB expression and ELISA analysis of IL-2 secretion). Predictions on the mechanisms through which SLAM receptor engagement facilitates these T cell responses have been speculated upon here, but not tested. To more thoroughly characterise the intracellular pathways involved in these T cell responses, more in-depth biochemical studies assessing recruitment of intracellular adaptors, phosphorylation, and activation of transcription factors would be of use.

Despite these limitations, the findings reported here regarding the effect of 2B4

engagement on Jurkat T cell activation and the roles of CRACC and CD150 on IL-2 production do suggest an important role played by SLAM family members in the complex process of T cell activation, and all further studies suggested could help elucidate potential roles for these receptors as immunotherapeutic targets.

5.3.2 Determining the role of extracellular size in TCR and CAR-T cell antigen recognition

5.3.2.1 Essential findings

In Chapter 3, we expanded our investigation on the role of accessory receptors in T cell activation to include CAR-T cell studies, as CAR-T cells reportedly exploit accessory receptors with less efficacy than TCR-T cells, despite the critical role these molecules play in activation [161]. We built upon previous work showing that elongation of accessory receptors increases their effect on CAR-T cell antigen recognition, using CombiCells to precisely quantify the potency of the elongated PD-1 receptor [2]. We again deployed the CombiCell system to assess the efficacy of a novel CAR receptor, the Compact CAR, engineered to be size-optimised for accessory receptor engagement. We found that the Compact CAR exhibited increased sensitivity and efficacy compared to the standard CAR in both CombiCell sensitivity assays and longitudinal cell-killing assays. We generated truncated variants of the standard CAR in an effort to determine whether changes to extracellular dimensions alone are sufficient to restore CAR sensitivity, but we found no such sensitivity improvements for any of the size variants we tested.

5.3.2.2 Significance, future work, and limitations

In the context of CAR-T cell activation, our co-signalling receptor studies highlight the importance of extracellular dimensionality in mediating receptor activity, with elongated accessory receptors performing poorly when paired with the relatively

shorter TCR but exhibiting enhanced performance with their size-optimised CAR partners [2]. This conclusion is further supported by the enhanced sensitivity of the Compact CAR, which matches the extracellular dimensions of the TCR and exhibits improved activity compared to the standard CAR across both sensitivity assays and longitudinal cell killing assays [2]. However, the Compact CAR exhibits several structural differences from the standard CAR in its hinge, and truncations of the standard CAR did not produce the same sensitivity enhancements observed for the Compact CAR [2].

Of note, we tested a limited number of hinge size variants, and it has been reported that even small deviations in the extracellular dimensions of receptor/ligand pairs can be enough to disrupt optimal co-signalling [2]. We therefore highly recommend testing additional truncations through a systematic screening process involving removal of each subsequent amino acid from the standard CAR hinge in an effort to determine whether optimisation of standard CAR size could be sufficient to restore its sensitivity to that of the TCR. Based on the results of such a screening process, additional investigations into standard and Compact CAR flexibilities and steric constraints could be merited.

In conclusion, the findings of these experiments underscore the importance of spatial considerations in CAR design when attempting to enhance CAR sensitivity to low-density antigens.

5.3.3 Refining the CombiCell system by investigating size-matching between native and SpyCatcher-presented ligands

5.3.3.1 Essential findings

In Chapter 4, we attempted to determine whether the CombiCell platform itself introduces a size-mismatch between native and SpyCatcher-presented surface ligands by comparing the potency of SpyTagged and endogenous CD58. We tested the sensitivities of Jurkat T cells with CD2 receptors of varying lengths in systems expressing either endogenous CD58 or SpyTagged CD58. We found that both elongated and WT CD2 receptors exhibited equivalent sensitivities when presented with the endogenous CD58/SpyTagged pMHC pairing, but the elongated CD2 receptor showed a decrease in sensitivity compared to the WT when presented with the SpyTagged CD58/SpyTagged pMHC pairing. We hypothesised that the lack of a phenotype for elongated CD2 could be the result of a size-mismatch phenotype contributed by the extracellular domain of surface SpyCatcher and created a hypothesis suggesting that the relative dimensions of receptor/ligand pairs, rather than absolute receptor lengths, govern T cell sensitivities.

We therefore developed novel surface SpyCatchers of varying dimensions and found that by decreasing the extracellular size of the surface SpyCatcher hinge region (thereby bringing the SpyTagged ligand closer to the surface of the CombiCell), we could increase effector T cell sensitivities to endogenous CD58. This finding remained consistent for both GPI-anchored surface SpyCatchers and transmembrane surface SpyCatchers. Overall, these findings suggest a potential size discrepancy between endogenous CD58 and SpyTagged CD58 and provide evidence to support the idea that truncation of surface SpyCatcher hinge regions can enhance exploitation of endogenous CD58.

5.3.3.2 Significance, future work, and limitations

The importance and utility of the CombiCell platform itself is supported by the contents of this thesis, which has shown that T cell activation is a highly context-specific phenomenon, requiring the presence of essential adaptor molecules, precise T cell/APC interface dimensions, and specific ligand concentrations and combinations [1, 2, 133, 176]. Deviations to these criteria can mask important effector functions, making it of high importance to employ a high-throughput and physiologically relevant platform when interrogating the roles of these co-signalling molecules in T cell activation. However, we note here that the CombiCell system introduces a potential size discrepancy between SpyTagged and endogenously-presented ligands, which can lead to a reduction in T cell sensitivity to endogenous ligands. Although we were able to generate novel CombiCells with truncated surface SpyCatchers and thereby improve the sensitivity of effector T cells to endogenous ligands, several additional experimental controls are required to further validate the refinements we have made to the CombiCell system.

Because the SpyCatcher-presented CD58 concentrations used in our experiments led to greater CD58 surface densities than endogenous CD58 expression, we recommend additional control studies using CD58 expression levels matched between the two systems. These experiments would allow us to directly quantify the extent of the sensitivity difference exerted by using CombiCells. To perform these control studies, we could increase the surface density of endogenous CD58 through overexpression of the ligand, or we could lower the concentration of SpyTagged CD58 utilised in the CombiCell assays to match the expression levels of endogenous CD58.

Furthermore, although our refined surface SpyCatchers led to improvements in T cell sensitivities to endogenous ligands, these changes were not reflected in studies using the elongated CD2 receptor. We speculated that our CD2 elongation was not matched in size to either the original SpyCatcher hinge length or the truncated

SpyCatcher hinge length. Based on this assumption, additional experiments using an elongated CD2 variant that had been size-optimised to the original surface SpyCatcher hinge length (i.e. elongated by around 5 nm) would theoretically exhibit differential activity in response to the original and truncated surface SpyCatchers, providing an additional screening metric through which we could validate our refined system.

Finally, we suggest the addition of several controls to our experimental repertoire, including a CD58-negative condition and an endogenous CD58 condition, in order to highlight the activity of T cells in the absence of CD58-mediated co-stimulation and provide a baseline for the activity of T cells under fully endogenous conditions.

The scope of the CombiCell validation investigations in this thesis are confined to a study of extracellular dimensions. However, using SpyTagged ligands has the potential to introduce several other artifacts including changes to diffusion kinetics and decreased responsivity of the artificial APC. Receptor/ligand engagement and subsequent signalling cascades and transcriptional changes can impact both effector and target cells; however our model system has been designed for these changes to only impact the effector [274]. Additionally, APC ligands exhibit diverse modes of membrane attachment, including lipid anchoring and transmembrane domains, and have the potential to associate directly or indirectly with the actin cytoskeleton [275]. The method of membrane attachment can influence ligand activity and diffusion rates, which is of relevance within the framework of the kinetic segregation model [276]. CombiCell investigations can be designed in such a way as to minimise the impact of these constraints, but it is important to be aware of the limitations of the platform.

In conclusion, the data suggest a potential artifact of the CombiCell system in the form of a size discrepancy between endogenous CD58 and SpyTagged CD58, providing and testing a potential resolution to this issue through truncation of both

GPI-anchored and transmembrane surface SpyCatcher hinges.

5.4 Conclusions

In summary, this thesis demonstrates that accessory receptors exhibit context-dependent functionality, and the impacts of their engagement on T cell signalling processes depend on receptor structure, intracellular signalling capacity, and critically, receptor/ligand extracellular spatial organisation.

Using the CombiCell system, we quantitatively assessed the effects of several different accessory receptor/ligand interactions on T cell antigen sensitivity, revealing that receptors with closely related signalling architectures (e.g. CD150, 2B4, CRACC, and CD2) can generate distinct functional outcomes, likely through recruitment of disparate intracellular adaptor molecules and enzymes. We further demonstrated, using both CAR-T cells and CombiCells with truncated surface SpyCatchers, that the magnitude of these functional effects is strongly influenced by the physical dimensions of the receptor/ligand complex.

We found that size optimising TCR or CAR/antigen and accessory receptor/ligand complexes can enhance the potency of co-signalling, and that this can be achieved through modifications to the accessory receptor/ligand complex, the antigen-engaging receptor itself, or the mode of ligand presentation. Our data underpins a hypothesis suggesting that the relative dimensions of receptor/ligand pairs, rather than their absolute lengths, govern T cell antigen sensitivity.

Collectively, our findings advance our understanding of the impact of co-signalling receptors on quantitative phenotypes such as antigen sensitivity, support the use of the CombiCell system for dissecting the contributions of individual receptors to cell-cell interactions, and provide important design considerations for the refinement of experimental platforms.

6 | Materials and Methods

6.1 Materials

6.1.1 General reagents

Table 6.1: Cell lines

Cell line	Description/origin	Additional Notes
U87	Gliblastoma	HLA-A*02:01 positive
A375	Malignant melanoma	Nuclear mCherry expressed
Jurkat E6.1	Acute T cell leukemia	TCR $\alpha\beta$ KO
CHO-K1	Hamster ovary	ICAM-1 KO
Nalm6	Acute lymphoblastic leukemia	HLA-A*01:01 positive
HEK-293T	Embryonic kidney	Used to produce lentivirus

Table 6.2: Antibodies for flow cytometry

Target (Clone)	Conjugate	Supplier	Catalogue number
Human CD45 (HI30)	BV421	BioLegend	304032
Human CD45 (HI30)	BV510	Biolegend	304036
Human CD69 (FN50)	AF647	BioLegend	310918
Human CD69 (FN50)	AF488	BioLegend	310916
Human 4-1BB (4B4-1)	AF647	BioLegend	309824
Human CD319 (162.1)	PE/Dazzle 594	BioLegend	331812
Human NTB-A (NT-7)	PE	BioLegend	317207
Human CD150 (A12; 7D4)	PE	BioLegend	306307
Human CD84 (CD84.1.21)	PE	BioLegend	326007
Human CD48 (BJ40)	PE	BioLegend	336707
Human CD244 (2-69)	PE	BioLegend	393507
Human CD229 (HLy-9.1.25)	PE	BioLegend	326107
Human CD58 (TS2/9)	PE	BioLegend	330905
Human CD58 (TS2/9)	APC	BioLegend	330918
Human CD58 (TS2/9)	PerCP/cy5.5	BioLegend	330913
Human CD2 (TS1/8)	BV421	BioLegend	309218
Human PD-1 (EH12.2H7)	BV421	BioLegend	329920
Human CD8α (RPA-T8)	PE	Abcepta	ATB10171
HLA-A,B,C (W6/32)	AF488	BioLegend	311413
HLA-A,B,C (W6/32)	AF647	BioLegend	311414

Table 6.3: Reagent kits

Reagent	Supplier	Catalogue Number
IL-2 Human Uncoated ELISA Kit	Thermo Fisher Scientific	88-7025-77
IFN-γ Human Uncoated ELISA Kit	Thermo Fisher Scientific	88-7316-86

Table 6.4: Instruments and equipment

Name	Company
BD LRS Fortessa X-20 cell analyzer	BD Biosciences
BD FACSAria III	BD Biosciences
CytoFLEX flow cytometer	Beckman Coulter
SpectraMax M3 microplate reader	Molecular Devices
Incucyte Live-Cell Analysis System	Sartorius
LSM 880 AiryScan	Zeiss

Table 6.5: Software

Name	Company
FlowJo	BD Biosciences
GraphPad Prism	GraphPad Software
PyMOL	Schrödinger, Inc.

6.1.2 In-house reagents

While several buffers and media were purchased from commercial vendors, the following solutions were produced in-house.

Table 6.6: In-house reagents

Common name	Composition
Complete DMEM	DMEM with 10% FBS, 1% PenStrep
Complete RPMI	RPMI with 10% FBS, 1% PenStrep
Flow cytometry staining solution	PBS with 1% BSA
ELISA wash buffer	PBS with 0.05% Tween20

6.2 Methods

6.2.1 Maintenance of immortal cell lines

HEK293 T cells (adherent) were maintained in complete DMEM at 37°C in a 10% CO_2 incubator. Every 2-3 days, cells were split using Trypsin (TrypLE Express; Thermo Fisher Scientific, 12604013) and seeded at a density of 1 million cells per 75 cm^2 flask.

U87 cells (adherent) were maintained in complete DMEM at 37°C in a 10% CO_2 incubator. Every 2-3 days, cells were split using Trypsin and seeded at a density of 2 million cells per 75 cm^2 flask.

CHO-K1 cells (adherent) were maintained in complete DMEM at 37°C in a 10% CO_2 incubator. Every 2-3 days, cells were split using Trypsin and seeded at a density of 1 million cells per 75 cm^2 flask.

A375 mCherry cells (adherent) were maintained in complete DMEM at 37°C in a 5% CO_2 incubator. Every 2-3 days, cells were split using Trypsin and seeded at a density of 2 million cells per 75 cm^2 flask.

Nalm6 cells (suspension) were maintained in complete RPMI at 37°C in a 5% CO_2 incubator. Every 2-3 days, cells were split and seeded at a density of 0.5 million cells/mL in a 25 cm^2 flask.

Jurkat E6.1 T cells (suspension) were maintained in complete RPMI at 37°C in a 5% CO_2 incubator. Every 2-3 days, cells were split and seeded at 1 million cells/mL in a 25 cm^2 flask.

6.2.2 Lentivirus production - pHR

Day -2: 0.8 million HEK 293T cells were seeded in 3 mL of complete DMEM in 6-well tissue culture plates (Corning, 3516) and incubated overnight.

Day -1: 1 mL of complete DMEM was removed and cells were transfected using X-tremeGENE^{TM} HP (Roche, 6366244001) with a pHR lentiviral transfer plasmid (0.8 μg) and lentiviral packaging plasmids pRSV-Rev (0.25 μg, Addgene, 12253), pMDLg/pRRE (0.53 μg, Addgene, 12251), and pMD2.G (0.35 μg, Addgene, 12259).

Day 0: 1 mL of complete DMEM was added to each well.

Day 1: Viral supernatant was harvested from each well and filtered through a 0.45 micron filter before being used to transduce 1 million target cells.

6.2.3 Lentivirus production - pLEX

Day -2: 0.8 million HEK 293T cells were seeded in 3 mL of complete DMEM in 6-well tissue culture plates (Corning, 3516) and incubated overnight.

Day -1: 1 mL of complete DMEM was removed and cells were transfected using X-tremeGENE^{TM} HP (Roche, 6366244001) with a pLEX lentiviral transfer plasmid (0.8 μg) and lentiviral packaging plasmids pRSV-Rev (0.25 μg, Addgene, 12253), pMDLg/pRRE (0.53 μg, Addgene, 12251), and pMD2.G (0.35 μg, Addgene, 12259). 6 wells were used for each pLEX construct.

Day 0: 1 mL of complete DMEM was added to each well.

Day 1: Viral supernatant was harvested from each well and filtered through a 0.45 micron filter. Supernatant was combined with Lenti-X^{TM} Concentrator (Takara Bio, 631231) at a ratio of 1 part virus concentrator to 4 parts viral supernatant and inverted to mix. This mixture was chilled for 4 hours at 4°C, then spun at 4°C for 1 hour at 2000g. The supernatant was discarded and the remaining pellet was gently resuspended in 1 mL of complete RPMI and used to transduce 1 million target cells.

6.2.4 Isolation, viral transduction, and maintenance of CD8+ T cells

T cell isolation and virus production protocols were coordinated, with Day 1 of both protocols corresponding to the day of transduction.

Day 0: Anonymised leukocyte cones used for for T cell isolation were purchased from the UK National Health Service's Blood and Transplantation service at John Radcliffe Hospital. This project has been approved by the Medical Sciences Inter-Divisional Research Ethics Committee of the University of Oxford (R51997/RE001). The blood was combined with RosetteSep^{TM} Human CD8^{+} Enirchment Cocktail (STEMCELL Technologies, 15063) at a concentration of 150 μL/mL and incubated for 20 minutes at room temperature. The sample was then diluted using an equal volume of PBS and layered on Ficoll Paque Plus (GE, 17-1440-02) at a Ficoll-to-sample ratio of 0.8:1.

The sample was centrifuged for 30 min at 1200g with the brake off. The buffy coat of cells, found at the Ficoll/plasma interface, was then collected and washed twice in PBS using centrifugation (5 min, 500g). The cell pellet was resuspended at a density of 1 million cells per mL in complete RPMI supplemented with recombinant human IL-2 (50 U/mL) (PeproTech, 200-02) and CD3/CD28 Human T-activator Dynabeads (Thermo Fisher Scientific, 11132D) at a 1:1 bead-to-cell ratio. Cells were incubated overnight at 5% CO_2, 37°C.

Day 1: 24 hours after activation, 1 million cells were isolated and transduced with filtered lentiviral supernatant.

Days 3 and 5: 48 and 96 hours after transduction, 1 mL of media was removed and replaced with 1 mL of complete RPMI supplemented with IL-2 (50 U/mL). For primary T cells requiring selection, antibiotic was also added 48 and 96 hours post-transduction. Geneticin^{TM} (G418 Sulfate, 50 mg/mL; Thermo Fisher Scien-

tific, 10131027) was added at a concentration of 300 μg/mL and puromycin (Sigma, P8833-10MG) was added at a concentration of 1 μg/mL.

Day 6: Dynabeads were magnetically removed and cells were resuspended in complete RPMI supplemented with IL-2 (50 U/mL). Following day 6, primary T cells were continually split every 2 days and maintained at a density of 1 million/mL in complete RPMI with IL2 (50 U/mL).

6.2.5 Production of U87 CombiCells

6.2.5.1 CRISPR/Cas9 knock-out of U87 proteins

β2M knockout of parental U87 cells

1 million U87 cells were re-suspended in 100 μL complete DMEM and washed with 1000 μL Opti-MEM (Gibco, 51985034) by centrifugation (5 min, 500g). The supernatant was discarded and the wash procedure was repeated three times to remove any trace of complete DMEM. U87 cells were then resuspended in 100 μL Opti-MEM and moved to an electroporation cuvette (BTX electroporation cuvette Plus; Fisher Scientific, 15447270).

3.6 μL Opti-MEM, 1 μL of each β2M sgRNA guide, and 3.4 μL of TrueCut Cas9 V2 enzyme (ThermoFisher, A36499) were combined in an RNA-free tube. This 10 μL mixture was transferred to the electroporation cuvette containing the cell suspension. Cells were shocked once (300V, 2 mesc, ECM 830 Square Wave Electroporation System) and transferred to a 25 cm^2 flask with 7 mL complete DMEM media, prewarmed. Cells were allowed to recover for 3 days and were then cultured according to standard practice. KO efficacy was verified using flow cytometry.

CD58 knockout of β2M KO U87 cells

1 million β2M KO U87 cells were re-suspended in 100 μL complete DMEM and washed with 1000 μL Opti-MEM (Gibco, 51985034) by centrifugation (5 min, 500g).

The supernatant was discarded and the wash procedure was repeated three times to remove any trace of complete DMEM. U87 cells were then resuspended in 100 uL Opti-MEM and moved to an electroporation cuvette (BTX electroporation cuvette Plus; Fisher Scientific, 15447270).

3.6 μL Opti-MEM, 1 μL of each CD58 KO sgRNA guide, and 3.4 μL of TrueCut Cas9 V2 enzyme (ThermoFisher, A36499) were combined in an RNA-free tube. This 10 μL mixture was transferred to the electroporation cuvette containing the cell suspension. Cells were shocked once (300V, 2 mesc, ECM 830 Square Wave Electroporation System) and transferred into a 25 cm^2 flask with 7 mL complete DMEM media. Cells were allowed to recover for 3 days and were then cultured according to standard practice. KO efficacy was verified using flow cytometry.

6.2.5.2 Lentiviral transduction

Single KO (β2M KO) and double KO (β2M KO/CD58 KO) U87 cells were transduced with surface SpyCatcher using lentivirus. One million U87 target cells in 4 mL of complete DMEM were combined with 3 mL of crude lentivirus supernatant and allowed to recover for 3-4 days. One week post-transduction, cells were sorted using flow cytometry (BD FACS Aria III) for matched surface SpyCatcher using SpyTagged mClover staining to compare surface expression levels.

6.2.6 Production of Jurkat TCR/CAR-T cells

Jurkat T cells for SLAM studies

Parental TRAC(-/-) TRBC(-/-) E6.1 Jurkat T cells previously described [277] were used as the parental Jurkat line from which all further Jurkat variants were derived. These parental cells were lentivirally transduced with the 1G4 TCR, human CD8α-P2A-CD8β, and CD2, as previously described [1]. Following all transductions, Jurkat T cells were sorted to ensure matched expression of surface proteins.

To sort, cells were stained in the dark for 30 min in a sterile PBS 1% BSA (Merck, A7906) solution containing a 1:1000 dilution of fluorescently-conjugated peptide-MHC tetramer (used to detect TCR and CAR expression) and 1:200 dilutions of fluorescently conjugated anti-human CD2 (Biolegend) and fluorescently conjugated anti-human CD8α (Abcepta). Following staining, sorting was performed used flow cytometry (BD FACSAria III).

To generate SLAM-overexpressing Jurkat T cell lines, the sorted 1G4 TCR/CD8α-P2A-CD8β/CD2$^+$ T cells were further transduced with lentivirus for SLAM proteins CD150, Ly9, 2B4, CD84, or CRACC. Each transduction used 3 mL of crude lentivirus supernatant for the transduction of 1 million Jurkats. Following all transductions, Jurkat T cells were re-sorted using flow cytometry (BD FACSAria III) and fluorescently-conjugated anti-SLAM antibodies (all BioLegend) to ensure SLAM-positive T cell populations.

Jurkat T cells for PD-1 studies

TRAC(-/-) TRBC(-/-) E6.1 Jurkat T cells underwent a CRISPR/Cas9 CD2 KO followed by transduction with a desired antigen receptor as well as CD2 WT or elongated CD2 (CD2-CD43(40)) and PD-1 WT or elongated PD-1 (PD-1-CD43(40)) [2]. Following all transductions, Jurkat T cells were sorted using flow cytometry (BD FACSAria III) using fluorescently conjugated anti-CD2 and anti-PD-1 antibodies (1:200 dilution, BioLegend) to ensure matched expression of surface proteins.

Jurkat T cells for CombiCell size-matching studies

TRAC(-/-) TRBC(-/-) E6.1 Jurkat T cells underwent a CRISPR/Cas9 CD2 KO followed by transduction with the 1G4 TCR alongside CD2 WT or an elongated CD2 variant (CD2-CD43(40) or CD2-CD43(234)), as described in [2]. Following all transductions, Jurkat T cells were sorted using flow cytometry (BD FACSAria III) using fluorescently conjugated anti-CD2 (1:200 dilution, BioLegend) to ensure matched expression of surface proteins.

6.2.7 Production of additional cell lines

Protocols for the generation of CHO-K1 CombiCells and Nalm6 β2M CombiCells have been previously described [1, 2], and these cell lines along with the A375 nuclear mCherry cells, U87 NLuciferase cells, and HEK-293T cells were obtained from Dushek lab cell stocks.

6.2.8 CombiCell co-culture assays - adherrent cells

Day 1: 50,000 adherrent cells (CHOs or U87s) per well were seeded in 96-well flat bottom tissue culture plates (Corning, 3596) and allowed to double overnight at 37°C in a 10% CO_2 incubator.

Day 2: SpyTagged ligands were diluted to their required concentrations in a total volume of 60 μL complete DMEM. Existing media from adherent cells was aspirated and the 60 μL diluted ligand mixture was added. The cells were then incubated at 37°C, 10% CO_2 for 45 min. Following incubation, the ligand mixture was aspirated and cells were washed with 200 μL complete DMEM. 50,000 effector cells (Jurkats or primary T cells) were added to each well in 200 μL complete RPMI. The co-culture was then centrifuged (5 min, 50g) to ensure effector-to-target cell contact and incubated for 20 hours at 37°C, 5% CO_2.

Day 3: Cells were again centrifuged (5 min, 50g) to allow for removal of supernatant. 120 μL of the co-culture supernatant was taken for ELISA analysis. The remaining cells were dislodged using 40 μL of 0.5 μM EDTA (UltraPure^{TM} 0.5M EDTA, pH 8.0; Thermo Fisher Scientific, 15-575-020) diluted 1:5 in PBS. The cells were then transferred to v-bottom plates (Corning, 3894) for flow cytometry analysis.

6.2.9 CombiCell co-culture assays - suspension cells

Day 1: 100,000 Nalm6 cells in suspension were added to each well of 96-well tissue culture v-bottom plates (Corning, 3894) and centrifuged (5 min, 500g) to remove media. SpyTagged ligands were diluted to their required concentrations in a total volume of 60 μL complete RPMI. Existing media was removed from the Nalm6 cells and diluted ligands were added and incubated for 45 min at 37°C, 5% CO_2. SpyTagged ligand-coupled Nalm6 cells were then washed with 200 μL complete RPMI and moved to 96-well flat bottom tissue culture plates (Corning, 3596). 50,000 effector cells (Jurkats or primary T cells) were added to each well in 200 μL complete RPMI. The co-culture was then centrifuged (5 min, 50g) to ensure effector-to-target cell contacts and incubated for 20 hours at 37°C, 5% CO_2.

Day 2: Cells were again centrifuged (5 min, 50g) to allow for removal of 120 μl of co-culture supernatant, taken for ELISA analysis. The remaining cells were resuspended and transferred to v-bottom plates for flow cytometry analysis.

6.2.10 Peptide pulsing assays

Day 1: 50,000 adherent U87 cells per well expressing NLuciferase were seeded in 96-well tissue culture flat bottom plates (Corning, 3596) in 200 μL complete DMEM and allowed to double overnight at 37°C in a 10% CO_2 incubator.

Day 2: 9V peptides were diluted to their required concentrations in 200 μL complete DMEM. Existing media from U87 cells was aspirated and the 200 μL diluted ligand mixture was added. The cells were then incubated at 37°C, 10% CO_2 for 45 min. Following incubation, the ligand mixture was aspirated and cells were washed using 200 μL complete DMEM. 50,000 effector cells (Jurkats or primary T cells) were added to each well in 200 μL complete RPMI. The co-culture was then centrifuged (5 min, 50g) to ensure effector-to-target cell contacts and incubated for 20 hours at 37°C, 5% CO_2.

Day 3: Cells were again centrifuged (5 min, 50g) to allow for removal of supernatant. 120 μL of the co-culture supernatant was taken for ELISA analysis. The remaining cells were dislodged using 40 μL of 0.5 μM EDTA (UltraPure^{TM} 0.5M EDTA, pH 8.0; Thermo Fisher Scientific, 15-575-020) diluted 1:5 in PBS. The cells were then transferred to v-bottom plates (Corning, 3894) for flow cytometry analysis.

6.2.11 Flow Cytometry - detection of T cell activation

Tissue culture v-bottom plates (Corning, 3894) containing cell solutions from co-culture assays were washed by centrifugation (5 min, 500g) to remove residual media. Pellets were resuspended in 40 μL of a PBS 1% BSA (Merck, A7906) staining solution containing antibodies against T cell activation markers CD69 (1:200 dilution, Biolegend) and 4-1BB (1:200 dilution, Biolegend) for primary T cells or against CD69 alone (1:200 dilution, Biolegend) for Jurkat T cells (Tables 5.6 and 5.7). All T cell activation assays included an anti-CD45 antibody (1:200 dilution, Biolegend) to distinguish between T cells and CHO cells during flow cytometry analysis (Tables 5.6 and 5.7). Primary T cell assay staining solutions also utilised fluorescently-conjugated peptide-MHC tetramers (1:1000 dilution, in-house) which could be used to detect TCR and CAR expression.

Cells were incubated for 35-40 minutes in the dark at 4°C. Following staining, cells were washed with 110 μL PBS, centrifuged (5 min, 500g), and resuspended in 70 μL PBS. Samples were run on a flow cytometer (Fortessa X-20, BD BioSciences) and data was analyzed using FlowJo software (BD Biosciences).

6.2.12 Flow Cytometry - detection of loaded SpyTagged ligands

After SpyTagged ligand coupling and subsequent washing with complete DMEM during the initial CombiCell assay, 40 μL of 0.5 μM EDTA (UltraPure^{TM} 0.5M

EDTA, pH 8.0; Thermo Fisher Scientific, 15-575-020) diluted 1:5 in PBS was added to ligand-loaded CombiCells. The cells were dislodged, transferred to 96-well v-bottom plates (Corning, 3894), and centrifuged (5 min, 500g) to remove excess media. For ligand detection, fluorescently conjugated antibodies against proteins of interest were diluted in PBS with 1% BSA. All antibodies were used at a dilution of 1:200 (Table 5.8). CombiCells were resuspended in 40 μL of staining solution and incubated in the dark for 40 min at 4°C. Cells were then washed with 110 μL PBS using centrifugation (500g, 5 min), resuspended in 70 μL PBS, and run on a flow cytometer (Fortessa X-20, BD BioSciences). Data analysis was performed using FlowJo software (BD Biosciences).

6.2.13 Flow Cytometry - detection of T cell receptors

100,000 T cells per well were added to v-bottom plates (Corning, 3894) and centrifuged (5 min, 500g) to remove excess media. T cells were resuspended in 40 μL of PBS 1% BSA staining solution containing antibodies against target receptors (Table 5.9). All antibodies were used at a 1:200 dilution. To test for TCR and CAR surface expression, fluorescently-conjugated peptide MHC tetramers (in-house) were used (1:1000 dilution).

Cells resuspended in staining solution were incubated in the dark for 40 min at 4°C. Following staining, cells were washed with 110 μL PBS using centrifugation (500g, 5 min), resuspended in 70 μL PBS, and run on a flow cytometer (Fortessa X-20, BD BioSciences). Data analysis was performed using FlowJo software (BD Biosciences).

6.2.14 Flow Cytometry - detection of surface SpyCatcher

100,000 CombiCells per well were added to a v-bottom plate (Corning, 3894) and centrifuged (5 min, 500g) to remove excess media. Cells were resuspended in 40 μl of PBS 1% BSA staining solution containing SpyTag-mCLOVER3 (in-house) diluted

1:50. The cells were then incubated in the dark for 45 min at 4°C. Following staining, cells were washed with 110 μL PBS using centrifugation (500g, 5 min), resuspended in 70 μL PBS, and run on a flow cytometer (Fortessa X-20, BD BioSciences). Data analysis was performed using FlowJo software (BD Biosciences).

Table 6.7: Jurkat T cell activation panel

Target	Dilution	Clone	Conjugate	Supplier
Human CD45	1:200	HI30	BV421/BV510	Biolegend
Human CD69	1:200	FN50	AF647	Biolegend

Table 6.8: Primary T cell activation panel

Target	Dilution	Clone	Conjugate	Supplier
Human CD45	1:200	HI30	BV421/BV510	Biolegend
Human CD69	1:200	FN50	AF488	Biolegend
Human 4-1BB	1:200	4B4-1	AF647	Biolegend
TCR/CAR	1:1000	In-house reagent	PE	Dushek Lab

Table 6.9: SpyTagged ligand loading check panels

Target	Dilution	Clone	Conjugate	Supplier
Human CD58	1:200	TS2/9	PE	Biolegend
Human CD58	1:200	TS2/9	APC	Biolegend
Human CD58	1:200	TS2/9	PerCP/Cy5.5	Biolegend
Human CD48	1:200	BJ40	PE	Biolegend
Human PD-L1	1:200	MIH2	PE	Biolegend
HLA-A,B,C	1:200	W6/32	AF488	Biolegend
HLA-A,B,C	1:200	W6/32	AF647	Biolegend
Human CD319	1:200	162.1	PE/Dazzle 594	Biolegend
Human NTB-A	1:200	NT-7	PE	Biolegend
Human CD150	1:200	A12;7D4	PE	Biolegend
Human CD84	1:200	CD84.1.21	PE	Biolegend
Human CD244	1:200	2-69	PE	Biolegend
Human CD229	1:200	HLy-9.1.25	PE	Biolegend

Table 6.10: T cell receptor expression check panel

Target	Dilution	Clone	Conjugate	Supplier
Human CD2	1:200	TS1/8	BV421	Biolegend
Human CD8α	1:200	RPA-T8	PE	Abcepta
Human CD319	1:200	162.1	PE/Dazzle 594	Biolegend
Human NTB-A	1:200	NT-7	PE	Biolegend
Human CD150	1:200	A12;7D4	PE	Biolegend
Human CD84	1:200	CD84.1.21	PE	Biolegend
Human CD244	1:200	2-69	PE	Biolegend
Human CD229	1:200	HLy-9.1.25	PE	Biolegend
Human PD-1	1:200	EH12.2H7	BV421	Biolegend
TCR/CAR	1:1000	In-house reagent	PE	Dushek Lab

6.2.15 Surface density quantification of PD-L1 on CHO-K1 CombiCells

PD-L1 quantification was performed as described in [2].

100,000 CHO-K1 CombiCells from co-culture experiments loaded with a 3-fold titration of SpyTagged PD-L1 with a maximum concentration of 0.5 μM were lifted using 40 μL of 0.5 μM EDTA (UltraPure^{TM} 0.5M EDTA, pH 8.0; Thermo Fisher Scientific, 15-575-020) diluted 1:5 in PBS and split into two groups: one group of 60,000 cells per condition and one group of 30,000 cell per condition. This split was used in order to control for possible antibody depletion during staining steps.

Each group was added to 96-well tissue culture v-bottom plates (Corning, 3894) and stained with an anti-human PD-L1 PE antibody (PE, Clone: MIH2, BioLegend, 393608) at a concentration of 1.33×10^{-2} μM in 100 μl of PBS 1% BSA staining solution. The cells were then incubated on ice for 30 min and washed twice with PBS 1% BSA using centrifugation (5 min, 500g). Cell samples were run on a flow cytometer (Fortessa X-20, BD BioSciences) to determine total fluorescence. In order to translate this signal into number of molecules, Quantum R-PE MESF calibration beads (Bangs Laboratories Inc, 827A) were also run on the flow cytometer under

the same settings.

The total gMFI for both the cells and the calibration beads was then assessed using FlowJo (BD Biosciences). A calibration curve was generated according to manufacturer protocols to convert gMFI from PE staining into number of PE molecules using an f/p ratio of 1.07 (obtained from BioLegend). To determine the average number of PD-L1 molecules per cell for each loading condition, the calculated number of PE molecules per cell was then divided by this f/p ratio.

To translate this calculation into a surface density, brightfield microscopy was used to estimate cell surface areas. CHO-K1 CombiCells were spun down (5 min, 500g) and resuspended in a 90% MilliQ water, 10% PBS solution in order to swell the cells. The cells were imaged on an ibidi 18-well μ-slide (ibidi, 81816-90) using brightfield microscopy with a Zeiss 880 AiryScan laser scanning microscope (63x oil immersion objective, 1 AU pinhole setting) (Zeiss). All imaging was controlled with the Zen Black Software. A Z-stack (step size 1 μm) was utilised to scan the cells and the resulting image stacks were assessed using Fiji (ImageJ version 1.54p). The total circular area for each of the cellular cross-sections was measured for each image stack slice, and the maximum circular area was then used to determine cell radius and surface area.

The average cell surface area was calculated as 1455 μm^2 (calculated using N=7 samples). The surface density was then estimated by dividing the number of PD-L1 molecules per cell by the surface area.

6.2.16 Longitudinal killing assays

Incucyte killing assays were performed as described in [2].

Day 1: A375 cells expressing nuclear mCherry were seeded in a 96-well flat-bottom plate (Corning, 3596) at a density of 12,000 cells/well and incubated overnight in 100 μL of complete DMEM at 37°C, 5% CO2.

Day 2: Effector cells (Primary T cells) were serially diluted to the appropriate E:T ratios (1:1, 1:2, 1:4, 1:8, and 1:16) and added to each well in 100 μl complete RPMI. For each E:T ratio, T cells were plated in triplicate to create technical replicates.

The number of mCherry^{+}*ve* A375 cells in each well was recorded every 2 hours using the Incucyte Live-Cell Analysis System (Sartorius), and the resulting data was used to generate viability curves using GraphPad Prism (GraphPad Software).

6.2.17 Cytokine detection assays

10 μL of supernatant from stimulation assays was added to Nunc MaxiSorp 96-well plates (Thermo Fisher Scientific, 442404) and used for ELISA analysis. The IL-2 Human uncoated ELISA kit (ThermoFisher Scientific, 88-7025-77) and the IFN-γ Human uncoated ELISA kit (ThermoFisher Scientific, 88-7316-86) were used according to the manufacturer's instructions. Absorbances at 450 nm and 570 nm were determined using a SpectraMax M5 plate reader (Molecular Devices) and used to quantify cytokine levels.

6.2.18 AlphaFold SpyCatcher size measurements

Structural models of the full-length hCD52 surface SpyCatcher were generated using AlphaFold 3. The amino acid sequences of the full extracellular domain of surface SpyCatcher was entered into the web-based prediction tool [278]. Predictions were performed using default settings. Five ranked models were generated for each input, and the top-ranked model based on pLDDT was selected for further analysis. Molecular graphics were rendered with PyMOL (Schrödinger, Inc.) and end-to-end distances were measured using the built-in distance measurement tool [263].

6.2.19 Elongated CD2 size estimates

Elongated CD2 variants utilised CD43-based extensions. For the CD2-CD43(40) variant, the CD2 extracellular domain (P06729, 25-209) was fused to a GGGGS flexible linker and a 40 amino acid CD43 extension (P16150, 213-253). For the CD2-CD43(234) variant, the CD2 extracellular domain (P06729, 25-209) was fused to the GGGGS flexible linker and a 234 amino acid CD43 extension (P16150, 19-253). Available electron microscopy of the mucin CD43 suggests that it adopts an extended conformation with each amino acid contributing on average 0.2 nm to the overall size [2, 237] and the GGGGS flexible linker contributing an estimated 0.85 nm assuming a persistence length of 0.38 nm [2].

6.2.20 Data analysis

Gating and further data analysis on FACS files was performed using FlowJo software (BD Biosciences). Cell populations were gated by size in order to exclude doublets and cellular debris. T cells were distinguished from CHO and U87 CombiCells cells on the basis of their CD45 expression.

Nonlinear regression curves (agonist vs. response) were fit using GraphPad Prism (GraphPad Software) and used to generate dose-response curves, from which EC50 and EMax values were extracted. EC50 in this study is defined as the concentration of antigen required to elicit a 50% maximal response. EMax is defined as the maximum response cytokine response at high ligand concentrations. Statistical analyses were also performed using Prism, with experiment-specific statistical tests outlined in the figure captions.

6.2.21 Peptide and protein production

6.2.21.1 Peptides

The NY-ESO-1 derived 9V peptide (SLLMWITQV) was obtained from Peptide Protein research, UK at purity $> 95\%$.

6.2.21.2 pMHC tetramer

Tetramers were created in-house by combining monomeric biotinylated 9V peptide-MHC with steptavidin-PE at a molar ratio of 1:4 with continual shaking. The mixture was centrifuged at 13,000g for removal of insoluble proteins and stored in 0.1% azide at 4°C.

6.2.21.3 SpyTagged proteins

SpyTagged pMHC: SpyTagged pMHC was generated as described in [1]. The heavy chain of HLA-A*02:01 (UniProt residues 25-298) with a C-terminal SpyTag003 and β2M-microglobulin were expressed in *E.coli* as inclusion bodies, refolded *in vitro* together with the 9V variant of the NY-ESO-1 peptide as described in [160], and purified using size-exclusion chromatography. Chromatography was performed in HBS-EP buffer (10 mM M HEPES pH 7.4, 150 mM NaCl, 3 mM EDTA, 0.005% v/v Tween-20) using a Superdex S75 column (GE Healthcare, USA).

SpyTagged co-stimulatory ligands:

SpyTagged ligands were generated as described in [1, 2].

The soluble extracellular domains of SpyTagged ligands CD58, CD48, CD150, Ly9, CD84, CRACC, and PD-L1 fused to a C-terminal SpyTag003 (RGVPHIVMVDAYKRYK) followed by a Histag (HHHHHH) for purification were produced in Expi293^{TM} cells (ThermoFisher Scientific, A14527). Cells were grown in Expi293^{TM} Expression Medium (ThermoFisher Scientific, A1435101) on a shaking platform (130

rpm) in a 37°C incubator with 8% CO_2 and passaged every 2-3 days. The suspension was maintained a volume of less than 33.3% of total flask capacity with a cell density of between 0.5 and 3 million cells per mL. Prior to transfection, cells adjusted to a density of 3 million per ml and counted to ensure a viability above 95%.

Day 0: For 100 ml transfection, 320 μl of ExpiFectamine^{TM} 293 Transfection reagent (ThermoFisher Scientific, A14524) was combined with 6 ml of Opti-MEM (ThermoFisher Scientific, 31985062) and incubated for 5 min. 100 μg of expression plasmid was also combined with 6 ml of Opti-MEM, and this DNA mixture was added to the ExpiFectamine^{TM} solution and incubated for 15 min before being added to the cell culture.

Day 1: 24 hours post-transfection, 600 μl of enhancer 1 and 6 ml of enhancer 2 were added to the culture, which was then left to shake for 4-5 days so that protein expression could occur.

Day 5/6: To harvest the cells, the suspension was centrifuged and the supernatant was collected and filtered using a 0.22 μm filter. The mixture was adjusted with imidazole (to a final concentration of 1 mM), PMSF (to a final concentration of 1 mM), and Ni-NTA Agarose (Qiagen, 30310) (2 ml added for each 50 ml of supernatant). This mixture was incubated at 4°C overnight on a rolling platform, then poured through a gravity flow column to collect the Ni-NTA Agarose. The collected Ni-NTA Agarose was washed with 10 ml of wash buffer (50 mM NaH_2PO_4, 300 mM NaCl, and 5 mM imidazole at pH 8) three times. The protein was then eluted using 15 ml of elution buffer (50 mM NaH_2PO_4, 300 mM NaCl, and 250 mM imidazole at pH 8). The protein was concentrated down to 500 μl using a protein concentrator with a 10,000 molecular weight cut-off. The buffer was exchanged into a size exclusion buffer (25 mM NaH_2PO_4 and 150 mM NaCl at pH 7.5), and this solution was then loaded onto a Superdex 200 10/300 GL size exclusion column (Cytiva, 17-5175-01). Samples from all observed peaks were analysed using a reducing SDS-PAGE

gel, and fractions corresponding to desired peaks were frozen at -70°C.

mCLOVER-SpyTag003

Quantification of surface SpyCatcher was performed using an mCLOVER protein generated in-house.

SpyTag003 fused to monomeric mCLOVER3 with a C-terminal HisTag was expressed in *E.coli*. Bacteria were then pelleted using centrifugation (15 min at 6000g and 4°C) and washed in BugBuster (Merck Milliproe 70921) supplemented with DNase I, magnesium sulfate, lysozyme, and protease inhibitors. This lysate solution was combined with 10 mM imidazole and Ni-NTA agarose (Qiagen, 30310) and loaded onto gravity flow columns to collect the Ni-NTA Agatorse. The columns were then washed with a His-Tag wash buffer (50 mM NaH_2PO_4, 300 mM NaCl, and 20 mM imidazole at pH 8) and the SpyTag-mCLOVER was eluted with elution buffer (50 mM NaH_2PO_4, 300 mM NaCl, and 250 mM imidazole at pH 8). The purified protein was exchanged into PBS and kept at -70°C.

6.3 Sequences

6.3.1 SpyCatcher Variants

IgK signal sequences in red; SpyCatcher003 sequence in blue; flexible linker sequence in black; CD52-derived hinge region in magenta, with only TSQTSSPS remaining in the protein for hCD52 variants; transmembrane-derived hinge region also in magenta.

Full length (FL) hCD52 surface SpyCatcher: Insert in lentiviral vector pHR

ETDTLLLWVLLLWVPGSTGD VTTLSGLSGEQGPSGDMTTEEDSATHIKFSK
RDEDGRELAGATMELRDSSGKTISTWISDGHVKDFYLYPGKYTFVETAAPD

GYEVATPIEFTVNEDGQVTVDGEATEGDAHT GSSGSGGS TSQTSSPSASS-
NISGGIFLFFVANAIIHLFCFS*

Δ8 hCD52 surface SpyCatcher: Insert in lentiviral vector pHR

ETDTLLLWVLLLWVPGSTGD VTTLSGLSGEQGPSGDMTTEEDSATHIKFSK
RDEDGRELAGATMELRDSSGKTISTWISDGHVKDFYLYPGKYTFVETAAPD
GYEVATPIEFTVNEDGQVTVDGEATEGDAHT TSQTSSPSASSNISGGIFLFF-
VANAIIHLFCFS*

Δ15 hCD52 SpyCatcher: Insert in lentiviral vector pHR

ETDTLLLWVLLLWVPGSTGD VTTLSGLSGEQGPSGDMTTEEDSATHIKFSK
RDEDGRELAGATMELRDSSGKTISTWISDGHVKDFYLYPGKYTFVETAAP
DGYEVATPIEFTVNEDGQVTVDGEATEGDAHT SASSNISGGIFLFFVANAI-
IHLFCFS*

Full length (FL) mouse CD80 SpyCatcher: Insert in lentiviral vector pHR

ETDTLLLWVLLLWVPGSTGD VTTLSGLSGEQGPSGDMTTEEDSATHIKFSK
RDEDGRELAGATMELRDSSGKTISTWISDGHVKDFYLYPGKYTFVETAAPD
GYEVATPIEFTVNEDGQVTVDGEATEGDAHT GSSGSGGS PPDSKNTLVLF-
GAGFGAVITVVVIVVIIKCFCKHRSCFRRNEASRETNNSLTFGPEEALAEQTVFL*

Δ14 mouse CD80 SpyCatcher: Insert in lentiviral vector pHR

ETDTLLLWVLLLWVPGSTGD VTTLSGLSGEQGPSGDMTTEEDSATHIKFSK
RDEDGRELAGATMELRDSSGKTISTWISDGHVKDFYLYPGKYTFVETAAPD
GYEVATPIEFTVNEDGQVTVDGEATEGDAHT TLVLFGAGFGAVITVVVIVVI-
IKCFC*

Full length (FL) human CD28 SpyCatcher: Insert in lentiviral vector pHR

ETDTLLLWVLLLWVPGSTGD VTTLSGLSGEQGPSGDMTTEEDSATHIKFSK
RDEDGRELAGATMELRDSSGKTISTWISDGHVKDFYLYPGKYTFVETAAP

DGYEVATPIEFTVNEDGQVTVDGEATEGDAHT GPSKPFWVLVVVGGVLA-
CYSLLVTVAFIIFWVRSKRSRLLHSDYMNMTPRRPGPTRKHYQPYAPPRDFAAYRS*

Δ3 human CD28 SpyCatcher: Insert in lentiviral vector pHR

ETDTLLLWVLLLWVPGSTGD VTTLSGLSGEQGPSGDMTTEEDSATHIKFSK
RDEDGRELAGATMELRDSSGKTISTWISDGHVKDFYLYPGKYTFVETAAP
DGYEVATPIEFTVNEDGQVTVDGEATEGDAHT KPFWVLVVVGGVLACYS-
LLVTVAFIIFWVRSKRSRLLHSDYMNMTPRRPGPT*

Full length (FL) human CD86 SpyCatcher: Insert in lentiviral vector pHR

ETDTLLLWVLLLWVPGSTGD VTTLSGLSGEQGPSGDMTTEEDSATHIKFSK
RDEDGRELAGATMELRDSSGKTISTWISDGHVKDFYLYPGKYTFVETAAPD
GYEVATPIEFTVNEDGQVTVDGEATEGDAHT LEDPQPPPDHIPWITAVLP
TVIICVMVFCLILWKWKKKKRPRNSYKCGTNTMEREESEQTKKREKIHIPE
RSDEAQRVFKSSKTSSCDKSDTCF

Δ10 human CD86 SpyCatcher: Insert in lentiviral vector pHR

ETDTLLLWVLLLWVPGSTGD VTTLSGLSGEQGPSGDMTTEEDSATHIKFSK
RDEDGRELAGATMELRDSSGKTISTWISDGHVKDFYLYPGKYTFVETAAP
DGYEVATPIEFTVNEDGQVTVDGEATEGDAHT IPWITAVLPTVIICVMVF-
CLILWKWKKKKRPRNSY*

6.3.2 SLAM Family Expression Sequences

6.3.2.1 SLAM Receptor Sequences

CD150: Insert in lentiviral vector pHR; UniProt Q13291: 1-335

MDPKGLLSLTFVLFLSLAFGASYGTGGRMMNCPKILRQLGSKVLLPLTYER
INKSMNKSIHIVVTMAKSLENSVENKIVSLDPSEAGPPRYLGDRYKFYLENL
TLGIRESRKEDEGWYLMTLEKNVSVQRFCLQLRLYEQVSTPEIKVLNKTQE

NGTCTLILGCTVEKGDHVAYSWSEKAGTHPLNPANSSHLLSLTLGPQHADN
IYICTVSNPISNNSQTFSPWPGCRTDPSETKPWAVYAGLLGGVIMILIMVVIL
QLRRRGKTNHYQTTVEKKSLTIYAQVQKPGPLQKKLDSFPAQDPCTTIYVA
ATEPVPESVQETNSITVYASVTLPES

Ly9: Insert in lentiviral vector pHR; UniProt Q9HBG7: 1-655

MVAPKSHTDDWAPGPFSSKPQRSQLQIFSSVLQTSLLFLLMGLRASGKDSAP
TVVSGILGGSVTLPLNISVDTEIENVIWIGPKNALAFARPKENVTIMVKSYLG
RLDITKWSYSLCISNLTLNDAGSYKAQINQRNFEVTTEEEFTLFVYEQLQEP
QVTMKSVKVSENFSCNITLMCSVKGAEKSVLYSWTPREPHASESNGGSILTV
SRTPCDPDLPYICTAQNPVSQRSSLPVHVGQFCTDPGASRGGTTGETVVGV
LGEPVTLPLALPACRDTEKVVWLFNTSIISKEREEAATADPLIKSRDPYKNR
VWVSSQDCSLKISQLKIEDAGPYHAYVCSEASSVTSMTHVTLLIYRRLRKPKI
TWSLRHSEDGICRISLTCSVEDGGNTVMYTWTPLQKEAVVSQGESHLNVSW
RSSENHPNLTCTASNPVSRSSHQFLSENICSGPERNTKLWIGLFLMVCLLCVG
IFSWCIWKRKGRCSVPAFCSSQAEAPADTPEPTAGHTLYSVLSQGYEKLDT
PLRPARQQPTPTSDSSSDSNLTTEEDEDRPEVHKPISGRYEVFDQVTQEGA
GHDPAPEGQADYDPVTPYVTEVESVVGENTMYAQVFNLQGKTPVSQKEES
SATIYCSIRKPQVVPPPQQNDLEIPESPTYENFT

2B4: Insert in lentiviral vector pHR; UniProt Q9BZW8: 1-370

MLGQVVTLILLLLLKVYQGKGCQGSADHVVSISGVPLQLQPNSIQTKVDSIA
WKKLLPSQNGFHHILKWENGSLPSNTSNDRFSFIVKNLSLLIKAAQQQDSGL
YCLEVTSISGKVQTATFQVFVFDKVEKPRLQGQGKILDRGRCQVALSCLVS
RDGNVSYAWYRGSKLIQTAGNLTYLDEEVDINGTHTYTCNVSNPVSWESH
TLNLTQDCQNAHQEFRFWPFLVIIVILSALFLGTLACFCVWRRKRKEKQSE
TSPKEFLTIYEDVKDLKTRRNHEQEQTFPGGGSTIYSMIQSQSSAPTSQEPA
YTLYSLIQPSRKSGSRKRNHSPSFNSTIYEVIGKSQPKAQNPARLSRKELENF
DVYS

CD84: Insert in lentiviral vector pHR; UniProt Q9UIB8: 1-345

MAQHHLWILLLCLQTWPEAAGKDSEIFTVNGILGESVTFPVNIQEPRQVKII
AWTSKTSVAYVTPGDSETAPVVTVTHRNYYERIHALGPNYNLVISDLRMED
AGDYKADINTQADPYTTTKRYNLQIYRRLGKPKITQSLMASVNSTCNVTLT
CSVEKEEKNVTYNWSPLGEEGNVLQIFQTPEDQELTYTCTAQNPVSNNSDS
ISARQLCADIAMGFRTHHTGLLSVLAMFFLLVLILSSVFLFRLFKRRQGRIFP
EGSCLNTFTKNPYAASKKTIYTYIMASRNTQPAESRIYDEILQSKVLPSKEEP
VNTVYSEVQFADKMGKASTQDSKPPGTSSYEIVI

CRACC: Insert in lentiviral vector pHR; UniProt Q9UIB8: 1-335

MAGSPTCLTLIYILWQLTGSAASGPVKELVGSVGGAVTFPLKSKVKQVDSIV
WTFNTTPLVTIQPEGGTIIVTQNRNRERVDFPDGGYSLKLSKLKKNDSGIYY
VGIYSSSLQQPSTQEYVLHVYEHLSKPKVTMGLQSNKNGTCVTNLTCCMEH
GEEDVIYTWKALGQAANESHNGSILPISWRWGESDMTFICVARNPVSRNFSS
PILARKLCEGAADDPDSSMVLLCLLLVPLLLSLFVLGLFLWFLKRERQEEYIE
EKKRVDICRETPNICPHSGENTEYDTIPHTNRTILKEDPANTVYSTVEIPKK
MENPHSLLTMPDTPRLFAYENVI

6.3.2.2 SpyTagged Ligand Sequences - extracellular domain only

CD150: Insert in lentiviral vector pTT3; UniProt Q13291: 21-237

ASYGTGGRMMNCPKILRQLGSKVLLPLTYERINKSMNKSIHIVVTMAKSLEN
SVENKIVSLDPSEAGPPRYLGDRYKFYLENLTLGIRESRKEDEGWYLMTLE
KNVSVQRFCLQLRLYEQVSTPEIKVLNKTQENGTCTLILGCTVEKGDHVAY
SWSEKAGTHPLNPANSSHLLSLTLGPQHADNIYICTVSNPISNNSQTFSPWPG
CRTDPSETKP

CD48: Insert in lentiviral vector pTT3; UniProt P09326: 27-212

QGHLVHMTVVSGSNVTLNISESLPENYKQLTWFYTFDQKIVEWDSRKSKYF

ESKFKGRVRLDPQSGALYISKVQKEDNSTYIMRVLKKTGNEQEWKIKLQVL
DPVPKPVIKIEKIEDMDDNCYLKLSCVIPGESVNYTWYGDKRPFPKELQNS
VLETTLMPHNYSRCYTCQVSNSVSSKNGTVCLS

Ly9: Insert in lentiviral vector pTT3; UniProt Q9HBG7: 48-453

KDSAPTVVSGILGGSVTLPLNISVDTEIENVIWIGPKNALAFARPKENVTIMV
KSYLGRLDITKWSYSLCISNLTLNDAGSYKAQINQRNFEVTTEEEFTLFVYE
QLQEPQVTMKSVKVSENFSCNITLMCSVKGAEKSVLYSWTPREPHASESNG
GSILTVSRTPCDPDLPYICTAQNPVSQRSSLPVHVGQFCTDPGASRGGTTGE
TVVGVLGEPVTLPLALPACRDTEKVVWLFNTSIISKEREEAATADPLIKSRD
PYKNRVWVSSQDCSLKISQLKIEDAGPYHAYVCSEASSVTSMTHVTLLIYRR
LRKPKITWSLRHSEDGICRISLTCSVEDGGNTVMYTWTPLQKEAVVSQGES
HLNVSWRSSENHPNLTCTASNPVSRSSHQFLSENICSGPERNTK

CD84: Insert in lentiviral vector pTT3; UniProt Q9UIB8: 22-225

KDSEIFTVNGILGESVTFPVNIQEPRQVKIIAWTSKTSVAYVTPGDSETAPVV
TVTHRNYYERIHALGPNYNLVISDLRMEDAGDYKADINTQADPYTTTKRY
NLQIYRRLGKPKITQSLMASVNSTCNVTLTCSVEKEEKNVTYNWSPLGEEG
NVLQIFQTPEDQELTYTCTAQNPVSNNSDSISARQLCADIAMGFRTHHTG

CRACC: Insert in lentiviral vector pTT3; UniProt Q9UIB8: 23-220

SGPVKELVGSVGGAVTFPLKSKVKQVDSIVWTFNTTPLVTIQPEGGTIIVTQ
NRNRERVDFPDGGYSLKLSKLKKNDSGIYYVGIYSSSLQQPSTQEYVLHVYE
HLSKPKVTMGLQSNKNGTCVTNLTCCMEHGEEDVIYTWKALGQAANESH
NGSILPISWRWGESDMTFICVARNPVSRNFSSPILARKLCEGAAD

6.3.3 TCR and CAR Sequences

1G4 TCR: Insert in lentiviral transfer vectors pHR and pLEX with Neo resistance

(α chain) KQEVTQIPAALSVPEGENLVLNCSFTDSAIYNLQWFRQDPGKGLT

SLLLIQSSQREQTSGRLNASLDKSSGRSTLYIAASQPGDSATYLCAVRPTSGG
SYIPTFGRGTSLIVHPYIQNPDPAVYQLRDSKSSDKSVCLFTDFDSQTNVSQS
KDSDVYITDKTVLDMRSMDFKSNSAVAWSNKSDFACANAFNNSIIPEDTFF
PSPESSCDVKLVEKSFETDTNLNFQNLSVIGFRILLLKVAGFNLLMTLRLWSS

(β chain) GVTQTPKFQVLKTGQSMTLQCAQDMNHEYMSWYRQDPGMGLR
LIHYSVGAGITDQGEVPNGYNVSRSTTEDFPLRLLSAAPSQTSVYFCASSYV
GNTGELFFGEGSRLTVLEDLKNVFPPEVAVFEPSEAEISHTQKATLVCLATG
FYPDHVELSWWVNGKEVHSGVSTDPQPLKEQPALNDSRYALSSRLRVSATF
WQDPRNHFRCQVQFYGLSENDEWTQDRAKPVTQIVSAEAWGRADCGFTS
ESYQQGVLSATILYEILLGKATLYAVLVSALVLMAMVKRKDSRG

CD8α CAR [D52N-CD8α TM-CD28ζ] Insert in lentiviral transfer vector pLEX with puro resistance

MAEVQLLESGGGLVQPGGSLRLSCAASGFTFSTYQMSWVRQAPGKGLEWV
SGIVSSGGSTAYADSVKGRFTISRDNSKNTLYLQMNSLRAEDTAVYYCAGEL
LPYYGMDVWGQGTTVTVSSAKTTPKLEEGEFSEARVQSELTQPRSVSGSP
GQSVTISCTGTERDVGGYNYVSWYQQHPGKAPKLIIHNVIERSSGVPDRFSG
SKSGNTASLTISGLQAEDEADYYCWSFAGGYYVFGTGTDVTVLGQPKANP
TVDPDYKDDDDKTTTPAPRPPTPAPTIASQPLSLRPEACRPAAGGAVHTR
GLDFACDIYIWAPLAGTCGVLLLSLVITLYCRSKRSRLLHSDYMNMTPRRPG
PTRKHYQPYAPPRDFAAYRSRVKFSRSADAPAYQQGQNQLYNELNLGRRE
EYDVLDKRRGRDPEMGGKPRRKNPQEGLYNELQKDKMAEAYSEIGMKGE
RRRGKGHDGLYQGLSTATKDTYDALHMQALPPR

CD28 CAR H(40) [D52N-CD28 TM H(40)-CD28ζ] Insert in lentiviral transfer vector pLEX with Puro resistance

MAEVQLLESGGGLVQPGGSLRLSCAASGFTFSTYQMSWVRQAPGKGLEWV
SGIVSSGGSTAYADSVKGRFTISRDNSKNTLYLQMNSLRAEDTAVYYCAGEL
LPYYGMDVWGQGTTVTVSSAKTTPKLEEGEFSEARVQSELTQPRSVSGSP

GQSVTISCTGTERDVGGYNYVSWYQQHPGKAPKLIIHNVIERSSGVPDRFSG
SKSGNTASLTISGLQAEDEADYYCWSFAGGYYVFGTGTDVTVLGQPKANP
TVDPKIEVMYPPPYLDNEKSNGTIIHVKGKHLCPSPLFPGPSKPFWVLVVV
GGVLACYSLLVTVAFIIFWVRSKRSRLLHSDYMNMTPRRPGPTRKHYQPYA
PPRDFAAYRSLRVKFSRSADAPAYQQGQNQLYNELNLGRREEYDVLDKRR
GRDPEMGGKPRRKNPQEGLYNELQKDKMAEAYSEIGMKGERRRGKGHDG
LYQGLSTATKDTYDALHMQALPPR

CD28 CAR H(25) [D52N-CD28 TM H(25)-CD28ζ] Insert in lentiviral transfer vector pLEX with Puro resistance

MAEVQLLESGGGLVQPGGSLRLSCAASGFTFSTYQMSWVRQAPGKGLEWV
SGIVSSGGSTAYADSVKGRFTISRDNSKNTLYLQMNSLRAEDTAVYYCAGEL
LPYYGMDVWGQGTTVTVSSAKTTPKLEEGEFSEARVQSELTQPRSVSGSP
GQSVTISCTGTERDVGGYNYVSWYQQHPGKAPKLIIHNVIERSSGVPDRFSG
SKSGNTASLTISGLQAEDEADYYCWSFAGGYYVFGTGTDVTVLGQPKANP
TVDSNGTIIHVKGKHLCPSPLFPGPSKPFWVLVVVGGVLACYSLLVTVAFIIF
WVRSKRSRLLHSDYMNMTPRRPGPTRKHYQPYAPPRDFAAYRSLRVKFSR
SADAPAYQQGQNQLYNELNLGRREEYDVLDKRRGRDPEMGGKPRRKNPQ
EGLYNELQKDKMAEAYSEIGMKGERRRGKGHDGLYQGLSTATKDTYDAL
HMQALPPR

CD28 CAR H(21) [D52N-CD28 TM H(21)-CD28ζ] Insert in lentiviral transfer vector pLEX with Puro resistance

MAEVQLLESGGGLVQPGGSLRLSCAASGFTFSTYQMSWVRQAPGKGLEWV
SGIVSSGGSTAYADSVKGRFTISRDNSKNTLYLQMNSLRAEDTAVYYCAGEL
LPYYGMDVWGQGTTVTVSSAKTTPKLEEGEFSEARVQSELTQPRSVSGSP
GQSVTISCTGTERDVGGYNYVSWYQQHPGKAPKLIIHNVIERSSGVPDRFSG
SKSGNTASLTISGLQAEDEADYYCWSFAGGYYVFGTGTDVTVLGQPKANP
TVDIIHVKGKHLCPSPLFPGPSKPFWVLVVVGGVLACYSLLVTVAFIIFWVR

SKRSRLLHSDYMNMTPRRPGPTRKHYQPYAPPRDFAAYRSLRVKFSRSAD
APAYQQGQNQLYNELNLGRREEYDVLDKRRGRDPEMGGKPRRKNPQEGL
YNELQKDKMAEAYSEIGMKGERRRGKGHDGLYQGLSTATKDTYDALHMQ
ALPPR

Compact CAR: Insert in lentiviral vector pLEX with Neo resistance

MLLLVTSLLLCELPHPAFLLIPMAEVQLLESGGGLVQPGGSLRLSCAASGFTF
STYQMSWVRQAPGKGLEWVSGIVSSGGSTAYADSVKGRFTISRDNSKNTLY
LQMNSLRAEDTAVYYCAGELLPYYGMDVWGQGTTVTVSSASTKGPSVFPL
APSSKSTSGGTAALGCLVKDYFPEPVTVSWNSGALTSGVHTFPAVLQSSGL
YSLSSVVTVPSSSLGTQTYICNVNHKPSNTKVDKRVEPKSCGGGGSFWVLV
VVGGVLACYSLLVTVAFIIFWVRSKRSRLLHSDYMNMTPRRPGPTRKHYQP
YAPPRDFAAYRSRVKFSRSADAPAYQQGQNQLYNELNLGRREEYDVLDKR
RGRDPEMGGKPRRKNPQEGLYNELQKDKMAEAYSEIGMKGERRRGKGHD
GLYQGLSTATKDTYDALHMQALPPRGSGATNFSLLKQAGDVEENPGPMLL
LVTSLLLCELPHPAFLLIPQSELTQPRSVSGSPGQSVTISCTGTERDVGGYNY
VSWYQQHPGKAPKLIIHNVIERSSGVPDRFSGSKSGNTASLTISGLQAEDEAD
YYCWSFAGGYYVFGTGTDVTVLGGQPKANPTVTLFPPSSEELQANKATLV
CLISDFYPGAVTVAWKADGSPVKAGVETTKPSKQSNNKYAASSYLSLTPEQ
WKSHRSYSCQVTHEGSTVEKTVAPTECSGGGGSFWVLVVVGGVLACYSLL
VTVAFIIFWVRSKRSRLLHSDYMNMTPRRPGPTRKHYQPYAPPRDFAAYRS
RVKFSRSADAPAYQQGQNQLYNELNLGRREEYDVLDKRRGRDPEMGGKP
RRKNPQEGLYNELQKDKMAEAYSEIGMKGERRRGKGHDGLYQGLSTATK
DTYDALHMQALPPR

Bibliography

[1] A. Patel, V. Andre, S. B. Eguiguren, M. I. Barton, J. Burton, E. M. Denham, J. Pettmann, A. M. Mørch, M. A. Kutuzov, J. A. Siller-Farfán, M. L. Dustin, P. A. van der Merwe, and O. Dushek, "Using CombiCells, a platform for titration and combinatorial display of cell surface ligands, to study T-cell antigen sensitivity modulation by accessory receptors," *EMBO J.*, vol. 43, no. 1, pp. 132–150, 2024.

[2] J. Burton, J. A. Siller-Farfán, V. Andre, E. Jenkins, M. I. Barton, S. Bustamante Eguiguren, J. Cabezas Caballero, S. J. Davis, T. R. Weikl, P. A. van der Merwe, and O. Dushek, "Optimising CAR-T cell sensitivity by engineering matched extracellular sizes between CAR/antigen and CD2/CD58 adhesion complexes," *bioRxiv*, 2025, preprint.

[3] J. S. Marshall, R. Warrington, W. Watson, and H. L. Kim, "An introduction to immunology and immunopathology," *Allergy, Asthma & Clinical Immunology*, vol. 14, no. Suppl 2, p. 49, 2018.

[4] T. Pradeu, B. P. Thomma, S. E. Girardin, and B. Lemaitre, "The conceptual foundations of innate immunity: Taking stock 30 years later," *Immunity*, vol. 57, no. 4, pp. 613–631, 2024.

[5] R. Wang, C. Lan, K. Benlagha, N. O. S. Camara, H. Miller, M. Kubo, S. Heegaard, P. Lee, L. Yang, H. Forsman, X. Li, Z. Zhai, and C. Liu, "The interaction of innate immune and adaptive immune system," *MedComm (2020)*, vol. 5, no. 10, p. e714, 2024.

[6] S. Uthaisangsook, N. K. Day, S. L. Bahna, R. A. Good, and S. Haraguchi, "Innate immunity and its role against infections," *Annals of Allergy, Asthma & Immunology*, vol. 88, no. 1, pp. 1–6, 2002.

[7] H. Chi, M. Pepper, and P. G. Thomas, "Principles and therapeutic applications of adaptive immunity," *Cell*, vol. 187, no. 9, pp. 2052–2078, Apr. 2024.

[8] K. Seo and J. K. Choi, "Comprehensive analysis of TCR and BCR repertoires: Insights into methodologies, challenges, and applications," *Genomics & Informatics*, vol. 23, no. 1, p. 6, Feb. 2025.

[9] Y. Wen, Y. Jing, L. Yang, D. Kang, P. Jiang, N. Li, J. Cheng, J. Li, X. Li, Z. Peng, X. Sun, H. Miller, Z. Sui, Q. Gong, B. Ren, W. Yin, and C. Liu, "The regulators of BCR signaling during B cell activation," *Blood Science*, vol. 1, no. 2, pp. 119–129, 2019.

[10] J. E. Smith-Garvin, G. A. Koretzky, and M. S. Jordan, "T cell activation," *Annual Review of Immunology*, vol. 27, pp. 591–619, 2009.

[11] S. Halle, K. A. Keyser, F. R. Stahl, A. Busche, A. Marquardt, X. Zheng, M. Galla, V. Heissmeyer, K. Heller, J. Boelter, K. Wagner, Y. Bischoff, R. Martens, A. Braun, K. Werth, A. Uvarovskii, H. Kempf, M. Meyer-Hermann, R. Arens, M. Kremer, G. Sutter, M. Messerle, and R. Förster, "In vivo killing capacity of cytotoxic T cells is limited and involves dynamic interactions and T cell cooperativity," *Immunity*, vol. 44, no. 2, pp. 233–245, 2016.

[12] E. V. Rothenberg, J. Moore, and M. A. Yui, "Launching the T-cell-lineage developmental programme," *Nature Reviews Immunology*, vol. 8, pp. 9–21, 2008.

[13] D. Roth, "V(D)J recombination: Mechanism, errors, and fidelity," *Microbiology Spectrum*, vol. 2, no. 6, pp. 1–12, 2014.

[14] E. Market and F. N. Papavasiliou, "V(D)J recombination and the evolution of the adaptive immune system," *PLoS Biology*, vol. 1, no. 1, p. e16, 2003.

[15] N.-p. Weng, "Numbers and odds: TCR repertoire size and its age changes impacting on T cell functions," *Seminars in Immunology*, vol. 69, p. 101810, 2023.

[16] S. C. Jameson, K. A. Hogquist, and M. J. Bevan, "Positive selection of thymocytes," *Annual Review of Immunology*, vol. 13, no. 1, pp. 93–126, 1995.

[17] W.-L. Lo and E. S. Huseby, "The partitioning of TCR repertoires by thymic selection," *Journal of Experimental Medicine*, vol. 221, no. 10, p. e20230897, 2024.

[18] J. Ekeruche-Makinde, J. J. Miles, H. A. van den Berg, A. Skowera, D. K. Cole, G. Dolton, A. J. Schauenburg, M. P. Tan, J. M. Pentier, S. Llewellyn-Lacey, K. M. Miles, A. M. Bulek, M. Clement, T. Williams, A. Trimby, M. Bailey, P. Rizkallah, J. Rossjohn, M. Peakman, D. A. Price, S. R. Burrows, A. K. Sewell, and L. Wooldridge, "Peptide length determines the outcome of TCR/peptide-MHC I engagement," *Blood*, vol. 121, no. 7, pp. 1112–1123, 2013.

[19] M. N. Artyomov, M. Lis, S. Devadas, M. M. Davis, and A. K. Chakraborty, "CD4 and CD8 binding to MHC molecules primarily acts to enhance Lck delivery," *Proceedings of the National Academy of Sciences of the United States of America*, vol. 107, no. 39, pp. 16 916–16 921, 2010.

[20] S. Liu, S. Wei, Y. Sun, G. Xu, S. Zhang, and J. Li, "Molecular characteristics, functional definitions, and regulatory mechanisms for cross-presentation mediated by the major histocompatibility complex: A comprehensive review," *International Journal of Molecular Sciences*, vol. 25, no. 1, p. 196, 2023.

[21] K. Kedzierska and M. Koutsakos, "The ABC of major histocompatibility complexes and T cell receptors in health and disease," *Viral Immunology*, vol. 33, pp. 160–178, 2020.

[22] T. Hansen and M. Bouvier, "MHC class I antigen presentation: learning from viral evasion strategies," *Nature Reviews Immunology*, vol. 9, pp. 503–513, 2009.

[23] C. M. Poh, J. Zheng, R. Channappanavar, Z. W. Chang, T. H. O. Nguyen, L. Rénia, K. Kedzierska, S. Perlman, and L. L. M. Poon, "Multiplex screening assay for identifying cytotoxic CD8+ T cell epitopes," *Frontiers in Immunology*, vol. 11, p. 400, Mar 11 2020.

[24] P. A. Roche and K. Furuta, "The ins and outs of MHC class II-mediated antigen processing and presentation," *Nature Reviews Immunology*, vol. 15, no. 4, pp. 203–216, Apr. 2015.

[25] N. Vrisekoop, J. P. Monteiro, J. N. Mandl, and R. N. Germain, "Revisiting thymic positive selection and the mature T cell repertoire for antigen," *Immunity*, vol. 41, no. 2, pp. 181–190, 2014.

[26] L. Klein, B. Kyewski, P. M. Allen, and K. A. Hogquist, "Positive and negative selection of the T cell repertoire: what thymocytes see (and don't see)," *Nature Reviews Immunology*, vol. 14, no. 6, pp. 377–391, Jun 2014.

[27] R. A. Mariuzza, P. Agnihotri, and J. Orban, "The structural basis of T-cell receptor (TCR) activation: An enduring enigma," *Journal of Biological Chemistry*, vol. 295, no. 4, pp. 914–925, 2020.

[28] J. Wang, K. Lim, A. Smolyar, M. K. Teng, J. H. Liu, A. G. D. Tse, J. Liu, R. E. Hussey, Y. Chishti, C. T. Thomson, R. M. Sweet, S. G. Nathenson, H. C. Chang, J. C. Sacchettini, and E. L. Reinherz, "Atomic structure of an $\alpha\beta$ T cell receptor (TCR) heterodimer in complex with an anti-TCR Fab fragment derived from a mitogenic antibody," *The EMBO Journal*, vol. 17, no. 1, pp. 10–26, 1998.

[29] A. Morath and W. W. Schamel, "$\alpha\beta$ and $\gamma\delta$ T cell receptors: Similar but different," *Journal of Leukocyte Biology*, vol. 107, no. 6, pp. 1045–1055, 2020.

[30] S. Giri and G. Lal, "Differentiation and functional plasticity of $\gamma\delta$ T cells under homeostatic and disease conditions," *Molecular Immunology*, vol. 130, pp. 66–75, 2021.

[31] B. A. Irving and A. Weiss, "The cytoplasmic domain of the T cell receptor zeta chain is sufficient to couple to receptor-associated signal transduction pathways," *Cell*, vol. 64, no. 5, pp. 891–901, 1991.

[32] W.-L. Lo, N. H. Shah, N. Ahsan, V. Horkova, O. Stepanek, A. R. Salomon, J. Kuriyan, and A. Weiss, "Lck promotes Zap70-dependent LAT phosphorylation by bridging Zap70 to LAT," *Nature Immunology*, vol. 19, no. 7, pp. 733–741, 2018.

[33] A. K. Chakraborty and A. Weiss, "Insights into the initiation of TCR signaling," *Nature Immunology*, vol. 15, no. 9, pp. 815–823, 2014.

[34] V. Di Bartolo, D. Mège, V. Germain, M. Pelosi, E. Dufour, F. Michel, G. Magistrelli, A. Isacchi, and O. Acuto, "Tyrosine 319, a newly identified phosphorylation site of ZAP-70, plays a critical role in T cell antigen receptor signaling," *Journal of Biological Chemistry*, vol. 274, no. 10, pp. 6285–6294, 1999.

[35] B. Malissen, C. Grégoire, M. Malissen, and R. Roncagalli, "Integrative biology of T cell activation," *Nature Immunology*, vol. 15, no. 9, pp. 790–797, 2014.

[36] P. A. van der Merwe and O. Dushek, "Mechanisms for T cell receptor triggering," *Nature Reviews Immunology*, vol. 11, pp. 47–55, 2011.

[37] J. A. Cooper and H. Qian, "A mechanism for SRC kinase-dependent signaling by noncatalytic receptors," *Biochemistry*, vol. 47, no. 21, pp. 5681–5688, 2008.

[38] J. J. Boniface, J. D. Rabinowitz, C. Wolfing, J. Hampl, Z. Reich, J. D. Altman, R. M. Kantor, C. Beeson, H. M. McConnell, and M. M. Davis, "Initiation of signal transduction through the T cell receptor requires the multivalent engagement of peptide/MHC ligands," *Immunity*, vol. 9, no. 4, pp. 459–466, 1998.

[39] Y. Sykulev, M. Joo, I. Vturina, T. J. Tsomides, and H. N. Eisen, "Evidence that a single peptide-MHC complex on a target cell can elicit a cytolytic T cell response," *Immunity*, vol. 4, no. 6, pp. 565–571, June 1996.

[40] A. Trautmann and C. Randriamampita, "Initiation of TCR signalling revisited," *Trends in Immunology*, vol. 24, no. 8, pp. 425–428, Aug. 2003.

[41] R. M. Locksley, S. L. Reiner, F. Hatam, D. R. Littman, and N. Killeen, "Helper T cells without CD4: control of leishmaniasis in CD4-deficient mice," *Science*, vol. 261, pp. 1448–1451, 1993.

[42] M. W. Schilham, W. P. Fung-Leung, A. Rahemtulla, T. Kuendig, L. Zhang, J. Potter, R. G. Miller, H. Hengartner, and T. W. Mak, "Alloreactive cytotoxic T cells can develop and function in mice lacking both CD4 and CD8," *European Journal of Immunology*, vol. 23, no. 6, pp. 1299–1304, June 1993.

[43] M. Krogsgaard, Q. J. Li, C. Sumen, J. B. Huppa, M. Huse, and M. M. Davis, "Agonist/endogenous peptide-MHC heterodimers drive T cell activation and sensitivity," *Nature*, vol. 434, no. 7030, pp. 238–243, Mar. 2005.

[44] J. Juang, P. J. Ebert, D. Feng, K. C. Garcia, M. Krogsgaard, and M. M. Davis, "Peptide-MHC heterodimers show that thymic positive selection requires a more restricted set of self-peptides than negative selection," *Journal of Experimental Medicine*, vol. 207, no. 6, pp. 1223–1234, June 2010.

[45] S. T. Kim, K. Takeuchi, Z.-Y. A. Sun, M. Touma, C. E. Castro, A. Fahmy, M. J. Lang, G. Wagner, and E. L. Reinherz, "The alphabeta T cell receptor

is an anisotropic mechanosensor," *Journal of Biological Chemistry*, vol. 284, no. 45, pp. 31 028–31 037, 2009.

[46] L. Kjer-Nielsen, C. S. Clements, A. W. Purcell, A. G. Brooks, J. C. Whisstock, S. R. Burrows, J. McCluskey, and J. Rossjohn, "A structural basis for the selection of dominant alphabeta T cell receptors in antiviral immunity," *Immunity*, vol. 18, no. 1, pp. 53–64, Jan. 2003.

[47] T. Beddoe, Z. Chen, C. S. Clements, L. K. Ely, S. R. Bushell, J. P. Vivian, L. Kjer-Nielsen, S. S. Pang, M. A. Dunstone, Y. C. Liu, W. A. Macdonald, M. A. Perugini, M. C. Wilce, S. R. Burrows, A. W. Purcell, T. Tiganis, S. P. Bottomley, J. McCluskey, and J. Rossjohn, "Antigen ligation triggers a conformational change within the constant domain of the alphabeta T cell receptor," *Immunity*, vol. 30, no. 6, pp. 777–788, June 2009.

[48] M. S. Kuhns, A. T. Girvin, L. O. Klein, R. Chen, K. D. Jensen, E. W. Newell, J. B. Huppa, B. F. Lillemeier, M. Huse, Y. H. Chien, K. C. Garcia, and M. M. Davis, "Evidence for a functional sidedness to the alphabeta TCR," *Proceedings of the National Academy of Sciences of the United States of America*, vol. 107, no. 11, pp. 5094–5099, Mar. 2010.

[49] L. Li, J. O. Fierer, T. A. Rapoport, and M. Howarth, "Structural analysis and optimization of the covalent association between SpyCatcher and a peptide tag," *Journal of Molecular Biology*, vol. 426, pp. 309–317, 2014.

[50] Z.-Y. J. Sun, K. S. Kim, G. Wagner, and E. L. Reinherz, "Mechanisms contributing to T cell receptor signaling and assembly revealed by the solution structure of an ectodomain fragment of the CD3$\epsilon\gamma$ heterodimer," *Cell*, vol. 105, pp. 913–923, 2001.

[51] J. P. Secrist, L. A. Burns, L. Karnitz, G. A. Koretzky, and R. T. Abraham, "Stimulatory effects of the protein tyrosine phosphatase inhibitor, pervanadate,

on T-cell activation events," *Journal of Biological Chemistry*, vol. 268, pp. 5886–5893, 1993.

[52] V. Imbert, J. Peyron, D. Farahi Far, B. Mari, P. Auberger, and B. Rossi, "Induction of tyrosine phosphorylation and T-cell activation by vanadate peroxide, an inhibitor of protein tyrosine phosphatases," *Biochemical Journal*, vol. 297, no. Pt 1, pp. 163–173, Jan. 1994.

[53] R. A. Fernandes, C. Yu, A. M. Carmo, E. J. Evans, P. A. van der Merwe, and S. J. Davis, "What controls T cell receptor phosphorylation?" *Cell*, vol. 142, no. 5, pp. 668–669, Sept. 2010.

[54] K. Nika, C. Soldani, M. Salek, W. Paster, A. Gray, R. Etzensperger, L. Fugger, P. Polzella, V. Cerundolo, O. Dushek, T. Höfer, A. Viola, and O. Acuto, "Constitutively active Lck kinase in T cells drives antigen receptor signal transduction," *Immunity*, vol. 32, no. 6, pp. 766–777, June 2010.

[55] S. J. Davis and P. A. van der Merwe, "The kinetic-segregation model: TCR triggering and beyond," *Nature Immunology*, vol. 7, no. 8, pp. 803–809, Aug 2006.

[56] J. Lin and A. Weiss, "The tyrosine phosphatase CD148 is excluded from the immunologic synapse and down-regulates prolonged T cell signaling," *Journal of Cell Biology*, vol. 162, pp. 673–682, 2003.

[57] R. Varma, G. Campi, T. Yokosuka, T. Saito, and M. L. Dustin, "T cell receptor-proximal signals are sustained in peripheral microclusters and terminated in the central supramolecular activation cluster," *Immunity*, vol. 25, pp. 117–127, 2006.

[58] K. Choudhuri, M. Parker, A. Milicic, D. K. Cole, M. K. Shaw, A. K. Sewell, G. Stewart-Jones, T. Dong, K. G. Gould, and P. A. van der Merwe, "Peptide-major histocompatibility complex dimensions control proxi-

mal kinase-phosphatase balance during T cell activation," *Journal of Biological Chemistry*, vol. 284, no. 38, pp. 26 096–26 105, Sept. 2009.

[59] K. Choudhuri, D. Wiseman, M. H. Brown, K. Gould, and P. A. van der Merwe, "T cell receptor triggering is critically dependent on the dimensions of its peptide-MHC ligand," *Nature*, vol. 436, pp. 578–582, 2005.

[60] V. Horejsi, "Lipid rafts and their roles in T-cell activation," *Microbes and Infection*, vol. 7, pp. 310–316, 2005.

[61] A. Hashimoto-Tane, T. Yokosuka, C. Ishihara, M. Sakuma, W. Kobayashi, and T. Saito, "T-cell receptor microclusters critical for T-cell activation are formed independently of lipid raft clustering," *Molecular and Cellular Biology*, vol. 30, no. 14, pp. 3421–3429, July 2010.

[62] V. Golubovskaya and L. Wu, "Different subsets of T cells, memory, effector functions, and CAR-T immunotherapy," *Cancers (Basel)*, vol. 8, no. 3, p. 36, Mar 15 2016.

[63] R. N. Germain, "T-cell development and the CD4-CD8 lineage decision," *Nature Reviews Immunology*, vol. 2, no. 5, pp. 309–322, 2002.

[64] A. Viola, M. Salio, L. Tuosto, S. Linkert, O. Acuto, and A. Lanzavecchia, "Quantitative contribution of CD4 and CD8 to T cell antigen receptor serial triggering," *Journal of Experimental Medicine*, vol. 186, no. 10, pp. 1775–1779, 1997.

[65] J. Cabezas-Caballero, A. Huhn, M. A. Kutuzov, V. Andre, A. Shomuradova, B. W. A. Peeters, G. M. Gillespie, P. A. van der Merwe, and O. Dushek, "Generation of T cells with reduced off-target cross-reactivities by engineering co-signalling receptors," *Nature Biomedical Engineering*, 2026, epub ahead of print, Jan 2, 2026.

[66] Y. Li, Y. Yin, and R. A. Mariuzza, "Structural and biophysical insights into the role of CD4 and CD8 in T cell activation," *Frontiers in Immunology*, vol. 4, p. 206, Jul 22 2013.

[67] I. Raphael, S. Nalawade, T. N. Eagar, and T. G. Forsthuber, "T cell subsets and their signature cytokines in autoimmune and inflammatory diseases," *Cytokine*, vol. 74, no. 1, pp. 5–17, 2015.

[68] X. Zhu and J. Zhu, "CD4 T helper cell subsets and related human immunological disorders," *International Journal of Molecular Sciences*, vol. 21, no. 21, p. 8011, 2020.

[69] J. C. Waite and D. Skokos, "Th17 response and inflammatory autoimmune diseases," *International Journal of Inflammation*, vol. 2012, p. 819467, 2012.

[70] J. A. Roco, L. Mesin, S. C. Binder, C. Nefzger, P. Gonzalez-Figueroa, P. F. Canete, J. Ellyard, Q. Shen, P. A. Robert, J. Cappello, H. Vohra, Y. Zhang, C. R. Nowosad, A. Schiepers, L. M. Corcoran, K. M. Toellner, J. M. Polo, M. Meyer-Hermann, G. D. Victora, and C. G. Vinuesa, "Class-switch recombination occurs infrequently in germinal centers," *Immunity*, vol. 51, no. 2, pp. 337–350.e7, Aug. 2019.

[71] C. G. Vinuesa, M. A. Linterman, D. Yu, and I. C. MacLennan, "Follicular helper T cells," *Annual Review of Immunology*, vol. 34, pp. 335–368, 2016.

[72] J. C. Nolz, G. R. Starbeck-Miller, and J. T. Harty, "Naive, effector and memory CD8 T-cell trafficking: parallels and distinctions," *Immunotherapy*, vol. 3, no. 10, pp. 1223–1233, 2011.

[73] S. M. Kaech, E. J. Wherry, and R. Ahmed, "Effector and memory T-cell differentiation: implications for vaccine development," *Nature Reviews Immunology*, vol. 2, no. 4, pp. 251–262, 2002.

[74] C. H. Koh, S. Lee, M. Kwak, B. S. Kim, and Y. Chung, "CD8 T-cell subsets: heterogeneity, functions, and therapeutic potential," *Experimental & Molecular Medicine*, vol. 55, no. 11, pp. 2287–2299, 2023.

[75] M. W. Delfs, Y. Furukawa, R. N. Mitchell, and A. H. Lichtman, "CD8+ T cell subsets Tc1 and Tc2 cause different histopathologic forms of murine cardiac allograft rejection," *Transplantation*, vol. 71, no. 5, pp. 606–610, 2001.

[76] T. S. C. Hinks, R. D. Hoyle, and E. W. Gelfand, "CD8+ Tc2 cells: underappreciated contributors to severe asthma," *European Respiratory Review*, vol. 28, 2019.

[77] J. Alcain, A. D. P. Infante Cruz, G. Barrientos, S. Vanzulli, G. Salamone, and M. Vermeulen, "Mechanisms of unconventional CD8 Tc2 lymphocyte induction in allergic contact dermatitis: Role of H3/H4 histamine receptors," *Frontiers in Immunology*, vol. 13, p. 999852, Oct. 2022.

[78] A. Visekruna, J. Ritter, T. Scholz, L. Campos, A. Guralnik, L. Poncette, H. Raifer, S. Hagner, H. Garn, V. Staudt, T. Bopp, S. Reuter, C. Taube, K. Loser, and M. Huber, "Tc9 cells, a new subset of CD8(+) T cells, support Th2-mediated airway inflammation," *European Journal of Immunology*, vol. 43, no. 3, pp. 606–618, Mar. 2013.

[79] Y. Lu, B. Hong, H. Li, Y. Zheng, M. Zhang, S. Wang, J. Qian, and Q. Yi, "Tumor-specific IL-9-producing CD8+ Tc9 cells are superior effector than type-I cytotoxic Tc1 cells for adoptive immunotherapy of cancers," *Proceedings of the National Academy of Sciences of the United States of America*, vol. 111, no. 6, pp. 2265–2270, Feb. 2014.

[80] H. Hamada, M. d. L. Garcia-Hernandez, J. B. Reome, S. K. Misra, T. M. Strutt, K. K. McKinstry, A. M. Cooper, S. L. Swain, and R. W. Dutton,

"Tc17, a unique subset of CD8 T cells that can protect against lethal influenza challenge," *Journal of Immunology*, vol. 182, no. 6, pp. 3469–3481, Mar. 2009.

[81] R. I. Klein Geltink and A. Pillai, "Executive coaching unleashes Tc22 anti-tumor capacity," *Science Immunology*, vol. 7, no. 67, 2022.

[82] J. Su, Q. Xie, Y. Xu, X. C. Li, and Z. Dai, "Role of CD8(+) regulatory T cells in organ transplantation," *Burns & Trauma*, vol. 2, no. 1, pp. 18–23, 2014.

[83] Q. Zou, B. Wu, J. Xue, X. Fan, C. Feng, S. Geng, M. Wang, and B. Wang, "CD8+ Treg cells suppress CD8+ T cell responses by IL-10-dependent mechanism during H5N1 influenza virus infection," *European Journal of Immunology*, vol. 44, no. 1, pp. 103–114, 2014.

[84] D. L. Farber, N. A. Yudanin, and N. P. Restifo, "Human memory T cells: generation, compartmentalization and homeostasis," *Nature Reviews Immunology*, vol. 14, pp. 24–35, 2014.

[85] A. Gehad, J. E. Teague, T. R. Matos, V. Huang, C. Yang, R. Watanabe, J. T. O'Malley, C. L. Trimble, T. S. Kupper, and R. A. Clark, "A primary role for human central memory cells in tissue immunosurveillance," *Blood Advances*, vol. 2, no. 3, pp. 292–298, 2018.

[86] J. I. Gray, L. M. Westerhof, and M. K. L. MacLeod, "The roles of resident, central and effector memory CD4 T-cells in protective immunity following infection or vaccination," *Immunology*, vol. 154, pp. 574–581, 2018.

[87] R. Ullrich, H. L. Schieferdecker, K. Ziegler, E. O. Riecken, and M. Zeitz, "$\gamma\delta$ T cells in the human intestine express surface markers of activation and are preferentially located in the epithelium," *Cellular Immunology*, vol. 128, no. 2, pp. 619–627, July 1990.

[88] Y. Hu, Q. Hu, Y. Li, L. Lu, Z. Xiang, Z. Yin, D. Kabelitz, and Y. Wu, "$\gamma\delta$ T cells: origin and fate, subsets, diseases and immunotherapy," *Cellular*

Molecular Immunology, vol. 20, no. 1, pp. 1–17, 2023.

[89] M. Deseke and I. Prinz, "Ligand recognition by the $\gamma\delta$ TCR and discrimination between homeostasis and stress conditions," *Cellular & Molecular Immunology*, vol. 17, pp. 914–924, 2020.

[90] D. Fenoglio, A. Poggi, S. Catellani, F. Battaglia, A. Ferrera, M. Setti, G. Murdaca, and M. R. Zocchi, "Vdelta1 T lymphocytes producing IFN-gamma and IL-17 are expanded in HIV-1-infected patients and respond to Candida albicans," *Blood*, vol. 113, no. 26, pp. 6611–6618, June 2009.

[91] X. León-Lara, T. Yang, A. S. Fichtner, E. Bruni, C. von Kaisenberg, B. Eiz-Vesper, D. Dodoo, B. Adu, and S. Ravens, "Evidence for an Adult-Like Type 1-Immunity Phenotype of Vδ1, Vδ2 and Vδ3 T Cells in Ghanaian Children With Repeated Exposure to Malaria," *Frontiers in Immunology*, vol. 13, p. 807765, Feb. 2022.

[92] M. D. Hu, N. B. Golovchenko, G. L. Burns, P. M. Nair, T. J. t. Kelly, J. Agos, M. Z. Irani, W. S. Soh, M. R. Zeglinski, A. Lemenze, E. M. Bonder, I. Sandrock, I. Prinz, D. J. Granville, S. Keely, A. J. M. Watson, and K. L. Edelblum, "$\gamma\delta$ intraepithelial lymphocytes facilitate pathological epithelial cell shedding via CD103-mediated granzyme release," *Gastroenterology*, vol. 162, no. 3, pp. 877–889.e7, Mar. 2022.

[93] O. Toutirais, F. Cabillic, G. Le Friec, S. Salot, P. Loyer, M. Le Gallo, M. Desille, C. T. de La PintiÃ¨re, P. Daniel, F. Bouet, and V. Catros, "DNAX accessory molecule-1 (CD226) promotes human hepatocellular carcinoma cell lysis by Vγ9Vδ2 T cells," *European Journal of Immunology*, vol. 39, no. 5, pp. 1361–1368, May 2009.

[94] H. Raskov, A. Orhan, J. P. Christensen, and I. Gögenur, "Cytotoxic CD8+ T cells in cancer and cancer immunotherapy," *British Journal of Cancer*, vol.

124, no. 2, pp. 359–367, Jan. 2021.

[95] Y.-P. Lai, C.-C. Lin, W.-J. Liao, C.-Y. Tang, and S.-C. Chen, "CD4+ T cell-derived IL-2 signals during early priming advances primary CD8+ T cell responses," *PLoS ONE*, vol. 4, no. 11, p. e7766, 2009.

[96] R. M. Anthony, J. F. J. Urban, F. Alem, H. A. Hamed, C. T. Rozo, J. L. Boucher, N. Van Rooijen, and W. C. Gause, "Memory T(H)2 cells induce alternatively activated macrophages to mediate protection against nematode parasites," *Nature Medicine*, vol. 12, no. 8, pp. 955–960, Aug. 2006.

[97] D. M. Brown, S. Lee, M. d. L. Garcia-Hernandez, and S. L. Swain, "Multifunctional CD4 cells expressing gamma interferon and perforin mediate protection against lethal influenza virus infection," *Journal of Virology*, vol. 86, pp. 6792–6803, 2012.

[98] D. A. Morgan, F. W. Ruscetti, and R. Gallo, "Selective in vitro growth of T lymphocytes from normal human bone marrows," *Science*, vol. 193, no. 4257, pp. 1007–1008, 1976.

[99] S. H. Ross and D. A. Cantrell, "Signaling and function of interleukin-2 in T lymphocytes," *Annual Review of Immunology*, vol. 36, pp. 411–433, 2018.

[100] R. Setoguchi, S. Hori, T. Takahashi, and S. Sakaguchi, "Homeostatic maintenance of natural Foxp3+ CD25+ CD4+ regulatory T cells by interleukin (IL)-2 and induction of autoimmune disease by IL-2 neutralization," *Journal of Experimental Medicine*, vol. 201, pp. 723–735, 2005.

[101] S. Feau, V. Facchinetti, F. Granucci, S. Citterio, D. Jarrossay, S. Seresini, M. P. Protti, A. Lanzavecchia, and P. Ricciardi-Castagnoli, "Dendritic cell-derived IL-2 production is regulated by IL-15 in humans and in mice," *Blood*, vol. 105, no. 2, pp. 697–702, 2005.

[102] D. Peerlings, M. Mimpen, and J. Damoiseaux, "The IL-2 - IL-2 receptor pathway: Key to understanding multiple sclerosis," *Journal of Translational Autoimmunity*, vol. 4, p. 100123, 2021.

[103] Y. Minami, T. Kono, T. Miyazaki, and T. Taniguchi, "The IL-2 receptor complex: its structure, function, and target genes," *Annual Review of Immunology*, vol. 11, pp. 245–268, 1993.

[104] M. Allouche, Y. Sahraoui, Y. Augery-Bourget, M. Perrakis, C. Jasmin, and V. Georgoulias, "Interleukin 2 receptors," *Leukemia Research*, vol. 14, no. 8, pp. 699–703, 1990.

[105] O. Boyman and J. Sprent, "The role of interleukin-2 during homeostasis and activation of the immune system," *Nature Reviews Immunology*, vol. 12, pp. 180–190, 2012.

[106] Q. Sa, J. Woodward, and Y. Suzuki, "IL-2 produced by $CD8^+$ immune T cells can augment their IFN-γ production independently from their proliferation in the secondary response to an intracellular pathogen," *The Journal of Immunology*, vol. 190, no. 5, pp. 2199–2207, Mar 2013.

[107] M. L. Janas, P. Groves, N. Kienzle, and A. Kelso, "IL-2 regulates perforin and granzyme gene expression in $CD8^+$ T cells independently of its effects on survival and proliferation," *The Journal of Immunology*, vol. 175, no. 12, pp. 8003–8010, 2005.

[108] V. Kalia and S. Sarkar, "Regulation of effector and memory CD8 T cell differentiation by IL-2-a balancing act," *Frontiers in Immunology*, vol. 9, p. 2987, Dec 2018.

[109] W. Cui and S. M. Kaech, "Generation of effector $CD8^+$ T cells and their conversion to memory T cells," *Immunological Reviews*, vol. 236, pp. 151–166, Jul 2010.

[110] D. S. Green, H. A. Young, and J. C. Valencia, "Current prospects of type II interferon γ signaling and autoimmunity," *Journal of Biological Chemistry*, vol. 292, no. 34, pp. 13 925–13 933, Aug 2017.

[111] G. M. Lavigne, H. Russell, B. Sherry, and R. Ke, "Autocrine and paracrine interferon signalling as 'ring vaccination' and 'contact tracing' strategies to suppress virus infection in a host," *Proceedings of the Royal Society B: Biological Sciences*, vol. 288, no. 1945, p. 20203002, Feb. 2021.

[112] C. M. Horvath, "The Jak-STAT pathway stimulated by interferon gamma," *Science Signaling*, vol. 2004, no. 260, p. tr8, Nov 2004.

[113] M. Imran, A. S. Alshrari, A. Khan, and A. R. Alzahrani, "IFN-γ-driven macrophage responses in the immunity to Mycobacterium tuberculosis and Mycobacterium leprae," *Frontiers in Cellular and Infection Microbiology*, vol. 15, p. 1679691, 2025.

[114] S. Tötemeyer, M. Sheppard, A. Lloyd, D. Roper, C. Dowson, D. Underhill, P. Murray, D. Maskell, and C. Bryant, "IFN-γ enhances production of nitric oxide from macrophages via a mechanism that depends on nucleotide oligomerization domain-2," *Journal of Immunology*, vol. 176, no. 8, pp. 4804–4810, Apr 2006.

[115] J. K. Whitmire, N. Benning, and J. L. Whitton, "Cutting edge: early IFN-γ signaling directly enhances primary antiviral $CD4^+$ T cell responses," *Journal of Immunology*, vol. 175, no. 9, pp. 5624–5628, Nov 2005.

[116] F. Zhou, "Molecular mechanisms of IFN-γ to up-regulate MHC class I antigen processing and presentation," *International Reviews of Immunology*, vol. 28, no. 3-4, pp. 239–260, 2009.

[117] P. Groscurth and L. Filgueira, "Killing mechanisms of cytotoxic T lymphocytes," *Physiology*, vol. 13, no. 1, pp. 17–22, 1998.

[118] M. Mareboina, K. Bakhl, S. Agioti, N. S. Yee, I. Georgakopoulos-Soares, and A. Zaravinos, "Comprehensive analysis of granzymes and perforin family genes in multiple cancers," *Biomedicines*, vol. 13, no. 2, p. 408, Feb. 2025.

[119] I. Osińska, K. Popko, and U. Demkow, "Perforin: an important player in immune response," *Central-European Journal of Immunology*, vol. 39, no. 1, pp. 109–115, 2014.

[120] J. A. Trapani, "Granzymes: a family of lymphocyte granule serine proteases," *Genome Biology*, vol. 2, no. 12, pp. reviews3014.1–reviews3014.7, 2001.

[121] T. Nguyen and J. Russell, "The regulation of FasL expression during activation-induced cell death (AICD)," *Immunology*, vol. 103, no. 4, pp. 426–434, Aug. 2001.

[122] A. Ashkenazi and V. M. Dixit, "Apoptosis control by death and decoy receptors," *Current Opinion in Cell Biology*, vol. 11, no. 2, pp. 255–260, Apr. 1999.

[123] D. Cibrián and F. Sánchez-Madrid, "CD69: from activation marker to metabolic gatekeeper," *European Journal of Immunology*, vol. 47, no. 6, pp. 946–953, Jun 2017.

[124] R. Singh, Y.-H. Kim, S.-J. Lee, H.-S. Eom, and B. K. Choi, "4-1BB immunotherapy: advances and hurdles," *Experimental & Molecular Medicine*, vol. 56, pp. 32–39, 2024.

[125] J. C. Crispin, A. Martínez, P. de Pablo, C. Velasquillo, and J. Alcocer-Varela, "Participation of the CD69 antigen in the T-cell activation process of patients with systemic lupus erythematosus," *Scandinavian Journal of Immunology*, vol. 48, no. 2, pp. 196–200, Aug 1998.

[126] L. R. Shiow, D. B. Rosen, N. Brdicková, Y. Xu, J. An, L. L. Lanier, J. G. Cyster, and M. Matloubian, "CD69 acts downstream of interferon-alpha/beta

to inhibit S1P1 and lymphocyte egress from lymphoid organs," *Nature*, vol. 440, no. 7083, pp. 540–544, Mar 2006.

[127] D. Cibrian, M. L. Saiz, H. de la Fuente, R. Sánchez-Díaz, O. Moreno-Gonzalo, I. Jorge, A. Ferrarini, J. Vázquez, C. Punzón, M. Fresno, M. Vicente-Manzanares, E. Daudén, P. M. Fernández-Salguero, P. Martín, and F. Sánchez-Madrid, "CD69 controls the uptake of L-tryptophan through LAT1-CD98 and AhR-dependent secretion of IL-22 in psoriasis," *Nature Immunology*, vol. 17, no. 8, pp. 985–996, Aug 2016.

[128] W. W. Shuford, K. Klussman, D. D. Tritchler, D. T. Loo, J. Chalupny, A. W. Siadak, T. J. Brown, J. Emswiler, H. Raecho, C. P. Larsen, T. C. Pearson, J. A. Ledbetter, A. Aruffo, and R. S. Mittler, "4-1BB costimulatory signals preferentially induce $CD8^+$ T cell proliferation and lead to the amplification in vivo of cytotoxic T cell responses," *Journal of Experimental Medicine*, vol. 186, no. 1, pp. 47–55, Jul 7 1997.

[129] I. K. Jang, B. K. Choi, S. K. Lee, Y. H. Kim, H. S. Park, H. M. Kim, and J. Y. Lee, "Human 4-1BB (CD137) signals are mediated by TRAF2 and activate nuclear factor-kappa B," *Biochemical and Biophysical Research Communications*, vol. 242, pp. 613–620, 1998.

[130] K. Shah, A. Al-Haidari, J. Sun, and J. U. Kazi, "T cell receptor (TCR) signaling in health and disease," *Signal Transduction and Targeted Therapy*, vol. 6, no. 1, p. 412, 2021.

[131] O. Dushek and D. Coombs, "Analysis of serial engagement and peptide-MHC transport in T cell receptor microclusters," *Biophysical Journal*, vol. 94, no. 9, pp. 3447–3460, 2008.

[132] J. Pettmann, A. Huhn, E. Abu Shah, M. A. Kutuzov, D. B. Wilson, M. L. Dustin, S. J. Davis, P. A. van der Merwe, and O. Dushek, "The discriminatory

power of the T cell receptor," *eLife*, vol. 10, p. e67092, 2021.

[133] L. Chen and D. B. Flies, "Molecular mechanisms of T cell co-stimulation and co-inhibition," *Nature Reviews Immunology*, vol. 13, no. 4, pp. 227–242, Apr 2013.

[134] C. H. June, J. A. Ledbetter, M. M. Gillespie, T. Lindsten, and C. B. Thompson, "T-cell proliferation involving the CD28 pathway is associated with cyclosporine-resistant interleukin 2 gene expression," *Molecular and Cellular Biology*, vol. 7, no. 12, pp. 4472–4481, 1987.

[135] C. E. Edmead, J. R. Lamb, and G. F. Hoyne, "The T cell surface protein, CD28," *International Journal of Biochemistry & Cell Biology*, vol. 29, no. 8-9, pp. 1053–1057, Aug-Sep 1997.

[136] M. T. Lotze, S. H. Olejniczak, and D. Skokos, "CD28 co-stimulation: novel insights and applications in cancer immunotherapy," *Nature Reviews Immunology*, vol. 24, no. 12, pp. 878–895, Dec 2024.

[137] H. S. Lim, S. P. Cordoba, O. Dushek, J. Goyette, A. Taylor, C. E. Rudd, and P. A. van der Merwe, "Costimulation of IL-2 production through CD28 is dependent on the size of its ligand," *The Journal of Immunology*, vol. 195, no. 11, pp. 5432–5439, 2015.

[138] J. Göhring, L. Schrangl, G. J. Schütz, and J. B. Huppa, "Mechanosurveillance: Tiptoeing T cells," *Frontiers in Immunology*, vol. 13, p. 886328, 2022.

[139] C. Binder, F. Cvetkovski, F. Sellberg, S. Berg, H. Paternina Visbal, D. H. Sachs, E. Berglund, and D. Berglund, "CD2 immunobiology," *Frontiers in Immunology*, vol. 11, p. 1090, June 2020.

[140] S. L. McArdel, C. Terhorst, and A. H. Sharpe, "Roles of CD48 in regulating immunity and tolerance," *Clinical Immunology*, vol. 164, pp. 10–20, Mar. 2016.

[141] Y. Kaizuka, A. D. Douglass, S. Vardhana, M. L. Dustin, and R. D. Vale, "The coreceptor CD2 uses plasma membrane microdomains to transduce signals in T cells," *Journal of Cell Biology*, vol. 185, no. 3, pp. 521–534, 2009.

[142] S. Ikemizu, L. M. Sparks, P. A. van der Merwe, K. Harlos, D. I. Stuart, E. Y. Jones, and S. J. Davis, "Crystal structure of the CD2-binding domain of CD58 (lymphocyte function-associated antigen 3) at 1.8-A resolution," *Proceedings of the National Academy of Sciences of the United States of America*, vol. 96, no. 8, pp. 4289–4294, Apr. 1999.

[143] Y. Zhang, Q. Liu, S. Yang, and Q. Liao, "CD58 immunobiology at a glance," *Frontiers in Immunology*, vol. 12, p. 705260, 2021.

[144] P. A. van der Merwe, A. N. Barclay, D. W. Mason, E. A. Davies, B. P. Morgan, M. Tone, A. K. Krishnam, C. Ianelli, and S. J. Davis, "Human cell-adhesion molecule CD2 binds CD58 (LFA-3) with a very low affinity and an extremely fast dissociation rate but does not bind CD48 or CD59," *Biochemistry*, vol. 33, no. 33, pp. 10 149–10 160, Aug 23 1994.

[145] Q. Zhu, J. Li, N. Liu, L. Han, Z. Wu, Y. Wang, X. Lin, J. Wei, and W. Han, "CD2 augmentation enhances car-T-cell efficacy via immunological synapse remodeling and T-cell exhaustion mitigation," *Cellular & Molecular Immunology*, vol. 22, pp. 935–948, 2025.

[146] H. Ohno, C. Ushiyama, M. Taniguchi, R. N. Germain, and T. Saito, "CD2 can mediate TCR/CD3-independent T cell activation," *Journal of Immunology*, vol. 146, no. 11, pp. 3742–3746, Jun 1 1991.

[147] J. Leitner, D. Herndler-Brandstetter, G. J. Zlabinger, B. Grubeck-Loebenstein, and P. Steinberger, "CD58/CD2 is the primary costimulatory pathway in human $CD28^{-}CD8^{+}$ T cells," *Journal of Immunology*, vol. 195, no. 2, pp. 477–487, 2015.

[148] N. Killeen, S. G. Stuart, and D. R. Littman, "Development and function of T cells in mice with a disrupted CD2 gene," *EMBO Journal*, vol. 11, no. 12, pp. 4329–4336, Dec 1992.

[149] L. V. Riella, A. M. Paterson, A. H. Sharpe, and A. Chandraker, "Role of the PD-1 pathway in the immune response," *American Journal of Transplantation*, vol. 12, pp. 2575–2587, 2012.

[150] J. A. Perry, L. Shallberg, J. T. Clark, J. A. Gullicksrud, J. H. DeLong, B. B. Douglas, A. P. Hart, Z. Lanzar, K. O'Dea, C. Konradt, J. Park, J. R. Kuchroo, D. Grubaugh, A. G. Zaretsky, I. E. Brodsky, R. W. Malefyt, D. A. Christian, A. H. Sharpe, and C. A. Hunter, "PD-L1-PD-1 interactions limit effector regulatory T cell populations at homeostasis and during infection," *Nature Immunology*, vol. 23, no. 5, pp. 743–756, May 2022.

[151] E. Hui, J. Cheung, J. Zhu, X. Su, M. J. Taylor, H. A. Wallweber, D. K. Sasmal, J. Huang, J. M. Kim, I. Mellman, and R. D. Vale, "T cell costimulatory receptor cd28 is a primary target for pd-1-mediated inhibition," *Science*, vol. 355, no. 6332, pp. 1428–1433, 2017.

[152] Y. Gartshteyn, A. D. Askanase, and A. Mor, "SLAM associated protein signaling in T cells: Tilting the balance toward autoimmunity," *Frontiers in Immunology*, vol. 12, p. 654839, 2021.

[153] A. Veillette, "SLAM-family receptors: immune regulators with or without SAP-family adaptors," *Cold Spring Harbor Perspectives in Biology*, vol. 2, no. 3, p. a002469, Mar. 2010.

[154] C. Chu, Y. Wang, X. Zhang, X. Ni, J. Cao, W. Xu, Z. Dong, P. Yuan, W. Wei, Y. Ma, L. Zhang, L. Wu, and H. Qi, "SAP-regulated T Cell-APC adhesion and ligation-dependent and -independent Ly108-CD3ζ interactions," *The Journal of Immunology*, vol. 193, no. 8, pp. 3860–3871, 2014.

[155] H. Ahmed, A. R. Mahmud, M. F. Siddiquee, A. Shahriar, P. Biswas, M. E. K. Shimul, S. Z. Ahmed, T. I. Ema, N. Rahman, M. A. Khan, M. F. R. Mizan, and T. B. Emran, "Role of T cells in cancer immunotherapy: Opportunities and challenges," *Cancer Pathogenesis & Therapy*, vol. 1, no. 2, pp. 116–126, Dec 20 2022.

[156] S. Du, J. Yan, Y. Xue, Y. Zhong, and Y. Dong, "Adoptive cell therapy for cancer treatment," *Exploration (Beijing)*, vol. 3, no. 4, p. 20210058, Jul 2 2023.

[157] Q. Sun, Z. Hong, C. Zhang, X. Liu, F. Xie, Y. Yu, X. Chen, and Z. Zhou, "Immune checkpoint therapy for solid tumours: clinical dilemmas and future trends," *Signal Transduction and Targeted Therapy*, vol. 8, p. 320, 2023.

[158] J. Huang, M. Brameshuber, X. Zeng, J. Xie, Q. Li, Y.-h. Chien, S. Valitutti, and M. M. Davis, "A single peptide-major histocompatibility complex ligand triggers digital cytokine secretion in CD4+ T cells," *Immunity*, vol. 39, no. 5, pp. 846–857, 2013.

[159] Z. Zeng, H. Y. Chew, J. G. Cruz, G. R. Leggatt, and J. W. Wells, "Investigating T cell immunity in cancer: Achievements and prospects," *International Journal of Molecular Sciences*, vol. 22, no. 6, p. 2907, Mar. 2021.

[160] M. Aleksic, O. Dushek, H. Zhang, E. Shenderov, J. L. Chen, V. Cerundolo, D. Coombs, and P. A. van der Merwe, "Dependence of T cell antigen recognition on T cell receptor-peptide MHC confinement time," *Immunity*, vol. 32, no. 2, pp. 163–174, Feb. 2010.

[161] J. Burton, J. A. Siller-Farfán, J. Pettmann, B. Salzer, M. Kutuzov, P. A. van der Merwe, and O. Dushek, "Inefficient exploitation of accessory receptors reduces the sensitivity of chimeric antigen receptors," *Proceedings of the Na-*

tional Academy of Sciences of the United States of America, vol. 120, no. 2, p. e2216352120, 2023.

[162] J. L. Cannons, S. G. Tangye, and P. L. Schwartzberg, "SLAM family receptors and SAP adaptors in immunity," *Annual Review of Immunology*, vol. 29, pp. 665–705, 2011.

[163] C. Detre, M. Keszei, X. Romero, G. C. Tsokos, and C. Terhorst, "SLAM family receptors and the SLAM-associated protein (SAP) modulate T cell functions," *Seminars in Immunopathology*, vol. 32, no. 2, pp. 157–171, June 2010.

[164] G. Luo, R. Ni, X. Huang, Y. Li, and D. Luo, "The role of signaling lymphocytic activation molecule (slam) family receptors in health and disease progression: Focusing on cancer and therapy," *Clinical Immunology*, vol. 280, p. 110574, Nov. 2025.

[165] S. Sanzone, M. Zeyda, M. D. Saemann, M. Soncini, W. Holter, G. Fritsch, W. Knapp, F. Candotti, T. M. Stulnig, and O. Parolini, "SLAM-associated protein deficiency causes imbalanced early signal transduction and blocks downstream activation in T cells from X-linked lymphoproliferative disease patients," *Journal of Biological Chemistry*, vol. 278, no. 32, pp. 29 593–29 599, Aug. 2003.

[166] E. Cao, U. A. Ramagopal, A. A. Fedorov, E. V. Fedorov, Q. Yan, J. W. Lary, J. L. Cole, S. G. Nathenson, and S. C. Almo, "NTB-A receptor crystal structure: insights into homophilic interactions in the signaling lymphocytic activation molecule receptor family," *Immunity*, vol. 25, no. 4, pp. 559–570, 2006.

[167] M. H. Brown, K. Boles, P. A. van der Merwe, V. Kumar, P. A. Mathew, and A. N. Barclay, "2B4, the natural killer and T cell immunoglobulin superfamily

surface protein, is a ligand for CD48," *Journal of Experimental Medicine*, vol. 188, no. 11, pp. 2083–2090, 1998.

[168] S. Mehrle, J. Schmidt, M. W. Büchler, C. Watzl, and A. Märten, "Enhancement of anti-tumor activity in vitro and in vivo by CD150 and SAP," *Molecular Immunology*, vol. 45, no. 3, pp. 796–804, 2008.

[169] J. Qi, A. Crinier, B. EscaliÃ¨re, Y. Ye, Z. Wang, T. Zhang, L. Batista, H. Liu, L. Hong, N. Wu, M. Zhang, L. Chen, Y. Liu, L. Shen, E. Narni-Mancinelli, E. Vivier, and B. Su, "Single-cell transcriptomic landscape reveals tumor specific innate lymphoid cells associated with colorectal cancer progression," *Cell Reports Medicine*, vol. 2, no. 8, p. 100353, July 2021.

[170] M. Assidi, "Strong prognostic value of SLAMF7 protein expression in patients with lymph node-positive breast cancer," *Oncology Letters*, vol. 24, no. 6, p. 433, Oct. 2022.

[171] M. A. Dimopoulos, S. Lonial, D. White, P. Moreau, K. Weisel, J. San-Miguel, O. Shpilberg, S. Grosicki, I. Sšpička, A. Walter-Croneck, H. Magen, M. V. Mateos, A. Belch, D. Reece, M. Beksac, A. Spencer, H. Oakervee, R. Z. Orlowski, M. Taniwaki, C. Röllig, H. Einsele, M. Matsumoto, K. L. Wu, K. C. Anderson, Y. M. Jou, A. Ganetsky, A. K. Singhal, and P. G. Richardson, "Elotuzumab, lenalidomide, and dexamethasone in RRMM: final overall survival results from the phase 3 randomized ELOQUENT-2 study," *Blood Cancer Journal*, vol. 10, no. 9, p. 91, Sept. 2020.

[172] A. Veillette, M.-E. Cruz-Muñoz, and M.-C. Zhong, "SLAM family receptors and SAP-related adaptors: matters arising," *Trends in Immunology*, vol. 27, no. 5, pp. 228–234, 2006.

[173] K. Kato, M. Koyanagi, H. Okada, T. Takanashi, Y. W. Wong, A. F. Williams, K. Okumura, and H. Yagita, "CD48 is a counter-receptor for mouse CD2 and

is involved in T cell activation," *Journal of Experimental Medicine*, vol. 176, no. 5, pp. 1241–1249, 1992.

[174] Z. Dong, M. E. Cruz-Muñoz, M. C. Zhong, R. Chen, S. Latour, and A. Veillette, "Essential function for SAP family adaptors in the surveillance of hematopoietic cells by natural killer cells," *Nature Immunology*, vol. 10, pp. 973–980, 2009.

[175] A. G. Castro, T. M. Hauser, B. G. Cocks, J. Abrams, S. Zurawski, T. Churakova, F. Zonin, D. Robinson, S. G. Tangye, G. Aversa, K. E. Nichols, J. E. de Vries, L. L. Lanier, and A. O'Garra, "Molecular and functional characterization of mouse signaling lymphocytic activation molecule (SLAM): differential expression and responsiveness in Th1 and Th2 cells," *Journal of Immunology*, vol. 163, no. 11, pp. 5860–5870, 1999.

[176] J. Kramer, P. A. van der Merwe, and O. Dushek, "Platforms for studying cell-cell recognition by immune cells," *Immunology and Cell Biology*, vol. 103, no. 7, pp. 636–647, 2025.

[177] C.-J. Hsu, W.-T. Hsieh, A. Waldman, F. Clarke, E. S. Huseby, J. K. Burkhardt, and T. Baumgart, "Ligand mobility modulates immunological synapse formation and T cell activation," *PLoS ONE*, vol. 7, no. 2, p. e32398, 2012.

[178] R. E. Hynds, E. Vladimirou, and S. M. Janes, "The secret lives of cancer cell lines," *Disease Models Mechanisms*, vol. 11, no. 11, p. dmm037366, 2018.

[179] D. Hatlem, T. Trunk, D. Linke, and J. C. Leo, "Catching a SPY: Using the SpyCatcher-SpyTag and related systems for labeling and localizing bacterial proteins," *International Journal of Molecular Sciences*, vol. 20, no. 9, p. 2129, 2019.

[180] M. Gunes, S. T. Rosen, I. Shachar, and E. G. Gunes, "Signaling lymphocytic activation molecule family receptors as potential immune therapeutic targets in solid tumors," *Frontiers in Immunology*, vol. 15, p. 1297473, 2024.

[181] R. T. Abraham and A. Weiss, "Jurkat t cells and development of the t-cell receptor signalling paradigm," *Nature Reviews Immunology*, vol. 4, no. 4, pp. 301–308, Apr. 2004.

[182] D. Howie, M. Simarro, J. Sayos, M. Guirado, J. Sancho, and C. Terhorst, "Molecular dissection of the signaling and costimulatory functions of CD150 (SLAM): CD150/SAP binding and CD150-mediated costimulation," *Blood*, vol. 99, no. 3, pp. 957–965, 2002.

[183] P. A. Valdez, H. Wang, D. Seshasayee, M. van Lookeren Campagne, A. Gurney, W. P. Lee, and I. S. Grewal, "NTB-A, a new activating receptor in T cells that regulates autoimmune disease," *Journal of Biological Chemistry*, vol. 279, no. 18, pp. 18 662–18 669, Apr. 2004.

[184] S. Margraf, L. I. Garner, T. J. Wilson, and M. H. Brown, "A polymorphism in a phosphotyrosine signalling motif of CD229 (Ly9, SLAMF3) alters SH2 domain binding and T-cell activation," *Immunology*, vol. 146, no. 3, pp. 392–400, 2015.

[185] G. Papadaki, O. Ani, T. Florio, M. Young, J. Danon, Y. Sun, D. Dersh, and N. Sgourakis, "Decoupling peptide binding from T cell receptor recognition with engineered chimeric MHC-I molecules," *Frontiers in Immunology*, vol. 14, p. 1116906, 2023.

[186] J.-L. Chen, P. Dunbar, U. Gileadi, E. Jäger, S. Gnjatic, Y. Nagata, E. Stockert, D. Panicali, Y.-T. Chen, A. Knuth, L. Old, and V. Cerundolo, "Identification of NY-ESO-1 peptide analogues capable of improved stimulation of tumor-

reactive CTL," *The Journal of Immunology*, vol. 165, no. 2, pp. 948–955, 2000.

[187] C. A. Velikovsky, L. Deng, L. K. Chlewicki, M. M. Fernández, V. Kumar, and R. A. Mariuzza, "Structure of natural killer receptor 2B4 bound to CD48 reveals basis for heterophilic recognition in signaling lymphocyte activation molecule family," *Immunity*, vol. 27, no. 4, pp. 572–584, 2007.

[188] N. Mavaddat, D. W. Mason, P. D. Atkinson, E. J. Evans, R. J. Gilbert, D. I. Stuart, J. A. Fennelly, A. N. Barclay, S. J. Davis, and M. H. Brown, "Signaling lymphocytic activation molecule (CDw150) is homophilic but self-associates with very low affinity," *Journal of Biological Chemistry*, vol. 275, no. 36, pp. 28 100–28 109, 2000.

[189] R. R. Bartelt, N. Cruz-Orcutt, M. Collins, and J. C. D. Houtman, "Comparison of T cell receptor-induced proximal signaling and downstream functions in immortalized and primary T cells," *PLoS ONE*, vol. 4, no. 5, p. e5430, 2009.

[190] X.-Z. Ma, T. Jin, D. Sakac, S. Fahim, X. Zhang, Y. Katsman, M. Bali, and D. R. Branch, "Abnormal splicing of SHP-1 protein tyrosine phosphatase in human T cells: implications for lymphomagenesis," *Experimental Hematology*, vol. 31, no. 2, pp. 131–142, 2003.

[191] X. Romero, D. Benítez, S. March, R. Vilella, M. Miralpeix, and P. Engel, "Differential expression of SAP and EAT-2-binding leukocyte cell-surface molecules CD84, CD150 (SLAM), CD229 (Ly9) and CD244 (2B4)," *Tissue Antigens*, vol. 64, no. 2, pp. 132–144, 2004.

[192] M. P. Karampetsou, D. Comte, K. Kis-Toth, C. Terhorst, V. C. Kyttaris, and G. C. Tsokos, "Decreased SAP expression in T cells from patients with systemic lupus erythematosus contributes to early signaling abnormalities and

reduced IL-2 production," *The Journal of Immunology*, vol. 196, no. 12, pp. 4915–4924, 2016.

[193] H. Pahima, P. G. Puzzovio, and F. Levi-Schaffer, "2B4 and CD48: A powerful couple of the immune system," *Clinical Immunology*, vol. 204, pp. 64–68, 2019.

[194] J. B. Ames, V. Vyas, J. D. Lusin, and R. A. Mariuzza, "NMR structure of the natural killer cell receptor 2B4 (CD244): implications for ligand recognition," *Biochemistry*, vol. 44, no. 17, pp. 6416–6423, 2005.

[195] A. Kearney, A. Avramovic, M. A. Castro, A. M. Carmo, S. J. Davis, and P. A. van der Merwe, "The contribution of conformational adjustments and long-range electrostatic forces to the CD2/CD58 interaction," *Journal of Biological Chemistry*, vol. 282, no. 18, pp. 13 160–13 166, May 2007.

[196] R. R. Bartelt, N. Cruz-Orcutt, M. Collins, and J. C. D. Houtman, "Comparison of T cell receptor-induced proximal signaling and downstream functions in immortalized and primary T cells," *PLOS ONE*, vol. 4, no. 4, p. e5430, 2009.

[197] Y. Wei, J. Lee, M. Dziegelewski, M. S. Marlow, and D. B. Hayes, "Determination of the SLAMF1 self-association affinity constant with sedimentation velocity ultracentrifugation," *Analytical Biochemistry*, vol. 633, p. 114410, 2021.

[198] J.-O. Kim, H. W. Kim, K.-M. Baek, and C.-Y. Kang, "NF-κB and AP-1 regulate activation-dependent CD137 (4-1BB) expression in T cells," *FEBS Letters*, vol. 541, no. 1–3, pp. 163–170, 2003.

[199] E. Lupino, C. Ramondetti, and M. Piccinini, "IκB Kinase β Is Required for Activation of NF-κB and AP-1 in CD3/CD28-Stimulated Primary CD4+ T Cells," *The Journal of Immunology*, vol. 188, no. 6, pp. 2545–2555, 2012.

[200] C. W. Chow, M. Rincón, and R. J. Davis, "Requirement for transcription factor NFAT in interleukin-2 expression," *Molecular and Cellular Biology*, vol. 19, no. 3, pp. 2300–2307, 1999.

[201] M. T. Cooling, P. Hunter, and E. J. Crampin, "Sensitivity of NFAT cycling to cytosolic calcium concentration: implications for hypertrophic signals in cardiac myocytes," *Biophysical Journal*, vol. 96, no. 6, pp. 2095–2104, 2009.

[202] N. Hagberg, J. Theorell, H. Schlums, M.-L. Eloranta, Y. T. Bryceson, and L. Rönnblom, "Systemic lupus erythematosus immune complexes increase the expression of SLAM family members CD319 (CRACC) and CD229 (Ly-9) on plasmacytoid dendritic cells and CD319 on $CD56^{dim}$ NK cells," *Journal of Immunology*, vol. 191, no. 6, pp. 2989–2998, 2013.

[203] A. Bouchon, M. Cella, H. L. Grierson, J. I. Cohen, and M. Colonna, "Cutting edge: Activation of NK cell-mediated cytotoxicity by a SAP-independent receptor of the CD2 family," *Journal of Immunology*, vol. 167, no. 10, pp. 5517–5521, 2001.

[204] I. Tassi and M. Colonna, "The cytotoxicity receptor CRACC (CS-1) recruits EAT-2 and activates the PI3K and phospholipase C γ signaling pathways in human NK cells," *Journal of Immunology*, vol. 175, no. 12, pp. 7996–8002, 2005.

[205] D. M. Longo, B. Louie, E. Wang, Z. Pos, F. M. Marincola, R. E. Hawtin, and A. Cesano, "Inter-donor variation in cell subset specific immune signaling responses in healthy individuals," *American Journal of Clinical and Experimental Immunology*, vol. 1, no. 1, pp. 1–11, Apr. 2012.

[206] J. N. Brudno, M. V. Maus, and C. S. Hinrichs, "CAR T cells and T-cell therapies for cancer: A translational science review," *JAMA*, vol. 332, no. 22, pp. 1924–1935, 2024.

[207] J. Li, Y. Tang, and Z. Huang, "Efficacy and safety of chimeric antigen receptor (CAR)-T cell therapy in the treatment of relapsed and refractory multiple

myeloma: a systematic review and meta-analysis of clinical trials," *Translational Cancer Research*, vol. 11, no. 3, pp. 569–579, 2022.

[208] P. Lloret-Madrid, P. Chorão, M. Guerreiro, and P. Montesinos, "CAR-T cell therapy for acute myeloid leukemia: Where do we stand now?" *Current Oncology*, vol. 32, no. 6, p. 322, 2025.

[209] Y. Zhao, X. Bai, S. Guo, X. Zhang, J. Liu, M. Zhao, T. Xie, H. Meng, Y. Zhang, X. He, and M. Zhao, "Efficacy and safety of CAR-T therapy targeting CLL1 in patients with extramedullary diseases of acute myeloid leukemia," *Journal of Translational Medicine*, vol. 22, no. 1, p. 888, 2024.

[210] E. Pinto, L. Lione, M. Compagnone, M. Paccagnella, E. Salvatori, M. Greco, V. Frezza, E. Marra, L. Aurisicchio, G. Roscilli, and A. Conforti, "From ex vivo to in vivo chimeric antigen T cells manufacturing: new horizons for CAR T-cell based therapy," *Journal of Translational Medicine*, vol. 23, no. 1, p. 10, Jan. 2025.

[211] S. Feins, W. Kong, E. F. Williams, M. C. Milone, and J. A. Fraietta, "An introduction to chimeric antigen receptor (CAR) T-cell immunotherapy for human cancer," *American Journal of Hematology*, vol. 94, no. S1, pp. S3–S9, 2019.

[212] S. Guedan, H. Calderon, J. Posey, A. D., and M. V. Maus, "Engineering and design of chimeric antigen receptors," *Molecular Therapy: Methods & Clinical Development*, vol. 12, pp. 145–156, 2018.

[213] M. Jonnalagadda, A. Mardiros, R. Urak, X. Wang, L. J. Hoffman, A. Bernanke, W.-C. Chang, W. Bretzlaff, R. Starr, S. Priceman, J. R. Ostberg, S. J. Forman, and C. E. Brown, "Chimeric antigen receptors with mutated IgG4 Fc spacer avoid Fc receptor binding and improve T cell persistence and antitumor efficacy," *Molecular Therapy*, vol. 23, no. 4, pp. 757–768, 2015.

[214] S. E. James, P. D. Greenberg, M. C. Jensen, Y. Lin, J. Wang, B. G. Till, A. A. Raubitschek, S. J. Forman, and O. W. Press, "Antigen sensitivity of CD22-specific chimeric TCR is modulated by target epitope distance from the cell membrane," *The Journal of Immunology*, vol. 180, no. 10, pp. 7028–7038, 2008.

[215] J. Jayaraman, M. P. Mellody, A. J. Hou, R. P. Desai, A. W. Fung, A. H. T. Pham, Y. Y. Chen, and W. Zhao, "CAR-T design: Elements and their synergistic function," *EBioMedicine*, vol. 58, p. 102931, Aug 2020.

[216] R. D. Guest, R. E. Hawkins, N. Kirillova, E. J. Cheadle, J. Arnold, A. OâNeill, J. Irlam, K. A. Chester, J. T. Kemshead, and D. M. Shaw, "The role of extracellular spacer regions in the optimal design of chimeric immune receptors: evaluation of four different scfvs and antigens," *Journal of Immunotherapy*, vol. 28, no. 3, pp. 203–211, 2005.

[217] G. Bernard and L. Evgin, "Non-signaling but all important: how the linker, hinge, and transmembrane domains in the CAR hold it all together," *Frontiers in Immunology*, vol. 16, p. 1664403, 2025.

[218] L. Alabanza, M. Pegues, C. Geldres, V. Shi, J. J. W. Wiltzius, S. A. Sievers, S. Yang, and J. N. Kochenderfer, "Function of novel anti-CD19 chimeric antigen receptors with human variable regions is affected by hinge and transmembrane domains," *Molecular Therapy*, vol. 25, no. 11, pp. 2452–2465, 2017.

[219] S. Hirobe, K. Imaeda, M. Tachibana, and N. Okada, "The effects of chimeric antigen receptor (CAR) hinge domain post-translational modifications on CAR-T cell activity," *International Journal of Molecular Sciences*, vol. 23, no. 7, p. 4056, 2022.

[220] Y. Muller, D. Nguyen, L. Ferreira, P. Ho, C. Raffin, R. Valencia, Z. Congrave-Wilson, T. Roth, J. Eyquem, F. Van Gool, A. Marson, L. Perez, J. Wells,

J. Bluestone, and Q. Tang, "The CD28-transmembrane domain mediates chimeric antigen receptor heterodimerization with CD28," *Frontiers in Immunology*, vol. 12, p. 639818, 2021.

[221] M. M. Honikel and S. H. Olejniczak, "Co-stimulatory receptor signaling in CAR-T cells," *Biomolecules*, vol. 12, no. 9, p. 1303, Sept. 2022.

[222] M. S. Cook, E. King, K. R. Flaherty, K. Siddika, S. Papa, R. Benjamin, and A. Schurich, "CAR-T cells containing CD28 versus 4-1BB co-stimulatory domains show distinct metabolic profiles in patients," *Cell Reports*, vol. 44, no. 7, p. 115973, 2025.

[223] P. Lu, X.-a. Lu, X. Zhang, M. Xiong, J. Zhang, X. Zhou, F. Qi, J. Yang, and T. He, "Which is better in CD19 CAR-T treatment of r/r B-ALL, CD28 or 4-1BB? A parallel trial under the same manufacturing process," *Journal of Clinical Oncology*, vol. 36, no. 15_supplement, p. 3041, 2018.

[224] P. Zhang, X. Feng, X. Niu, Z. Liu, M. Li, M. Liu, D. Yan, G. Zhang, and X. Wan, "CD28 is superior to 4-1BB costimulation in generating CAR-NK cells for tumor immunotherapy," *Experimental Hematology & Oncology*, vol. 14, p. 28, 2025.

[225] K. M. Cappell and J. N. Kochenderfer, "A comparison of chimeric antigen receptors containing CD28 versus 4-1BB costimulatory domains," *Nature Reviews Clinical Oncology*, vol. 18, no. 11, pp. 715–727, 2021.

[226] S. Majumdar, H. Echelibe, M. Bettini, and M. L. Bettini, "The impact of CD3ζ ITAM multiplicity and sequence on CAR T-cell survival and function," *Frontiers in Immunology*, vol. 15, p. 1509980, 2025.

[227] G. de Oliveira Canedo, C. Roddie, and P. J. Amrolia, "Dual-targeting CAR T cells for B-cell acute lymphoblastic leukemia and B-cell non-Hodgkin lymphoma," *Blood Advances*, vol. 9, no. 4, pp. 704–721, 2025.

[228] E. Hamed, E. S. K. Mergani, R. O. M. Suliman, E. A. I. Eltayeb, A. Mohamed, and R. Hassan, "Long-term outcomes of CAR-T cell therapy in DLBCL," *Journal of Clinical Oncology*, vol. 43, no. 16_supplement, p. e19004, 2025, conference Abstract.

[229] R. Litvin and B. T. Hill, "Long-term outcomes and late toxicities of CAR t-cell therapy in large B-cell lymphoma," *Expert Opinion on Biological Therapy*, vol. 26, no. 1, pp. 39–50, 2026.

[230] A. Zinzi, M. Gaio, V. Liguori, C. Cagnotta, D. Paolino, G. Paolisso, G. Castaldo, G. F. Nicoletti, F. Rossi, A. Capuano, and C. Rafaniello, "Late relapse after CAR-T cell therapy for adult patients with hematologic malignancies: A definite evidence from systematic review and meta-analysis on individual data," *Pharmacological Research*, vol. 190, p. 106742, Apr 2023.

[231] R. G. Majzner and C. L. Mackall, "Tumor antigen escape from CAR T-cell therapy," *Cancer Discovery*, vol. 8, no. 10, pp. 1219–1226, 2018.

[232] D. T. Harris, M. V. Hager, S. N. Smith, Q. Cai, J. D. Stone, P. Kruger, M. Lever, O. Dushek, T. M. Schmitt, P. D. Greenberg, and D. M. Kranz, "Comparison of T cell activities mediated by human TCRs and CARs that use the same recognition domains," *Journal of Immunology*, vol. 200, no. 3, pp. 1088–1100, 2018.

[233] R. G. Majzner, S. P. Rietberg, E. Sotillo, R. Dong, V. T. Vachharajani, L. Labanieh, J. H. Myklebust, M. Kadapakkam, E. W. Weber, A. M. Tousley, R. M. Richards, S. Heitzeneder, S. M. Nguyen, V. Wiebking, J. Theruvath, R. C. Lynn, P. Xu, A. R. Dunn, R. D. Vale, and C. L. Mackall, "Tuning the antigen density requirement for CAR T-cell activity," *Cancer Discovery*, vol. 10, no. 5, pp. 702–723, 2020.

[234] J. D. Stone, D. T. Harris, C. M. Soto, A. S. Chervin, D. H. Aggen, E. J. Roy,

and D. M. Kranz, "A novel T cell receptor single-chain signaling complex mediates antigen-specific T cell activity and tumor control," *Cancer Immunology, Immunotherapy*, vol. 63, no. 11, pp. 1163–1176, 2014.

[235] R. Oren, M. Hod-Marco, M. Haus-Cohen, S. Thomas, D. Blat, N. Duvshani, G. Denkberg, Y. Elbaz, F. Benchetrit, Z. Eshhar, H. Stauss, and Y. Reiter, "Functional comparison of engineered T cells carrying a native TCR versus TCR-like antibody–based chimeric antigen receptors indicates affinity/avidity thresholds," *Journal of Immunology*, vol. 193, no. 11, pp. 5733–5743, 2014.

[236] J. H. Wang, A. Smolyar, K. Tan, J. H. Liu, M. Kim, Z. Y. Sun, G. Wagner, and E. L. Reinherz, "Structure of a heterophilic adhesion complex between the human CD2 and CD58 (LFA-3) counterreceptors," *Cell*, vol. 97, no. 6, pp. 791–803, June 1999.

[237] J. G. Cyster, D. M. Shotton, and A. F. Williams, "The dimensions of the T lymphocyte glycoprotein CD43 and its relationship to the T cell receptor," *The EMBO Journal*, vol. 10, no. 4, pp. 893–902, 1991.

[238] D. Y. Lin, Y. Tanaka, M. Iwasaki, A. G. Gittis, H. Su, B. Mikami, T. Okazaki, T. Honjo, N. Minato, and D. N. Garboczi, "The PD-1/PD-L1 complex resembles the antigen-binding Fv domains of antibodies and T cell receptors," *Proceedings of the National Academy of Sciences of the United States of America*, vol. 105, no. 8, pp. 3011–3016, 2008.

[239] L. Sušac, M. T. Vuong, C. Thomas, S. von Bülow, C. O'Brien-Ball, A. M. Santos, R. A. Fernandes, G. Hummer, R. Tampé, and S. J. Davis, "Structure of a fully assembled tumor-specific T cell receptor ligated by pMHC," *Cell*, vol. 185, no. 17, pp. 3201–3213.e19, 2022.

[240] Y. Li, T. Moriyama, S. Yoshimura, X. Zhao, Z. Li, X. Yang, E. Paietta, M. R. Litzow, M. Konopleva, J. Yu, H. Inaba, R. C. Ribeiro, C.-H. Pui, and J. J.

Yang, "PAX5 epigenetically orchestrates CD58 transcription and modulates blinatumomab response in acute lymphoblastic leukemia," *Science Advances*, vol. 8, no. 50, p. eadd6403, 2022.

[241] P. Zhang, G. Zhang, and X. Wan, "Challenges and new technologies in adoptive cell therapy," *Journal of Hematology & Oncology*, vol. 16, no. 1, p. 97, 2023.

[242] S. Ramakrishna, S. L. Highfill, Z. Walsh, S. M. Nguyen, H. Lei, J. F. Shern, H. Qin, I. L. Kraft, M. Stetler-Stevenson, C. M. Yuan, J. D. Hwang, Y. Feng, Z. Zhu, D. Dimitrov, N. N. Shah, and T. J. Fry, "Modulation of target antigen density improves CAR T-cell functionality and persistence," *Clinical Cancer Research*, vol. 25, no. 17, pp. 5329–5341, Sept. 2019.

[243] D. V. Volkov, V. M. Stepanova, I. A. Yaroshevich, A. G. Gabibov, and Y. P. Rubtsov, "The impact of the intracellular domains of chimeric antigenic receptors on the properties of CAR T-cells," *Acta Naturae*, vol. 17, no. 3, pp. 4–17, 2025.

[244] S. Jutz, A. Hennig, W. Paster, O. Asrak, D. Dijanovic, F. Kellner, W. F. Pickl, J. B. Huppa, J. Leitner, and P. Steinberger, "A cellular platform for the evaluation of immune checkpoint molecules," *Oncotarget*, vol. 8, no. 39, pp. 64 892–64 906, May 2017.

[245] J. R. Sedy, M. Gavrieli, K. G. Potter, M. A. Hurchla, R. C. Lindsley, K. Hildner, S. Scheu, K. Pfeffer, C. F. Ware, and K. M. Murphy, "B and T lymphocyte attenuator regulates T cell activation through interaction with herpesvirus entry mediator," *Nature Immunology*, vol. 6, no. 1, pp. 90–98, 2005.

[246] H. Zola, "High-sensitivity immunofluorescence/flow cytometry: detection of cytokine receptors and other low-abundance membrane molecules," *Current Protocols in Cytometry*, p. Unit 6.3, 2004.

[247] L. Chen and D. B. Flies, "Molecular mechanisms of T cell co-stimulation and co-inhibition," *Nature Reviews Immunology*, vol. 13, no. 4, pp. 227–242, 2013.

[248] M. L. Dustin and J. T. Groves, "Receptor signaling clusters in the immune synapse," *Annual Review of Biophysics*, vol. 41, pp. 543–556, 2012.

[249] E. Abu-Shah, N. Trendel, P. Kruger, J. Nguyen, J. Pettmann, M. Kutuzov, and O. Dushek, "Human $CD8^+$ T cells exhibit a shared antigen threshold for different effector responses," *The Journal of Immunology*, vol. 205, no. 6, pp. 1503–1512, 2020.

[250] A. J. Torres, R. L. Contento, S. Gordo, K. W. Wucherpfennig, and J. C. Love, "Functional single-cell analysis of T-cell activation by supported lipid bilayer-tethered ligands on arrays of nanowells," *Lab on a Chip*, vol. 13, no. 1, pp. 90–99, 2013.

[251] M. Krogsgaard, N. Prado, E. J. Adams, X. L. He, D. C. Chow, D. B. Wilson, K. C. Garcia, and M. M. Davis, "Evidence that structural rearrangements and/or flexibility during TCR binding can contribute to T cell activation," *Molecular Cell*, vol. 12, no. 6, pp. 1367–1378, Dec. 2003.

[252] O. Dushek, M. Aleksic, R. J. Wheeler, H. Zhang, S. P. Cordoba, Y. C. Peng, J. L. Chen, V. Cerundolo, T. Dong, D. Coombs, and P. A. van der Merwe, "Antigen potency and maximal efficacy reveal a mechanism of efficient T cell activation," *Science Signaling*, vol. 4, no. 176, p. ra39, June 2011.

[253] T. Yokosuka, M. Takamatsu, W. Kobayashi-Imanishi, A. Hashimoto-Tane, M. Azuma, and T. Saito, "Programmed cell death 1 forms negative costimulatory microclusters that directly inhibit T cell receptor signaling by recruiting phosphatase SHP2," *Journal of Experimental Medicine*, vol. 209, no. 6, pp. 1201–1217, 2012.

[254] A. Hashimoto-Tane, M. Sakuma, H. Ike, T. Yokosuka, Y. Kimura, O. Ohara, and T. Saito, "Micro-adhesion rings surrounding TCR microclusters are essential for T cell activation," *Journal of Experimental Medicine*, vol. 213, no. 8, pp. 1609–1625, 2016.

[255] P. Demetriou, E. Abu-Shah, S. Valvo, S. McCuaig, V. Mayya, A. Kvalvaag, T. Starkey, K. Korobchevskaya, L. Y. W. Lee, M. Friedrich, E. Mann, M. A. Kutuzov, M. Morotti, N. Wietek, H. Rada, S. Yusuf, J. Afrose, A. Siokis, O. I. C. Investigators, M. Meyer-Hermann, A. A. Ahmed, D. Depoil, and M. L. Dustin, "A dynamic CD2-rich compartment at the outer edge of the immunological synapse boosts and integrates signals," *Nature Immunology*, vol. 21, no. 10, pp. 1232–1243, 2020.

[256] R. Varma, G. Campi, T. Yokosuka, T. Saito, and M. L. Dustin, "T cell receptor-proximal signals are sustained in peripheral microclusters and terminated in the central supramolecular activation cluster," *Immunity*, vol. 25, no. 1, pp. 117–127, Jul 2006.

[257] F. W. B. Craenmehr, A. Gräwe, V. A. Veenbrink, R. Bellan, M. Merkx, and P. Y. W. Dankers, "Employing the SpyTag-SpyCatcher reaction for the modification of supramolecular polymers with functional proteins," *Bioconjugate Chemistry*, vol. 36, no. 6, pp. 1197–1207, 2025.

[258] L. Jia, K. Minamihata, H. Ichinose, K. Tsumoto, and N. Kamiya, "Polymeric SpyCatcher scaffold enables bioconjugation in a ratio-controllable manner," *Biotechnology Journal*, vol. 12, no. 12, p. 1700195, 2017.

[259] V. Lampinen, S. Gröhn, S. Soppela, V. Blazevic, V. P. Hytönen, and M. M. Hankaniemi, "SpyTag/SpyCatcher display of influenza M2e peptide on norovirus-like particle provides stronger immunization than direct genetic fusion," *Frontiers in Cellular and Infection Microbiology*, vol. 13, p. 1216364, 2023.

[260] A. Treumann, M. R. Lifely, P. Schneider, and M. A. Ferguson, "Primary structure of cd52," *Journal of Biological Chemistry*, vol. 270, no. 11, pp. 6088–6099, 1995.

[261] T. Kinoshita, "Biosynthesis and biology of mammalian GPI-anchored proteins," *Open Biology*, vol. 10, no. 3, p. 190290, 2020.

[262] A. H. Keeble and M. Howarth, "Insider information on successful covalent protein coupling with help from SpyBank," 2018.

[263] Q. T. Lin and P. B. Stathopulos, "Protocol for deriving distance restraints from AlphaFold for use in solution NMR structure determination," *STAR Protocols*, vol. 6, no. 3, p. 103988, 2025.

[264] G. Forlani, J. Michaux, H. Pak, F. Huber, E. L. Marie Joseph, E. Ramia, B. J. Stevenson, M. Linnebacher, R. S. Accolla, and M. Bassani-Sternberg, "Ciita-transduced glioblastoma cells uncover a rich repertoire of clinically relevant tumor-associated HLA-II antigens," *Molecular Cellular Proteomics*, vol. 20, p. 100032, 2021.

[265] P. J. Bjorkman and P. Parham, "Structure of the human class I histocompatibility antigen, HLA-A2," *Nature*, vol. 329, pp. 506–512, 1987.

[266] W. Wriggers, S. Chakravarty, and P. A. Jennings, "Control of protein functional dynamics by peptide linkers," *Biopolymers*, vol. 80, no. 6, pp. 736–746, 2005.

[267] F. Zhang, B. Crise, B. Su, Y. Hou, J. K. Rose, A. Bothwell, and K. Jacobson, "Lateral diffusion of membrane-spanning and glycosylphosphatidylinositol-linked proteins: toward establishing rules governing the lateral mobility of membrane proteins," *Journal of Cell Biology*, vol. 115, no. 1, pp. 75–84, 1991.

[268] Q. Zhang and M. Fujita, "Why nature evolved GPI-anchored proteins: unique structure characteristics enable versatile cell surface functions," *Glycobiology*,

vol. 31, no. 6, pp. 661–670, 2021.

[269] S. V. Radhakrishnan, N. Bhardwaj, T. Luetkens, and D. Atanackovic, "Novel anti-myeloma immunotherapies targeting the SLAM family of receptors," *OncoImmunology*, vol. 6, no. 5, p. e1308618, 2017.

[270] R. Grosser, L. Cherkassky, N. Chintala, and P. S. Adusumilli, "Combination immunotherapy with CAR T cells and checkpoint blockade for the treatment of solid tumors," *Cancer Cell*, vol. 36, no. 5, pp. 471–482, 2019.

[271] A. Leithner, A. Kvalvaag, T. Mitra, S. Valvo, H. Dada, E. Compeer, M. I. Barton, S. B. Eguiguren, E. Jenkins, C. Lagerholm, O. Dushek, and M. L. Dustin, "Mixed-mobility supported lipid bilayers uncover the role of immobilized icam1 on T cell activation and immune synapse organization," *Proceedings of the National Academy of Sciences of the United States of America*, vol. 123, no. 11, p. e2530126123, 2026.

[272] A. Veillette, "NK cell regulation by SLAM family receptors and SAP-related adapters," *Immunological Reviews*, vol. 214, pp. 22–34, 2006.

[273] S. Meinke and C. Watzl, "NK cell cytotoxicity mediated by 2B4 and NTB-A is dependent on SAP acting downstream of receptor phosphorylation," *Frontiers in Immunology*, vol. 4, p. 3, 2013.

[274] I. Bethani, S. S. Skånland, I. Dikic, and A. Acker-Palmer, "Spatial organization of transmembrane receptor signalling," *The EMBO Journal*, vol. 29, no. 16, pp. 2677–2688, 2010.

[275] I. Hwang and J. Sprent, "Role of the actin cytoskeleton in T cell absorption and internalization of ligands from APC," *Journal of Immunology*, vol. 166, no. 8, pp. 5099–5107, 2001.

[276] S. Saha, I. H. Lee, A. Polley, J. T. Groves, M. Rao, and S. Mayor, "Diffusion of GPI-anchored proteins is influenced by the activity of dynamic cortical actin,"

Molecular Biology of the Cell, vol. 26, no. 22, pp. 4033–4045, 2015.

[277] K. Y. Chen, E. Jenkins, M. Körbel, A. Ponjavic, A. H. Lippert, A. M. Santos, N. Ashman, C. O'Brien-Ball, J. McBride, D. Klenerman, and S. J. Davis, "Trapping or slowing the diffusion of T cell receptors at close contacts initiates T cell signaling," *Proceedings of the National Academy of Sciences of the United States of America*, vol. 118, no. 39, p. e2024250118, Sept. 2021.

[278] T. Nakai, Y. Nakai, N. Takami, E. Nakai, and T. Okajima, "SpyRing-mediated cyclization of TEV protease, guided by AlphaFold, improves thermostability," *ACS Omega*, vol. 10, no. 30, pp. 33 862–33 871, 2025.